UC Irvine

UC Irvine Electronic Theses and Dissertations

Title

FLASH irradiation protects the central nervous system

Permalink

https://escholarship.org/uc/item/2g21h260

Author

Allen, Barrett Don

Publication Date

2023

Peer reviewed|Thesis/dissertation

eScholarship.org Powered by the California Digital Library
University of California

UNIVERSITY OF CALIFORNIA,
IRVINE

FLASH Irradiation Protects the Central Nervous System

DISSERTATION

Submitted in partial satisfaction of the requirement
for the degree of

DOCTOR OF PHILOSOPHY
in Environmental Health Sciences

by

Barrett Don Allen

Dissertation Committee:
Professor Charles Limoli, Chair
Professor Michael Kleinman
Associate Professor Masashi Kitazawa

Introduction ©2021 Elsevier Inc.

Chapter 2 ©2020 by Radiation Research Society

Chapter 3 ©2022 American Association for Cancer Research

Chapter 4 ©2023 Oxford University Press

All other materials ©2023 Barrett Don Allen

Dedication

To Rachel, whose unwavering love and support helped make this possible.

To Elizabeth and Dexter who put up with the long hours.

To my parents who encouraged me to continue.

To those we've lost to cancer.

Table of Contents

List of Figures

List of Tables

Acknowledgements

I would like to express my deepest gratitude to my committee chair, Dr. Charles Limoli, who has given amazing guidance to me over the decade, including in the choice to pursue my graduate education. He has always been one to share his knowledge and genuinely desires others to succeed. Without his persistent encouragement, this dissertation would not have been possible.

I would also like to thank my committee members, Professor Michael Kleinman and Dr. Masashi Kitazawa who both once guided me through their research of interest during my first year of rotations. Their thoughtful and experienced insight has helped form this body of work. I am indeed grateful for them.

I am also indebted to Dr. Marie-Catherine Vozenin, who remains the most important name in the field of FLASH radiotherapy. Her and her lab were intricate in every experiment that I performed throughout this dissertation. Without her, none of this material would have been possible.

I will always be grateful for Dr. Janet Baulch and Dr. Munjal Acharya who were endless resources for me throughout the years. Both are the most dedicated scientists I have met and have helped shape who I have become.

I thank Elsevier Inc. for permission to include copywritten material that made up chapter 1 of my dissertation. I also thank the Radiation Research Society for their permission to include material that made up chapter 2. I also thank the American Association for Cancer Research for their permission to publish copywritten material that made up chapter 3. I also thank Oxford University Press for their permission to use copywritten material that made up chapter 4 of my dissertation.

Vita

Barrett Don Allen

2017 – 2023	Ph.D. in Environmental Health Sciences; Toxicology, University of California, Irvine
2018 – 2019	Teaching Assistant, Developmental and Cellular Biology, University of California, Irvine
2013 – 2017	Staff Research Associate II, University of California, Irvine
2011 – 2013	Staff Research Associate II, University of California, San Francisco
2010 – 2011	Intern, University of California, San Francisco, Department of Neurosurgery
2007 – 2011	B.S. in Molecular and Cellular Biology, San Francisco State University

Fields of Study

Neurogenic factors involved in traumatic brain injury

Radiation induced central nervous system normal tissue damage

Modulation of radiation dose rate to improve normal tissue sparing

Publications

Allen BD, Alaghband Y, Kramár EA, Ru N, Petit B, Grilj V, Petronek MS, Pulliam CF, Kim RY, Doan NL, Baulch JE, Wood MA, Bailat C, Spitz DR, Vozenin MC, Limoli CL. Elucidating the neurological mechanism of the FLASH effect in juvenile mice exposed to hypofractionated radiotherapy. Neuro Oncol. 2022 Nov 5:noac248. PMID: 36334265.

Luderer U, Lim J, Ortiz L, Nguyen JD, Shin JH, Allen BD, Liao LS, Malott K, Perraud V, Wingen LM, Arechavala RJ, Bliss B, Herman DA, Kleinman MT. Exposure to environmentally relevant concentrations of ambient fine particulate matter ($PM_{2.5}$) depletes the ovarian follicle reserve and causes sex-dependent cardiovascular changes in apolipoprotein E null mice. Part Fibre Toxicol. 2022 Jan 7;19(1):5. PMID: 34996492.

Allen BD, Limoli CL. Breaking barriers: Neurodegenerative repercussions of radiotherapy induced damage on the blood-brain and blood-tumor barrier. Free Radic Biol Med. 2022 Jan;178:189-201. PMID: 34875340.

Parihar VK, Syage A, Flores L, Lilagan A, Allen BD, Angulo MC, Song J, Smith SM, Arechavala RJ, Giedzinski E, Limoli CL. The Cannabinoid Receptor 1 Reverse Agonist AM251 Ameliorates Radiation-Induced Cognitive Decrements. Front Cell Neurosci. 2021 Jun 28;15:668286. PMID: 34262437.

Klein PM, Parihar VK, Szabo GG, Zöldi M, Angulo MC, Allen BD, Amin AN, Nguyen QA, Katona I, Baulch JE, Limoli CL, Soltesz I. Detrimental impacts of mixed-ion radiation on nervous system function. Neurobiol Dis. 2021 Apr;151:105252. PMID: 33418069.

Allen BD, Acharya MM, Montay-Gruel P, Jorge PG, Bailat C, Petit B, Vozenin MC, Limoli C. Maintenance of Tight Junction Integrity in the Absence of Vascular Dilation in the Brain of Mice

Exposed to Ultra-High-Dose-Rate FLASH Irradiation. Radiat Res. 2020 Dec 1;194(6):625-635. PMID: 33348373.

Parihar VK, Angulo MC, Allen BD, Syage A, Usmani MT, Passerat de la Chapelle E, Amin AN, Flores L, Lin X, Giedzinski E, Limoli CL. Sex-Specific Cognitive Deficits Following Space Radiation Exposure. Front Behav Neurosci. 2020 Sep 16;14:535885. PMID: 33192361.

Montay-Gruel P, Markarian M, Allen BD, Baddour JD, Giedzinski E, Jorge PG, Petit B, Bailat C, Vozenin MC, Limoli C, Acharya MM. Ultra-High-Dose-Rate FLASH Irradiation Limits Reactive Gliosis in the Brain. Radiat Res. 2020 Dec 1;194(6):636-645. PMID: 32853387.

Alaghband Y, Cheeks SN, Allen BD, Montay-Gruel P, Doan NL, Petit B, Jorge PG, Giedzinski E, Acharya MM, Vozenin MC, Limoli CL. Neuroprotection of Radiosensitive Juvenile Mice by Ultra-High Dose Rate FLASH Irradiation. Cancers (Basel). 2020 Jun 24;12(6):1671. PMID: 32599789.

Allen BD, Syage AR, Maroso M, Baddour AAD, Luong V, Minasyan H, Giedzinski E, West BL, Soltesz I, Limoli CL, Baulch JE, Acharya MM. Mitigation of helium irradiation-induced brain injury by microglia depletion. J Neuroinflammation. 2020 May 19;17(1):159. PMID: 32429943.

Allen, B. D., Apodaca, L. A., Syage, A. R., Markarian, M., Baddour, A. A. D., Minasyan, H., … Acharya, M. M. (2019). Attenuation of neuroinflammation reverses Adriamycin-induced cognitive impairments. Acta Neuropathol Commun. 2019 Nov 21;7(1):186. PMID: 31753024

Montay-Gruel P, Acharya MM, Petersson K, Alikhani L, Yakkala C, Allen BD, Ollivier J, Petit B, Jorge PG, Syage AR, Nguyen TA, Baddour AAD, Lu C, Singh P, Moeckli R, Bochud F, Germond JF, Froidevaux P, Bailat C, Bourhis J, Vozenin MC, Limoli CL. Long-term neurocognitive benefits of FLASH radiotherapy driven by reduced reactive oxygen species. Proc Natl Acad Sci U S A. 2019 May 16. PMID: 31097580

Parihar VK, Maroso M, Syage A, Allen BD, Angulo MC, Soltesz I, Limoli CL. Persistent nature of alterations in cognition and neuronal circuit excitability after exposure to simulated cosmic radiation in mice. Exp Neurol. 2018 Jul;305:44-55. Epub 2018 Mar 11. PMID: 29540322.

Allen BD, Acharya MM, Lu C, Giedzinski E, Chmielewski NN, Quach D, Hefferan M, Johe KK, Limoli CL. Remediation of Radiation-Induced Cognitive Dysfunction through Oral Administration of the Neuroprotective Compound NSI-189. Radiation Research. 2018 April; 189(4):345-353. PMID: 29351056

Acharya MM, Baddour AA, Kawashita T, Allen BD, Syage AR, Nguyen TH, Yoon N, Giedzinski E, Yu L, Parihar VK, Baulch JE. Epigenetic determinants of space radiation-induced cognitive dysfunction. Sci Rep. 2017 Feb 21;7:42885. PMID: 28220892.

Parihar VK, Allen BD, Caressi C, Kwok S, Chu E, Tran KK, Chmielewski NN, Giedzinski E, Acharya MM, Britten RA, Baulch JE, Limoli CL. Cosmic radiation exposure and persistent cognitive dysfunction. Scientific Reports. Oct 10 2016. PMID: 27721383

Acharya MM, Green KN, Allen BD, Najafi AR, Syage A, Minasyan H, Le MT, Kawashita T, Giedzinski E, Parihar VK, West BL, Baulch JE, Limoli CL. Elimination of microglia improves cognitive function following cranial irradiation. Scientific Reports. Aug 12 2016. PMID: 27516055

Acharya MM, Baulch JE, Lusardi TA, Allen BD, Chmielewski NN, Baddour AA, Limoli CL, Boison D. Adenosine kinase inhibition protects against cranial radiation-induced cognitive dysfunction. Frontiers in Molecular Neuroscience. June 3 2016. PMID: 27375429

Craver BM, Acharya MM, Allen BD, Benke SN, Hultgren NW, Baulch JE, Limoli CL. 3D surface analysis of hippocampal microvasculature in the irradiated brain. Environ Mol Mutagen. June 2016. PMID: 27175611

Baulch JE, Acharya MM, Allen BD, Ru N, Chmielewski NN, Martirosian V, Giedzinski E, Syage A, Park AL, Benke SN, Parihar VK, Limoli CL. Cranial grafting of stem cell-derived microvesicles improves cognition and reduces neuropathy in the irradiated brain. PNAS. April 26 2016. PMID: 27044087

Raber J, Allen AR, Sharma S, Allen B, Rosi S, Olsen RH, Davis MJ, Eiwaz M, Fike JR, Nelson GA. Effects or proton and combined proton and (56)Fe radiation on the hippocampus. Radiat Res. Jan 2016. PMID: 26720797

Parihar VK, Allen B, Tran KK, Macaraeg TG, Chu EM, Kwok SF, Chmielewski NN, Craver BM, Baulch JE, Acharya MM, Cucinotta FA, Limoli CL. What happens to your brain on the way to Mars. Science Advances May 1 2015. PMID: 26180843

Baulch JE, Craver BM, Tran KK, Yu L, Chmielewski N, Allen BD, Limoli CL. Persistent oxidative stress in human neural stem cells exposed to low fluences of charged particles. Redox Biol. March 11 2015 PMID: 25800120

Parihar VK, Allen BD, Tran KK, Craver BM, Chmielewski NN, Martirosian V, Rosi S, Morganti JM, Vlkolinsky R, Acharya MM, Nelson GA, Allen AR, Limoli CL. Targeted overexpression of mitochondrial catalase prevents radiation-induced cognitive dysfunction. Antiox and Redox Signaling. Jan 1 2015 PMID: 24949841

Allen AR, Chakraborti A, Sharma S, Baure J, Habdank-Kolaczkowski J, Allen BD, Leu D, Huang T-T, Rosi S, Raber J, Fike JR. Delayed administration of α-difluoromethylornithine prevents hippocampal dependent cognitive impairment after single and combined injury in mice. Radiat Res. Nov 2014. PMID: 25375198

Raber J., Rudobeck E, Campbell-Beachler M, Allen AR, Allen BD, Rosi S, Nelson G, Ramachandran S, Turner T, Fike JR, Vlkolinsky R. ^{28}Silicon radiation-induced enhancement of synaptic plasticity in the hippocampus of naïve and cognitively tested mice. Radiation Research March 27 2014. PMID: 24673255

Allen AR, Eilertson K, Sharma S, Schneider D, Baure J, Allen BD, Rosi S, Raber J, Fike JR. Effects of Radiation Combined Injury on Hippocampal Function are Modulated in Mice Deficient in Chemokine Receptor 2 (CCR2). Radiation Research July 2013. PMID: 23772926

Allen AR, Eilertson K, Chakraborti A, Sharma S, Baure J, Habdank-Kolaczkowski J, Allen BD, Rosi S, Raber J, Fike JR. Radiation exposure prior to traumatic brain injury induces responses that differ as a function of animal age. International Journal of Radiation Biology. October 2013. PMID: 24164494

Chakraborti A, Allen A, Allen B, Rosi S, Fike JR. Cranial irradiation alters dendritic spine density and morphology in the hippocampus. PLoS One. July 16 2012. PMID: 22815839

Abstract of the Dissertation

FLASH Irradiation Protects the Central Nervous System

By

Barrett Don Allen

Doctor of Philosophy in Environmental Health Science

University of California, Irvine, 2023

Professor Charles L. Limoli, Chair

Radiotherapy has long been used to control tumor growth by causing ionization of cellular macromolecules including DNA, RNA, lipids and proteins, leading to lethal or sublethal damage to a cell. Typically, convention radiotherapy (CONV-RT) is delivered at a dose rate between 0.07–0.1 $Gy \cdot s^{-1}$ and fractionated over an extended treatment plan (1 -2 months), allowing healthy normal tissue to mend sublethal damage while repair-compromised tumor tissue accumulates damage. Previous studies have identified that fractions under 2 Gy are required to reduce long-term neurocognitive damage[1]. These normal tissue dose tolerances limit the therapeutic benefit of radiotherapy. A recent breakthrough in radiation delivery modalities have shown that using ultra-high dose rates (>100 $Gy \cdot s^{-1}$), or 'FLASH' irradiation, can reduce cognitive damage, spare normal tissue injury, and minimize harm to critical systems like the blood brain barrier (BBB), all while maintaining isoefficient tumor control[2–4]. This new radiation modality has the potential to greatly extend the therapeutic benefit of radiotherapy while limiting the unintended neurological sequelae that are frequently caused by treatment.

At this point, our lab has produced substantial evidence that FLASH irradiation reduces damage done to the CNS normal tissue, protecting the homeostasis, and potentially reducing the onset and severity of late radiation-injury in brain tumor survivors subjected to cranial radiotherapy. Experiments performed by ourselves and collaborators have examined the FLASH effect using preclinical models of fish, rodents, cats, and mini-pigs[2,5–8] and has successfully been used clinically in a single patient to treat multiresistant CD30+ T-cell cutaneous lymphoma[4]. While a plethora of data is available on the FLASH effect, the underlying mechanisms are still not fully understood. Our lab has shown that oxygenation levels of the tissue play a vital role in radiation induce tissue damage through mitigation of reactive oxygen species (ROS)[2]; however, there are likely other key mechanisms at play. The importance of tissue oxygenation and the role the BBB plays in maintaining CNS homeostasis are why we consider the vasculature to be a key element in deciphering the FLASH effect.

The Limoli lab has been publishing regularly on the benefits of FLASH irradiation in pre-clinical models for the last 4 years, highlighting the normal tissue sparing effects in the CNS. My work in particular has focused on the effect of both CONV and FLASH irradiation on the normal tissue and the BBB. I performed initial experiments utilizing FLASH and CONV radiation to determine effects on the BBB at early timepoints which led to a publication in *Radiation Research*[9]. Following this, I spent time exploring the literature behind CNS vasculature, radiotherapy, and new experimental therapeutic techniques which culminated into a published review in *Free Radical Biology and Medicine*[10]. I have used this rationale to examine the cognitive and vasculature effects of FLASH on juveniles[11], a particularly radiation susceptible population. Results from the juvenile model have guided us to explore the neurological mechanistic basis of the effect we find in an adult model while simultaneously testing the

threshold of dose tolerance. Further experiments on a similar cohort of adult animals to measure blood flow and tissue oxygenation levels using spatial frequency and domain imaging. Results from this publication are expected to be concluded soon. The objective of this dissertation is to, in part, determine if the normal tissue sparing effect of FLASH irradiation reduces radiation-induced pathology of the BBB, further explicate the neuro-mechanistic basis of cognitive protection and determine the effects on tumor vascularization. Results produced from this body of work will not only provide additional justification for clinical translation, but it may also help illuminate key mechanistic differences between cancer and normal tissue that may one day be used for therapeutic gain.

My field of focus has been the effects of ultra-high dose rate FLASH radiotherapy in pre-clinical models. In particular, my work has focused on both clinical and FLASH dose rates and their effect on the normal tissue, cognition, neuroinflammation, and the BBB. My graduate work led to numerous publications and is challenging the fundamental principles used in the field to improve .

Introduction and Background

The role of the blood brain barrier (BBB) is to maintain homeostasis within the central nervous system (CNS). This is achieved through a unique microvasculature network that physically blocks and selectively transports specific molecules across the barrier via combined efforts of endothelial cells, tight junction (TJ) proteins, pericytes, basal lamina, and astrocytes that make up the neurovascular unit (NVU). When functioning properly, the NVU creates a tight seal around blood vessel walls that requires adsorptive and carrier mediated transportation of non-lipid soluble agents [12]. In addition, endothelial cells contain ATP dependent efflux transporters that actively push foreign material back into the lumen [12,13]. Conversely, CNS tumor vasculature, commonly referred to as the blood tumor barrier (BTB), is prone to irregularities when unregulated and disorganized vasculature growth causes disruptions in the barrier within glioblastomas (GBM) and secondary metastases [14–16]. The importance of a well-organized BBB is highlighted when this system fails to filter foreign material from the blood, and it is allowed to enter the brain. We can observe such failures in the BBB and BTB directly after radiotherapeutic interventions by measuring leakage into the parenchymal space [9,17–19]. While preserving the BBB is critical to maintaining homeostasis within the healthy CNS, exploration into new physical and chemical treatment options endeavor to therapeutically disrupt the BTB for drug delivery [20–23].

Current treatment plans for CNS tumors involve surgical resection, irradiation, and chemotherapeutic regimens. An estimated 86,000 new cases of CNS cancer occurred in 2019. Even with the latest treatment options available, the five-year survival rate for patients with all types of malignant tumors was 35.8%, while GBMs specifically had a five-year survival rate of only 6.8% [24]. This low rate of survival is in part attributed to insufficient drug intervention options due to the relative impenetrability of the BBB and even within the barrier compromised

BTB. In GBM, the integrity of the BTB is not uniform, leaving regions of the tumor variably exposed to drugs that are readily blocked by the BBB [25,26]. However, even with the compromised vasculature of the BTB, uptake of chemotherapeutic drugs paclitaxel and doxorubicin exhibit relatively low penetrance within metastatic tumors [27]. This indicates that while the BTB may be more susceptible to toxic leakage, other interventions are required to open the vasculature further within the tumor. This is likely the reason that many chemotherapeutic drugs fail during clinical trials as the variance in BBB and BTB permeability is not fully understood [28]. Clearly, failure to treat the entire tumor parenchyma compromises the efficacy of any chemotherapeutic treatment regimen leading to tumor recurrence, a routine, and confounding complication.

To circumvent these limitations, new methods must be implemented to permeabilize the vasculature of targeted regions to facilitate drug delivery, or to actively assist in denaturing the semi-intact BTB within the CNS while protecting the surrounding normal tissue. Others have highlighted the benefits of creating a porous BBB and/or BTB with the use of radiation [29,30], ultrasound [31,32] and receptor mediated transport [33] to improve drug delivery. The caveat to these strategies is that permeabilizing the BBB has non-targeted effects in normal tissues that may lead to indiscriminate damage to the brain. Further studies that define key differences between the BTB and BBB may provide new insight, allowing for targeted breakdown of tumor vasculature and improved chemotherapeutic treatment within the CNS.

This review describes the foundational differences between the BBB and BTB and the dichotomy between the deleterious effects and therapeutic opportunities that radiotherapy presents, emphasizing the current efforts to create leakage across the BBB/BTB and its implications for the penetrance of therapeutic interventions and neurotoxicity.

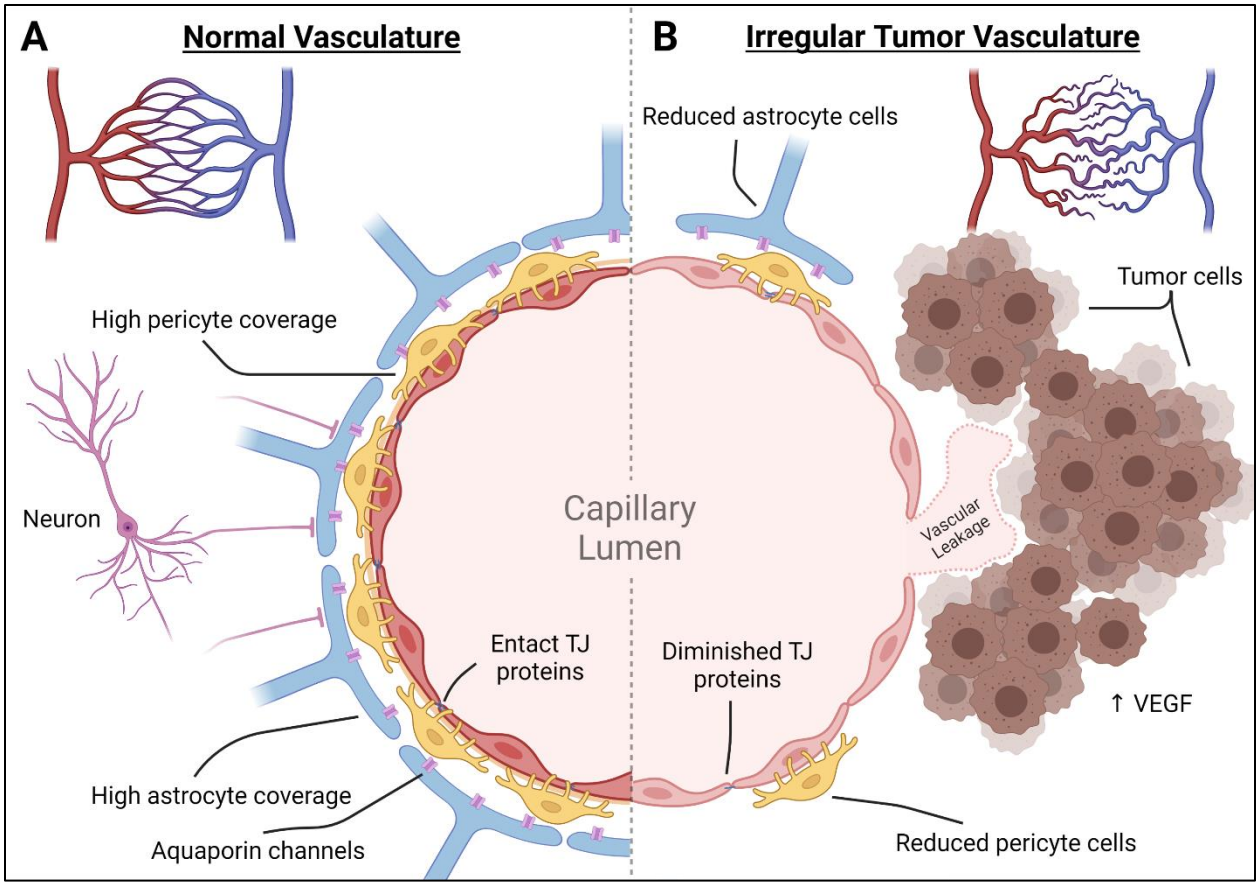

Figure 1.1: Comparison of the neurovascular unit of the blood brain barrier and blood tumor barrier.

Normal vasculature of the brain develops from pial arteries to arterioles to capillaries where transfer of nutrients and oxygen can take place. In the normal tissue, capillaries are spread out somewhat uniformly to ensure equal distribution. In the BTB, there is a reduced presence of capillary endings, and an irregular overlay creating areas of hypoxic tumor tissue. (**A**) In the normal tissue capillaries, the neurovascular unit controls the influx of materials by forming a non-fenestrated endothelial cell layer that is tightly bound together with TJ proteins. These are enveloped by pericyte cells and astrocytic endfeet that aid in maintaining the endothelial cell transport proteins, TJ proteins, induction of angiogenesis and influx of ions and fluids. This is

controlled by local input as well as neuronal demand that can interact directly or through astrocytic channels. (**B**) Within the BTB, barrier integrity is compromised. Tumor cells attach to the outer vascular wall and induce vascular growth through VEGF expression. The new capillary bed is irregular and leaves areas of the tumor hypoxic. The new vasculature becomes the foundation of the BTB and has been found to have reductions in astrocytic endfeet coverage, pericyte cells, TJ proteins, and neuron attachment. The resulting capillary wall of the BTB is susceptible to neurotoxic leakage.

Neurovascular Unit (NVU)

The NVU is a collection of all cell types that form and regulate the capillary network within the brain. Primarily the NVU defines a physical barrier, formed by the binding of endothelial cells via TJ proteins to create a non-fenestrated capillary wall. Endothelial cells play a primary role in controlling entry into the brain parenchyma through expression of transporter proteins. These cells are supported and encased by pericyte cells, the basement membrane and astrocytic endfeet that provide additional regulation and feedback from signaling within the brain. Local neurons also play a regulatory role by controlling nutrient demand and feedback signals among these cell types to modify molecular, ion and aqueous transport in a process called neurovascular coupling (NVC) (**Figure 1.1**).

<u>Endothelial cells and Tight Junction Proteins</u>

The microvasculature of the CNS relies primarily on the layer of endothelial cells bound together by TJ proteins encased within the basement membrane. This endothelial monolayer creates the interface via which molecules enter the brain. These cells harness carrier and receptor mediated efflux, organic anion and cation, nucleoside, and large amino acid transporter systems to maintain gradients and push unwanted waste and metabolites into the glymphatic waste

clearance system. Of particular importance are ATP-driven efflux pump transporters including the ATP-Binding Cassette (ABC), P-glycoprotein, breast cancer resistance protein, and multidrug resistance related proteins, as these work to actively remove chemotherapeutics and xenobiotics [34,35]. Facilitated transporters Glut1 and major facilitator superfamily domain-containing protein 2A (Mfsd2a) are also considered critical to proper BBB function and overall health. Glut1 is responsible for influx of glucose, the primary fuel for neurons, and Glut1 deficiency is known to cause mitochondrial disfunction and epilepsy in children [36]. Mfsd2a transporters are in part responsible for transport of essential omega-3 fatty acids in CNS endothelial cells. In transgenic knockout mouse models of Mfsd2a, levels of docosahexaenoic acid (DHA, an essential omega-3 fatty acid) are diminished along with leakage of 10kDa dextran observed from embryonic through adult stages. Further electron microscopy imaging has indicated that cells and TJ proteins were structurally intact, indicating a role for Mfsd2a in preventing foreign material from crossing the BBB [37]. Additionally, loss of Mfsd2a and concomitant reductions in DHA diminish mitochondrial activity, likely responsible for impaired cognition and ataxia in mice [38,39].

TJ proteins are essential to creating a sealed barrier between endothelial cells, forcing molecules to enter the CNS through active transporter mediated mechanisms as opposed to passive diffusion. This is achieved by a series of proteins that function together to create a non-fenestrated vasculature. Junctional adhesion molecule 1 (JAM-1) proteins help connect cells while simultaneously recruiting TJ proteins, including claudin family proteins ZO-1, and Occludin, that further tighten the seal between endothelial cells and facilitate cell-cell signaling [40–42]. Damage to these TJ protein populations can allow larger molecules to bypass endothelial cell regulatory mechanisms. While cells can lose TJ proteins, repair mechanisms are in place to

maintain structural integrity of the BBB. An in vitro study of TJ proteins performed under real-time confocal microscopy demonstrated that EGTA and laser insults reduced TJ integrity and increased permeability that was actively repaired by transient localized Rho activation [43]. The dynamic degradation and rapid repair of TJ proteins provides a brief window of permeability to the BBB, a feature that could be exploited clinically for drug delivery to the CNS.

Pericytes

Pericytes play a crucial part of the NVU as they regulate cerebral blood flow, stabilizing vessels, initiating angiogenesis, and maintaining the BBB. These cells make up a large portion of the BBB, almost matching the number of endothelial cells [44]. The versatility of pericytes is due to specialized subpopulations that support and regulate the BBB and assist angiogenesis within the BBB. Ensheathing pericytes physically control cerebral blood flow by contracting or relaxing within regions based on metabolic demand [45,46]. This is achieved through expression of α-smooth muscle actin (α-SMA), tropomyosin, and myosin [46–48] that actuate contractile processes.

Defining subpopulations of pericytes can be complicated as there is no defined marker for each type, rather they are referred to by protein expression that determines functionality of the particular cell. Further complicating the categorization of pericytes, expression of these defining proteins can be dependent on tissue-specific cell type, developmental stage of angiogenesis, or maturity of the cell. Pericytes with the platelet-derived growth factor-β (PDGFβ) receptor are recruited by endothelial cells via PDGFβ and transforming growth factor-β (TGF- β), where they implant within the basement membrane of the blood vessel to bolster the BBB [44,49]. These pericytes help to stabilize the vasculature [50], control the cell cycle of endothelial cells [49], control regulation of TJ proteins [44], and assist in angiogenesis by secreting notch homolog protein 3 (NOTCH3) and vascular endothelial growth factor (VEGF) [46,50]. Pericyte cells express desmin

and α-SMA that form contractile filaments and allow cells to exhibit control of blood flow by constriction on the blood vessels. Desmin and α-SMA expression in pericytes are found on venular and arterioles, while only desmin+ cells are found on capillaries [51,52]. This likely indicates that these cells have unique abilities that larger blood vessels require, while capillaries may require a specifically desmin+ pericytes to regulate blood flow. Pericytes have also been shown to exhibit immuno-regulatory functions through their capability to phagocytose other cells, respond to inflammatory markers, and present antigens to T cells [53]. In response to inflammatory cytokines interleukin-1b and tumor necrotic factor-alpha (TNF-□), pericytes can express matrix metalloprotease 9 which leads directly to BBB breakdown [54,55]. Since these cells are an integral part of the BBB, damage to pericytes can have detrimental effects on the BBB and the homeostasis of the CNS. In that light, loss of pericytes likely exacerbates several adverse neurological conditions including Alzheimer's Disease and ischemia [45,56].

Astrocytes and the Gliovascular Unit

Glial cells are an integral part of the NVU, and are intermediaries between neurons and the vasculature, defining a smaller subset of the NVU called the gliovascular unit (GVU). The GVU is primarily responsible for linking the needs of the neuronal population in which they are embeded and the vasculature system that delivers the required oxygen and nutrients into the perivascular space. In vitro studies of astrocytes cocultured with endothelial cells have suggested that a complex relationship exists between the two cell types. Endothelial cells have shown increased expression of ABC transporters and TJ proteins when they are co-cultured with either astrocytes or astrocyte conditioned media [57,58], suggesting that cytokine signals from astrocytes create a stronger BBB. This could be due to astrocytic expression of glucagon-like-peptide-1 (GLP-1R) which has been shown to reduce the permeability of the BBB [59]. Co-culture studies

have also shown the importance of TGFB1, as reduction of this astrocytic-derived signal reduces Msfd2a in endothelial cells, causing increased permeability [60]. However, astrocytes are also known to secrete vascular endothelial growth factor VEGF and NFkB that act as pro-inflammatory effectors as well as metalloproteinases (MMPs), chemokines and cytokines that can directly or indirectly damage the BBB. Angiogenesis induced by VEGF causes a breakdown of the BBB by downregulating CLDN5 and OCLN allowing vascular modifications [61,62]. Leakage of the BBB has been detected through measurements of FITC labeled dextran crossing into regions of the CNS undergoing angiogenesis expressing elevated VEGF [63,64]. It has also been found that over expression of MMP-9 causes the degradation of CLDN5 and OCLN in vitro [65] and reductions of other TJ proteins in a mouse model of ischemia [66]. Furthermore, blocking MMP-9 prevents the degradation of TJ proteins and preserves the functional integrity of the BBB in rat models of ischemia [67], suggesting the importance of this class of proteins for BBB integrity.

Neurovascular Coupling

Being highly specialized cells that require constant metabolic input, neurons act as overseers of the NVU and regulate blood flow through a process called neurovascular coupling or cerebral hyperemia. When neurons are activated, metabolic demand is increased to restore ionic gradients, recycle neurotransmitters, or produce ATP. Increase in this metabolic demand is largely driven by aerobic metabolism, requiring copious amounts of glucose and oxygen. Neurovascular coupling is thought to induce vascular dilation via release of many different vasoactive factors from regions of synaptically active neurons, increasing access to glucose and oxygen to fuel high metabolic demands. These factors include neurotransmitters, ions, and metabolic by-products released from neuron projections and interneurons extending to the

vasculature that act directly on the BBB or through distal paracrine signaling extending to reach upstream arteriole regions of the vasculature (> 100 mm) [68,69]. Of special note are the 3 isoforms of nitric oxide synthase (NOS) enzymes that catalyze nitric oxide (NO), a potent vasodilator, from L-arginine; neuronal NOS (nNOS), inducible NOS (iNOS), and endothelial NOS (eNOS). All three isoforms of NOS produce NO and are expressed within the brain. Conflicting reports of NOS1-knockout mice (nNOS) have shown a lack of dilation during stimulation [70] as well as normal NVC dilation function [71]. This may indicate that other isoforms of NOS may help stabilize the loss of neuronal NOS production, but also that neuronal activity is not the sole triggering event to activate dilation [72].

Control of dilation in the microenvironment of the brain is hypothesized to rely on retrograde neuronal signaling transmitted to the pial arteries and penetrating arterioles which are wrapped in contractile smooth muscle cells. Early studies in rabbits showed that activation of NMDA receptors led to NO-mediated dilation of upstream pial arterioles [73]. Since then, a host of other neurotransmitters have been linked to mediation of vascular changes, including dopamine, substance P, serotonin, γ-aminobutyric acid, noradrenaline, neuropeptide Y, somatostatin and acetylcholine [74,75]. While no consensus signaling pathway within the neurovascular unit has emerged, it is likely that these signals can travel a certain distance (>1mm) via endothelial hyperpolarization to upstream pial arteries to modify blood flow [76].

Glymphatics

Until recently, it was generally believed that the brain was responsible for recycling its own waste while only a small amount of protein was shed back through the BBB due to the lack of or of an ill-defined lymphatic system [77]. This idea changed when Iliff et al. demonstrated clearance of cerebral spinal fluid (CSF) and Aβ protein along perivenous drainage pathways and reported it

to be astrocytic protein aquaporin-4 (AQP4) dependent [78,79]. Since then, it has been largely accepted that the glymphatic system is responsible for maintaining and regulating cerebral fluid dynamics, hydrostatic pressure, waste product removal and ion concentrations.

The glymphatic system facilitates waste clearance in the brain through the several different mechanisms. Influx of CSF travels through the perivascular space surrounding penetrating arteries, crossing into the interstitial space through AQP4 channels. Here it mixes with interstitial fluids (ISF), releasing CSF waste consisting of metabolic byproducts, ions, and fluids into the parenchyma. The resulting ISF are then drawn from arteries, through the parenchyma and towards the veins of the paravenous space through a process called convective flow [80,81]. This exchange of ions and flush of interstitial fluid waste is regulated by arterial pulsations during deep sleep [79,80,82,83].

Proper waste clearance from the brain appears to be vital as neurodegeneration is being attributed to glymphatic disfunction in the elderly. One hypothesis attributes age related reductions of deep REM sleep with decreased arterial pulsations that drive clearance, creating favorable conditions for Aβ aggregation [80,82,84,85]. Additionally, cardiac health and systemic blood pressure are the drivers of arterial pulsations, directly controlling convective flow. This has been observed in murine models of both hypertension and diabetes where direct reductions in glymphatic function were found [86,87].

Blood tumor barrier

The vast majority of brain cancers form due to metastasis of primary tumors of the lungs, breast and skin [88]. This occurs when cells of the existing primary tumor release and enter the circulatory system (lymphatics and blood), traverse, infiltrate and implant themselves within the brain. As newly formed tumor cells grow and proliferate, nutrients are leeched from the existing blood

supply in a process called cooption [62,89,90] while simultaneously new vasculature is created through the increased expression of VEGF by astrocytes and pericytes (**Figure 1**). Clinically, anti-angiogenic agents fail to stop tumor growth because tumors have evolved multiple strategies to compensate for hypoxia and localized nutrient deprivation [91]. However, some studies have shown the benefit of using anti-angiogenic agents alongside radiotherapy. It has been shown that as tumors grow past 1-2 mm in diameter within the parenchyma of the brain, the protective nature of the BBB begins to diminish, coinciding with the onset of tumor hypoxia [92,93]. Hypoxia triggers HIF stabilization that drives VEGF expression, known to promote vascular permeability along-side its pro-angiogenesis functions, that contribute to irregularities in the BTB as the tumor vasculature responds to dynamic changes in the microenvironment [94–96]. However, use of anti-angiogenesis treatments that target VEGF/VEGF2 have led to mixed results. According to Liu et al., this is likely due to GBM endothelial cell transformation and genetic reprogramming that allows proliferation and migration even under conditions of down regulated VEGF [97,98]. This indicates that other unknown factors are involved in developing irregular, chemo-resistant vasculature of the BTB. Efforts have also been focused on normalizing the tumor vasculature through the use of angiogenic stimulators, (for reviews see [99,100]), with the overarching goal to reduce leakage, increase oxygenation, and to facilitate immune cell infiltration to enhance sensitivity to therapeutic intervention.

Tumor-derived angiogenesis plays only one part of BTB permeability as formation of the tumor vasculature is structurally compromised at many levels. Brain tumors exhibit altered expression of TJ proteins, contributing to vascular leakage via paracellular diffusion [101,102]. This is likely due to reductions in Kruppel-like transcription factor 4 (KLF4) expression, resulting in decreased mRNA production of TJ proteins Claudin5, ZO-1 and Occludin [102]. Further, measurements of

GBM in patients indicate down regulation of the critical TJ proteins Claudin1, 3, and 5 [101]. While these changes in TJ proteins are wide spread, resultant vascular permeability is heterogeneous across the BTB, evident from unequal distribution of low molecular weight compounds within brain tumors [103]. Despite research focused on manipulating the BTB in efforts to aid drug delivery, realizing bona-fide improvements in the therapeutic index have been difficult to obtain.

While endothelial cells within the BBB are the first line of defense against intrusion of foreign materials, their presence in the BTB can be compromised during tumor progression leading to enhanced leakage. Tumor growth can alter expression and integrity of TJ proteins while inducing angiogenesis and adversely impact the expression of transporter proteins that help maintain homeostasis. Mfsd2a, a DHA transporter, downregulated within the endothelial cells of the BTB, has been found to be attributed to widespread leakage [60]. Significant loss of perivascular astrocytes in the developing BTB and a subsequent decrease in TGFβ1 was speculated to decrease Mfsd2a expression, thereby reducing the protective properties of endothelial cells in the BTB [60]. Liquid chromatography with tandem mass spectrometry measurements of GBM vasculature samples show a significant decrease of facilitator transporter Glut1 and efflux transporters ABCB1 And ABCG2 [104]. Disruption of these transport markers likely play a large part in BTB permeability, as shown in knockout models showing increased influx of fluorescent labeled 10 kDa dextran into the normal tissue parenchyma [37].

Reduction in pericyte numbers correlates with increased permeability within the BTB. In a clinical study following GBM patients, pericyte coverage was inversely correlated to the prognosis of patients treated with chemotherapeutic drugs [105]. The authors attribute the extended life span of these patients to the increase in BTB permeability, allowing enhanced chemotherapeutic access to the tumors. In breast cancer metastasis of the brain, it was found that

PDGFRβ+ pericytes decreased by 75%, while Desmin+ pericyte cell numbers more than doubled along the BTB [103]. Desmin+ pericytes are less involved with protection of the BBB than their PDGFRβ+ counterparts and are found to migrate and accumulate in newly forming BTB to promote angiogenesis [106]. While further work is required to determine the individual roles of these different classes of pericytes, it is interesting to note that the BTB can alter subpopulations of these cells to actively modulate vascularization.

As gliomas grow and co-opt surrounding blood vessels, astrocytic endfeet are displaced from the vasculature, thereby disrupting homeostasis of the surrounding neurons [90,107–109]. As gliomas increasingly co-opt the NVU, they produce VEGF to elicit angiogenesis, promoting blood vessel dilation and regional NVU permeability along the BTB [15]. Astrocytic endfeet also play a role in brain metastasis, as activated astrocytes physically surround the growing lesion to trigger a neuroinflammatory response. Activated astrocytes have been found to upregulate astrocytic sphigosine-1 phosphate receptor 3 (S1P3) which was found to inhibit constriction of the BTB. Additionally, by knocking down S1P3 in an in vitro model of activated or reactive astrocytes, reduced permeability was found within both the BBB and BTB as well as decreases in secreted chemokines, growth factors and interleukins [110]. While astrocytes are not as directly involved in forming a physical barrier as pericytes and endothelial cells, they play key regulatory roles in the secretion of multiple factors that maintain equilibrium among the collective components of the NVU.

Radiation induced changed within the BBB and BTB.

Radiotherapy is frequently prescribed for the treatment of CNS tumors and vascular malformations, inducing damage to the target region as well as to any normal tissue along the path of the beam. Damage produced by irradiation of tissue is caused by both direct and indirect

pathways. Direct ionization of cellular macromolecules including DNA, RNA, lipids and proteins can induce lethal or sublethal damage to a cell [111]. Ionizing radiation also indirectly damages cells through the generation of reactive oxygen species that damage intracellular target molecules [111]. Resultant damage can lead to mitotic catastrophe, necrosis, apoptosis, autophagy, or senescence (**Figure 1.2**). As a potent radiosensitizer, oxygen levels play a large role in dictating therapeutic outcomes, and vascular irregularities common to tumors routinely lead to hypoxia that compromises curative intent. Dose fractionation, beam modalities, and stereotaxic approaches are used to maximize damage to the tumor while minimizing exposure to the surrounding normal tissue. However, unavoidable vascular injury to normal tissues can still impact both acute and late responses to radiotherapy. Of particular concern to clinicians is the development of edema and the increased risk of stroke, late effects that transpire in the irradiated brain alongside white matter necrosis, lacunar infarcts, and parenchymal calcification, although each transpires with temporally distinct onsets [112].

Shortly after CNS irradiation, injection of radioactive tracers or fluorescent dyes indicate leakage of the BBB in human clinical trials, and in in vitro and in vivo models [18,113–119]. Within the first 24 hours after irradiation, vascular leakage is attributed to radiation-induced cell death. In one study, a 25 Gy dose resulted in a 15% reduction of endothelial cells within the CNS 24h later [120]. Direct irradiation, or subsequent ROS production can induce apoptosis, typically starting at 4 hours post-irradiation and peaking at approximately 12 hours, leaving gaps within the barrier [121–123]. Functional alterations persisting in irradiated endothelial cells that survive exposure can contribute further to permeability. Interestingly, endothelial cell expression of P-glycoprotein as well as modified glutathione, which upregulates efflux transporters, has been shown to increase after radiation exposure [124,125]. Such an effect can compromise treatment efficacy, as radiation

induced overexpression of efflux transporters reduces the half-life of chemotherapeutics in the tumor.

Radiation exposure has also been shown to induce delayed vascular dilation within the brain, likely due to an increase in endothelial nitric oxide synthase (eNOS) production [113,114 115]. Over expression of eNOS has, in part been linked to induction of vasogenic edema [126,127] which can elevate intracranial pressure leading to white matter necrosis. Breakdown of the BBB allows for intravascular proteins and fluid exchange into the extracellular space. Areas of white matter are particularly susceptible due to lowered tissue density, increased number of parallel axonal tracts and the ability of fluids to enter and travel along the white matter tracts [128]. Furthermore, vasogenic edema contributes to only a portion of intracranial pressure build up, as the glymphatic system should work to reduce pressure and remove waste. It is likely that the glymphatic system is compromised after radiotherapy, however, to date few studies have directly interrogated glymphatic system function after clinical radiotherapy regimens.

As detailed above, TJ proteins between endothelial cells dictate the integrity of the BBB. While cranial irradiation leads to minimal changes in TJ protein levels within 24 hours, modifications are found within the subsequent weeks [9,118], where reduced levels of TJ proteins were observed. Protracted changes in TJ proteins may portend longer-term cerebrovascular complications such as stroke and edema [129–131]. Of particular interest is the expression of VEGF, as it has been shown to be upregulated after irradiation and is known to alter expression and phosphorylation of TJ proteins [62,132,133]. While anti-VEGF treatments have proved to be relatively ineffective in clinical efforts to forestall tumor vascularization and growth [134], they may reduce fenestrations and damage to TJs [135,136].

Pericytes of the BBB are particularly susceptible to radiation induced cell death and could contribute regions of necrosis in the brain through reduced vasculature homeostasis. In a post-mortem analysis of normal tissue after GBM treatment, Lee et al. found that radionecrotic tissues of the BBB were devoid of pericyte support cells even though no morphological changes to the vasculature were found [137]. The authors posit that the lack of pericyte support within the cerebral vasculature could be responsible for fibrinoid necrosis and telangiectasis; However, it could be possible that cell death of these pericytes is caused by some unknown factor in the regions of necrosis. While this study provides the first evidence linking pericyte loss to radiation necrosis, it has also been found that loss of these cells leads to increased neuroinflammation in pericyte deficient mouse models [138] and permanent vascular constriction [45]. It is therefore pertinent to the field of radiobiology to further investigate the radio-response of pericyte cells as they may play a vital role in regulating the neuroinflammatory response post-irradiation. Indeed, strategies able to augment or recruit pericytes to the BTB could improve GBM therapeutic outcome by improving vascularization, reducing hypoxia and enhancing radiosensitivity [100,139].

In addition to cells of the NVU being susceptible to radiation induced apoptosis, senescence remains a great concern as it initiates persistent injury signatures within the normal tissue. Endothelial cells that survive radiation exposure may enter senescence which leads to further breakdown of the vasculature [140–142]. Studies in senescence accelerated mice (SAMP8), increases in BBB leakage were found from the initial screening at 3 months of age until end of life at 12-15 months [143,144]. Such data suggest that BBB damage from senescent endothelial cells is not repaired and/or contributes to a senescence associated secretory phenotype (SASP) and may persist chronically. SASP modified cell expression alters interleukins, chemokines, growth factors, and proteases that create a protumorigenic environment by enabling tumor growth and

metastasis [145]. In addition to endothelial cells, radiation-induced senescence of astrocytes is of particular concern as these cells escape apoptosis and linger within the parenchyma to foster chronic inflammation [146]. Senescent astrocytes have been reported to secrete proinflammatory cytokines IL-6, IL-1β, TNF-α [147,148] which can mediate persistent inflammatory signaling in the irradiated brain [149,150].

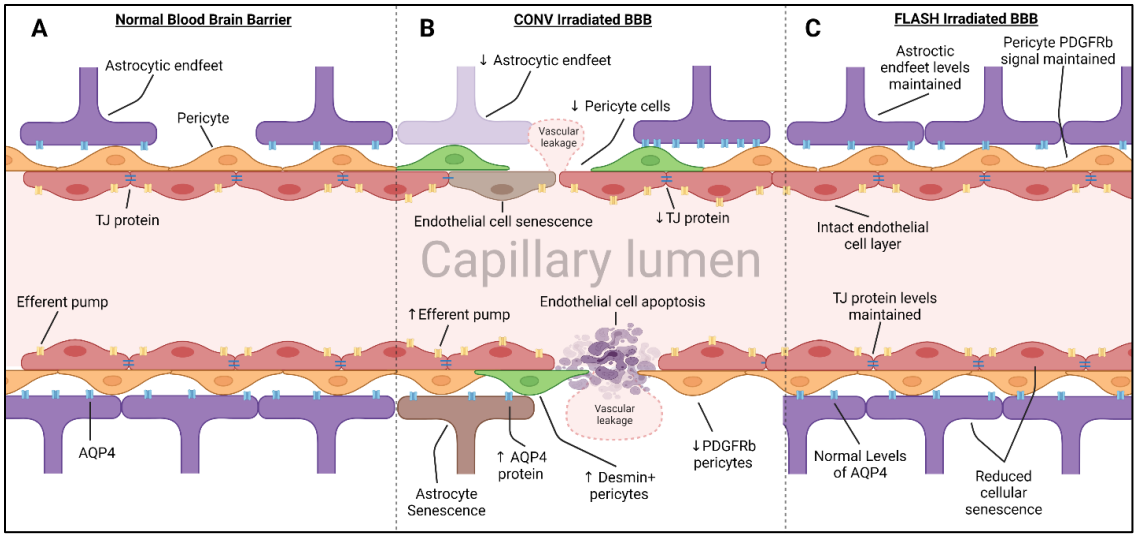

Figure 1.2: Irradiation of the blood brain barrier leads to damage of the neurovascular unit.

Vasculature of the BBB is susceptible to radiotherapy treatment, inducing modifications to protein expression and apoptosis and senescence of cells that alter homeostasis. (**A**) Normal BBB expresses high levels of TJ proteins, sealing gaps between endothelial cells, preventing paracellular crossing. Expression of efferent pumps on the lumen side of endothelial cells actively work to remove foreign materials and chemotherapeutic drugs from the brain. Pericytes embedded within the basement membrane provide support and regulation over dilation and TJ expression. Astrocytic endfeet express aquaporin protein (AQP4), regulating fluid transfer across the membrane. (**B**) Radiotherapy induces leakage of the BBB through apoptosis and senescence in cells of the NVU. Additionally, declines in TJ protein expression lead to vascular leakage through paracellular channels. Pericyte subpopulations respond to BBB damage by reducing expression of PDGFRβ and replacing it with desmin. Astrocytes produce irregular expression of AQP4, contributing directly to dysregulated fluid transfer into the CNS, causing edema. (**C**) Ultra-high dose rate FLASH irradiation protects the vasculature through reduced induction of cellular apoptosis and conservation of TJ proteins. Due to the normal tissue sparing effect observed in previous FLASH irradiation studies, we hypothesize that protection of the BBB is due to reduced toxicity to endothelial cells, pericytes, and astrocytic endfeet.

Bypassing the BBB and BTB

The idea that radiation alone or in combination with chemotherapy might provide an avenue for increasing the efficacy of brain tumor treatments has been a topic explored extensively [25,100,151]. Under normal, healthy conditions, endothelial cells of the BBB are known to actively remove anticancer agents by way of ATP dependent efflux transporters, reducing cytotoxicity [21–23,152]. By using tumor targeted therapies, clinicians could capitalize on the inherent leakiness of the BTB, while the intact BBB protects the normal tissue from treatments. While tumor morphology is generally thought to play a role in permeability, as masses of larger size exhibit more leakage than smaller tumors [93,153,154], some observations contradict this assertion [117]. To further complicate matters, tumor lineage must be considered, as phenotypic differences between GBM and metastatic tumors of various other origins influence success of induced permeabilization. Measurements of tumors indicated that morphometrically GBMs are far more engrafted into the normal tissue of the CNS while metastases are generally ovoidal in shape with a clearly defined border. Both tumor types have similar levels of cerebral blood flow, however GBMs are more prone to hemorrhaging, indicating potential predisposition to leakage on a greater scale than secondary tumors [155,156]. One factor to consider is that alterations to metastatic permeability are likely due to the genetic background of the founding tumor along with patient specific factors such as sex and age and origin of the metastasis. Differences in cytokine pattern expression from metastatic tumor origins could potentially lead to different vasculature phenotypes. One particular observation has shown that edema around secondary metastatic tumors is far higher when they originated in the lung as compared to the breast [157], likely due to increased aggressiveness and inflammation in lung cancer. Unfortunately, current literature lacks critical reviews of vasculature phenotypes of different metastatic tumors, as it may become clear that

bypassing the BTB will require therapeutic treatment tailored to metastasis origins. Numerous studies have been performed to bypass the BBB or BTB by use of both physical and chemical interventions to improve efficacy of drug delivery. While many of these techniques have proven to increase permeability of the BBB, few have been shown to improve clinical treatment efficacy.

-Radiation

As described, radiation alters the microenvironment of both tumor and normal tissues though a variety of mechanisms. The effects of radiation exposure on the BBB have been studied for decades [158–160], and while numerous animal studies have reported an increase in BBB permeability, these effects have been difficult to leverage for therapeutic gain when applied to the BTB. In part this may be due to difficulties in defining a reliable window of time following irradiation to deliver chemotherapeutic interventions. In studies of radiation induced BBB openings in mice, a single acute 20 Gy dose induced openings in the BBB that can manifest anywhere between 24 hours and 90 days post irradiation [140,161]. One particular study suggests that to induce permeability of the BBB, total doses of 20-30 Gy delivered at 3 Gy/fraction are required [162]; however, to reduce long-term neurotoxicity it also been suggested that fraction sizes of under 2 Gy are required [1]. Late responding tissues (*i.e.,* brain, spinal cord, lung, esophagus, kidney) to radiation toxicities have long been known to be sensitive to the dose/fraction. Additionally, the dynamics of radiation induced BTB permeability follow very different kinetics within a given tumor as they are heterogeneous, fluctuating with density and distance from sources of oxygen. These considerations are clearly impacted by tumor size as Teng et al. has found that while small metastatic tumors exhibit less leakage than larger, they display higher levels of radiation induced leakage in human patients [17]. Such data suggests limitations in the

amount of radiation induced vascular leakage that can be induced in tumors, prompting the search for alternative treatments to enhance the potential of this therapeutic strategy.

Radiotherapy fractionation schedules must also account for total dose, number of fractions, tissue organization, and target volumes to minimize early and late toxicities. While late toxicities in the brain and other tissues are largely attributed to functional changes in parenchymal cells involving secondary cascades of oxidative stress and inflammation, stromal compartments cannot be discounted. Indeed, precisely how different primary and secondary malignancies in the brain recruit, organize and re-program host stromal cells and the microenvironment will likely dictate the success of any strategy designed to transiently permeabilize the BTB. In support of this, other methods of permeabilizing the BTB are likely required to open the vasculature up enough to support therapeutic gains.

-Mechanical disruption of the BBB

Hyperosmotic agents and focused ultrasound (FUS) are two primary methods of mechanical BBB disruptions that increase permeability in the vasculature by exerting pressure on endothelial cells and TJ proteins. For several decades, osmotic disruption of the BBB has been studied with mixed results. Initially early studies discovered that injecting hyperosmotic solution of urea led to shrinkage of the endothelial cells, breaking TJ bonds and allowing agents within the blood to pass through paracellular pathways [163,164]. These principal findings led to the experimental use of mannitol, another hyperosmotic agent, just prior to chemotherapeutic delivery to prime the BBB and BTB for uptake. Limited clinical studies of mannitol, delivered via the carotid artery just prior to chemotherapy, have shown improved delivery of chemotherapeutic agents in both normal and tumor tissue [165,166]. However, use of hyperosmotic agents lack the specificity to open only the BTB, ultimately leading to difficulty in leveraging therapeutic gain as tumor and normal

tissue damage from chemotherapeutics will have to be balanced. Additionally, this treatment is particularly difficult to perform as a surgically implanted intra-arterial cranial catheter is required, involving an extended hospital stay and the use of general anesthesia and is not without risk.

One of the more promising and far less invasive methods of mechanical BBB disruption is the combined use of circulating microbubbles (MB) and FUS. Having first been investigated to induce thermal lesions within the brain (Lynn et al., 1942), increased permeability of the BBB was found as a side effect for a brief period of ~24 hours [167]. Currently accepted methods utilize an injection of lipid, albumin, or polymer MB which are then vibrated using FUS, causing a physical disruption of the vasculature for anywhere between 6 and 24 hours after treatment [167–169]. Though the exact mechanism of opening the BBB is unknown, it is hypothesized that rapid expansion and contraction of the microbubbles exerts pressure against the vessel walls to break the TJs of non-fenestrated capillaries.

While FUS holds promise as a novel technique to aid in drug delivery past the BBB, the overall safety is still being evaluated. FUS has been used within numerous regions of the human brain with only mild to moderate side effects [170]; however one of those side effects, a short lived inflammatory response, has received attention as of late. Upregulation of gene transcription associated with inflammation has been observed 6 hours post-FUS+MB that returned to baseline within 24 hours [171]. Additionally, numerous proinflammatory markers including in IBA-1, GFAP, CD68, and apoptosis (Tunel+) were found to increase within the first 24 hours [172]. Genomic analysis corroborated these findings as upregulation of inflammatory genes were correlated to an increase in BBB permeability after receiving FUS+MB [171]. While FUS+MB

induced inflammation is of concern and requires further interrogation, human clinical studies have continued showing minimal side effects.

-Manipulation of receptor-mediated transporters

Receptor mediated transporters embedded within endothelial cell of the BBB and BTB actively work to pull molecules across the vasculature. It has been hypothesized that manipulation of these transporters using chemical interventions and antigen masking could allow chemicals to cross into the parenchyma; however, these studies have found limited success. In one approach, strategies were developed to expose transferrin and insulin receptors by masking drugs with antibodies that would facilitate transport across the BTB [173]. Of particular interest to researchers was the manipulation of transferrin receptor as it has been found that they are over expressed within tumors [174]. Early clinical trials presented great success in a variety of cancer types [175], however phase-III trials indicated high level of toxicity for the transferrin conjugates [176]. Despite tumor overexpression of transferrin, limitations of this treatment are due to ubiquitous expression of this receptor throughout the body, allowing for dispersal of toxic drugs in a not specific manner.

Others have experimented using a class of antibodies called "angiopeps" that target lipoprotein receptor-related protein (LRP-1) [20,177]. Development of a new drug combining paclitaxel and the angiopep2 protein called ANG1005 was hypothesized to cross the BBB via LRP-1 mediated transcytosis. One study implementing ANG1005 using tumor-bearing and tumor-free mice found that it was able to cross both the BBB and BTB, but uptake was only 30-40% of the expected value in either [178]. The authors speculated that this was due to either multiple unknown uptake mechanisms or transport played a much smaller role in transiting these conjugates across the BBB/BTB than anticipated. Phase-II clinical trial in patients with breast cancer metastasis

underwent ANG1005 treatment leading to a an increased treatment effect [179]. Phase-III trials are underway and are expected to be completed in 2024. This drug, similar to many other treatments previously discussed is nonspecifically distributed and requires dose limitations due to normal tissue toxicity. The lack of tumor specificity in many of these treatments highlights the need to further understand differences between the BBB and BTB to hopefully lead to the development of targeted therapeutic treatments.

FLASH Radiotherapy

Modern day radiotherapy reduces normal tissue injury by implementing select fractionation schemes tailored to tumors residing in early (*e.g.* GI) or late (*e.g.* CNS) responding normal tissue beds. Fractionation along with advancements in conformal beam delivery have resulted in significant benefits, but collateral damage remains problematic for normal tissues, and dictates dose limiting toxicities that define the maximum tolerated dose that can be prescribed. In this light, evidence does not support the hypothesis that the vascular compartment is the dominant factor dictating neurocognitive outcomes following cranial radiotherapy, although for cerebrovascular complications, vascular and stromal compartments are likely to play prominent roles. Regardless of the target, recent developments in ultra-high dose rate "FLASH" radiotherapy using instantaneous dose rates $\geq 10^6$ Gy/sec may provide novel capability to resolve many long-standing issues related to dose limiting normal tissue toxicities. Central to this emerging radiation modality is that dose rate modulation can be used for therapeutic gain. Evidence in support of this comes from multiple preclinical models, but perhaps most convincingly in the CNS. FLASH radiotherapy has been found to elicit isoefficient tumor kill, but in the relative absence of normal tissue complications that confound standard-of-care conventional irradiation protocols using low dose rates of ≥ 0.01 Gy/sec [3,5,180,181]. While recent

interest in this new technique has been robust, to date, only one study has focused on the protective impact of FLASH radiotherapy on the BBB. In that work, FLASH irradiation was found to preserve TJ proteins and reduce eNOS dependent vasculature dilation, a beneficial effect not observed after conventional irradiation [9].

Given the widespread normal tissue benefits of FLASH radiotherapy, within and peripheral to the CNS, it is plausible that cells within the NVU exposed to ultra-high dose rate radiation will undergo reduced apoptosis and/or senescence, thereby aiding in the maintenance of BBB integrity (Figure 2-C.). Beyond the CNS, Velalopoulou et al., (2021) has shown peripheral vascular benefits using proton irradiation delivered at 69 Gy/sec (i.e. proton FLASH) to the hind limb in rodents. Irradiation of the highly vascularized hind limb by either proton FLASH or conventional proton dose rates produced an equal amount of low-grade lymphedema approximately 7 weeks later in rats. Conversely, standard dose rate irradiation, but not proton FLASH, led to severe late onset lymphedema, hypothesized to have developed from late forming fibrosis [182]. While the extent to which radiation induced disruptions to glymphatic clearance in the CNS remain uncertain, the study by Velalopoulou et. al. does suggest that protection of lymphatic clearance can be realized by FLASH. As the mechanism of action behind the protective effects of FLASH on normal tissue remain incompletely understood, additional studies are warranted to elucidate the extent of BBB protection and its potential differential impact on the BTB. This underscores the need for more definitive comparisons between radiation dose rates on the cerebral and tumor vasculature in efforts to translate this promising technology from the preclinical to clinical setting.

Conclusions and Future Perspectives

Radiotherapy is a double-edged sword when treating CNS tumors, while effective at forestalling tumor growth it invariably damages the delicate normal tissue structures that are critical to neurocognitive functionality. Despite ever improving radiotherapeutic modalities, overall survival of GBM patients remains dismal, and normal tissue complications resulting from cranial irradiation of primary and secondary CNS malignancies still confound quality of life. The latter is particularly true for childhood brain cancer, where despite success in eradicating tumors, longer term survival is plagued by neurocognitive and cerebrovascular complications. Fractionation schedules and stereotactic approaches have been adapted to reduce the amount of normal tissue damage, however, unintended consequences of treatment that manifest as cognitive dysfunction, edema, white matter necrosis, lacunar infarcts, and parenchymal calcification remain unmet medical needs.

This introduction highlights the current state of radiotherapeutic interventions and its limitations as a tool to permeabilize the BTB, where transient and incomplete opening of the tumor vasculature preclude optimal penetrance of drugs to the tumor parenchyma. While more focused research efforts have been placed on opening the BTB with radiation, the promise of alternative approaches involving focused ultrasound and angiopeps, have yet to be optimized. Given the foregoing, and the limitations of treating cerebral tumors with drugs, radiotherapy will likely remain a frontline treatment for controlling malignant growth in the brain. Thus, oncologists must balance curative intent that is largely dependent on delivering higher total doses, against the cost of elevating normal tissue damage, which becomes increasingly difficult with larger treatment volumes that may include critical structures.

This review has focused on differences that distinguish the radiobiological effects on the BBB from those observed for the BTB, highlighting the dysregulated development and leaky nature of the tumor vasculature that is primarily driven by hypoxia, cell senescence, and loss of proteins and transporters. While the current state of technology has not produced robust interventions to improve chemotherapeutic delivery to the tumor parenchyma in the brain, it remains a task worthy of continued investigation, especially given the adverse clinical outcomes facing brain tumor patients. Understanding key distinctions between the BBB and BTB will be critically important to address the efficacy of future interventions targeted to the vasculature. Ultimately this will lead to a more comprehensive understanding of the fundamental biological variations between normal and tumor tissues and how they can be exploited more effectively for therapeutic gain.

The FLASH effect protects the CNS vasculature at early points in adult female mice.

Abstract

Persistent vasculature abnormalities contribute to an altered CNS microenvironment that further compromises the integrity of the blood brain barrier and exposes the brain to a host of neurotoxic conditions. Standard radiotherapy (RT) at conventional (CONV) dose rate elicits short-term damage to the blood brain barrier (BBB) by disrupting supportive cells, vasculature volume and tight junction proteins. While current clinical applications of cranial radiotherapy use dose fractionation to reduce normal tissue damage, these treatments still cause significant complications. As dose escalation would enhance treatment of radiation resistant tumors, methods to subvert normal tissue damage are clearly needed. In this regard, we have recently developed a new modality of irradiation based upon the use of ultra-high dose rate FLASH-radiotherapy (FLASH-RT) that does not induce the classical pathogenic patterns caused by CONV irradiation. Our previous studies have optimized the physical parameters required to minimize normal brain toxicity (*i.e.* FLASH-RT, instantaneous intra-pulse dose rate, $6.9 \cdot 10^6$ Gy/s, at a mean dose rate of 2500 Gy/s) and are used in the present study to determine the impact of FLASH-RT on the integrity of the vasculature and the blood brain barrier. Both early (24-hour, 1-week) and late (1-month) time points post-RT were investigated using C57Bl/6J female mice exposed to whole brain irradiation delivered in single doses of 25 Gy and 10 Gy respectively, using CONV (0.09 Gy/s) or FLASH (>10^6 Gy/s) irradiation. While the majority of changes found 1 day following exposure were minimal, FLASH-RT was found to reduce levels of apoptosis in the neurogenic regions of the brain at this time. At the 1-week and 1-month times, it was found that the CONV irradiation induced vascular dilation, a well described sign of vascular alteration, while FLASH minimized these effects. These results were positively

correlated with and temporally coincident to changes in the immunostaining of the vasodilator eNOS colocalized to the vasculature, suggestive of possible dysregulation in blood flow at these latter times. Overall expression of the tight junction proteins Occludin and Claudin-5, that was significantly reduced after CONV-RT, remained unchanged in the FLASH-RT brains at 1- and 4-weeks post-RT. Our data further confirms that compared to isodoses of CONV irradiation known to elicit detrimental effects, FLASH-RT does not damage the normal vasculature. These data now provide the first evidence that FLASH-RT preserves microvasculature integrity in the brain, which may prove beneficial to cognition while allowing for better tumor control in the clinic.

Introduction

Radiotherapy is a frontline treatment for nearly all CNS malignancies[183,184], and is frequently implemented to eradicate certain vascular abnormalities such as arteriovenous malformations (AVM)[185]. While prescribed doses for the management of glioma, medulloblastoma and AVM vary, in nearly every instance such treatments elevate the risk of stroke. The link between cancer and cerebrovascular disease has been reviewed[186,187], and in the case of radiotherapy the risk of stroke is nearly doubled[188]. This is a particular concern for survivors of medulloblastoma[189,190], also prone to cerebral microbleeds[191] and vascular changes including vasculopathy resulting from their intensive cranio-spinal irradiation regimen using photons or protons[192,193]. Higher dose (up to 25Gy) gamma knife/stereotactic approaches for the treatment of vascular malformations also elevates the chance of hemorrhage, pointing to the longer-term risks of targeted non-cancer therapies in the brain[194–197].

A direct link between radiation-induced vascular damage and neurocognitive dysfunction remains to be completely elucidated, confounded by the fact that each of these normal tissue complications exhibits different dose response and temporal relationships[198]. Neurocognitive dysfunction can manifest after single doses in the range of 10 Gy, and in the relative absence of structural changes indicative of edema, typically requiring total fractionated doses in excess of 40 Gy for visualization by magnetic resonance (MR) and diffusion tensor (DT) imaging[199]. Regardless of the mechanistic link, what is certain is that radiation-induced normal tissue injury involves both stromal and parenchymal compartments of the brain, and includes a variety of changes that can manifest and persist long after the cessation of treatments. In this light, ultra-high dose rate FLASH-radiotherapy (FLASH-RT) has generated considerable excitement due to its marked capability to minimize normal tissue complications in a variety of organs using

multiple pre-clinical models, and at least to this point, without compromising tumor control[200,201]. In the brain, FLASH irradiation has been shown to spare a variety of neurocognitive indices, preserve host neuronal structure and attenuate neuroinflammation, evidenced by reductions in astrogliosis and microgliosis[2]. Despite the documented benefits of FLASH using fish, rodents, cats and mini-pigs[2,5,7,200], details regarding the impact of this novel irradiation modality on vascular endpoints is relatively unknown. Prior work analyzing the pulmonary vasculature has demonstrated the capability of FLASH-RT to reduce damage by preventing the activation of apoptotic cascades caused by conventional dose rates[202]. However, whether or not the benefits of FLASH-RT would extend to the complex blood brain barrier, responsible in part for maintaining CNS integrity was unknown, and provided the impetus for undertaking the present studies.

Our group has now published significant data demonstrating the neuroprotective effects of FLASH-RT and defined the critical physical parameters required[2,5]. Specifically, past studies in mice have defined dose rate cutoffs for neurocognitive sparing following acute (≤10 Gy), whole brain irradiation (WBI). Related work has found that neuroprotective benefits resulting from FLASH-RT when compared to conventional dose rate irradiation (CONV-RT) extend from early (1-month) to later (6-month) post-irradiation times[2]. In this study, we sought to evaluate the response of the vasculature in the brain to either irradiation modality at early times (24-hour and 1-week) after exposure to a relatively higher single dose (25 Gy, WBI) in efforts to approximate the radiotherapeutic management of certain vascular abnormalities. In addition, we analyzed vascular changes in the CNS at a later time (1-month), using a single dose (10 Gy, WBI) known to compromise long-term cognition. Here we provide some of the first evidence that FLASH-RT

provides significant protection to the CNS vasculature when compared against isodoses delivered at conventional dose rates.

Materials and Methods

Animals

All animal procedures were conducted in accordance to and Swiss ethics committee (VD3241) and the University of California, Irvine Institutional Animal Care and Use Committee (IACUC) for animal experimentation. Eight-week-old female C57Bl/6J mice were purchased from Charles River Laboratories (France) and aged until 10 weeks when they were irradiated.

Irradiation

Single fraction, WBI were performed on a prototype Oriatron 6e, 6MeV electron beam linear accelerator (LINAC) at the Lausanne University Hospital as previously described[203]. Dosimetry has been extensively described and published to ensure reproducible reliable delivery[203–206]. For short term studies, animals received a single dose of 25 Gy head-only using a 17mm graphite applicator at either conventional dose rate (CONV-RT; 0.09 Gy/s) or ultra-high dose rate FLASH radiotherapy (FLASH-RT, instantaneous intrapulse dose rate, $6.9 \cdot 10^6$ Gy/s at a mean dose rate of 2500 Gy/s) (**Table 2.1**). These animals were euthanized 24 hours (n=12 per group) or 1 week (n=12 per group) after irradiation and 30 min after lectin injection. To study long term vascular toxicity, a second cohort of animals (n=12 per group) received 10 Gy of the previously stated conventional dose rate or FLASH-RT (delivered at $5.6 \cdot 10^6$ Gy/sec in a single 1.8 μs pulse) (**Table 2.1**). These animals were euthanized 1 month after irradiation and 30 min after tomato lectin injection.

Lectin injection and perfusions

To accurately image microvasculature of the brain, half of all treatment groups were injected with tomato lectin (Vector Laboratories, Burlingame) 30 min prior to sacrifice. 100 μg of lectin

(1 μg/1 μL saline) was delivered via retro orbital iv. injections (Vector Labs: Dylight 488 Tomato Lectin) using a 32-gauge syringe. Animals were then intracardiacally perfused using 25 mL of heparinized saline, followed immediately by 75 mL of 4% paraformaldehyde using a Peri-Star^{TM} Pro peristaltic pump (World Precision Instruments) delivered at 16 mL/min. Brain tissue was extracted and allowed to fix overnight in 4% PFA at 4°C before being transferred to PBS + 0.01% NaN_3 for transportation and storage. Tissue later underwent a sucrose gradient (10%, 20%, 30% per volume) and OCT (Leica: Surgipath FSC 22 Clear) embedded before being coronally sectioned at 30 μm using a cryostat, and then stored in PBS + 0.01% NaN_3 at 4°C for later analysis.

Immunohistochemistry and image collection

Tight Junction Markers and eNOS:

Two sections per brain were selected from the ventral hippocampus approximately 300 μm apart. Immunofluorescence to detect the expression of Claudin-5 (CLDN5), Occludin (OCLN), and endothelial nitric oxide synthase (eNOS) were performed on lectin-injected tissues. Brain sections were initially washed and permeabilized with PBS + Triton (0.1%) and blocking was performed in 10% goat serum, 0.2% BSA, and 0.1% tween. Brain sections were incubated overnight at 4°C in 3% goat serum, 0.1% BSA and 0.1% tween with the primary antibodies against CLDN5 (Rabbit anti-CLDN5, Invitrogen: 34-1600; 1:200), OCLN (Mouse anti-OCLN, Invitrogen:33-1500; 1:250), eNOS (Rabbit anti-eNOS, Invitrogen: PA3-031A; 1:250). The following day, tissues were incubated for 1 hour at room temperature with the following secondary antibodies: Goat anti-Mouse 647 (Abcam: ab150115; 1:500), Goat anti-Rabbit 594 (Abcam: ab150080; 1:400), and Goat anti-Rabbit 647 (ThermoFisher Scientific: A27040; 1:400),

before being counterstained with DAPI. Tissues were then slide mounted and imaged at 40x using a Nikon (Nikon Eclipse Ti-E Confocal) or Olympus (Olympus FV3000 Confocal) at 40x.

Volumetric analysis:

Four hippocampal sections were selected from each lectin-perfused brain ~300 μm apart, mounted to slides, and imaged at 20x. Images were taken along the stratum radiatum and the molecular layer. This region was chosen due to its high level of vascularization and the relationship to cognitive effects. Z-stack images were taken at 20 μm thickness and then processed in IMARIS 3D rendering software using a process previously described 28.

IMARIS 3D Rendering:

All Z-stack images were imported into IMARIS (version 9.3.1, Bitplane AG, Zurich, Switzerland) and deconvoluted using an adaptive, theoretical PSF batch processing. Deconvoluted images were then processed for 3D surface analysis for Lectin, OCLN, and CLDN5, while a spot analysis was used to analyze eNOS. When analyzing for tight junction markers, volumes of Lectin and either OCLN or CLDN5 were colocalized and volumes recorded. To evaluate the cellular regulation of the microvasculature, eNOS measurements were quantified based on the volume of any spot within 5 μm of 3D rendered Lectin. This allowed for removal of eNOS expression from other cell types not associated with the microvasculature.

Apoptosis:

Interrogation of apoptosis was performed on 2 sections per region (SVZ and DG), per animal (n=4), 24 hours post-irradiation. A TUNEL assay kit was used (Apoptag In Situ Apoptosis Detection Kit, Sigma-Aldrich) to quantify the number of Tdt+ cells that colocalized with DAPI positive nuclei in either the SVZ or DG. IMARIS software allowed for quantification of DAPI positive cells, while Tdt+ positive cells were scored blind by hand.

Delivery Mode	Prescribed Dose (Gy)	Beam parameters							
		Graphite applicator type and size (mm)	Source-to-surface distance (mm)	Pulse repetition Frequency (Hz)	Pulse width (μs)	Number of pulses	Treatment time (s)	Mean dose rate (Gy/s)	Instantaneous dose rate (Gy/s)
CONV	10	Circular ∅17	800	10	1.0	1170 - 1180	116.9 - 117.9	0.09	8.5×10^{3}
	25	Circular ∅17	745	10	1.0	2620	261.9	0.1	9.5×10^{3}
FLASH	10	Circular ∅17	369-370	100	1.8	1	1.8×10^{-6}	5.6×10^{6}	5.6×10^{6}
	25	Circular ∅17	325	100	1.8	2	1.0×10^{-2}	2.5×10^{3}	6.9×10^{6}

Table 2.1: Irradiation Parameters, Adult Vasculature

Results

FLASH-RT does not induce vasogenic edema or eNOS in the microvasculature

Previous work has found that conventional dose-rate irradiation influences overall blood vessel volume[207]. To determine the potential effects of FLASH-RT on the vascular compartment, irradiated animals were injected with lectin and blood vessel volume was measured. Representative images demonstrating the IMARIS 3D rendering of lectin are shown (**Fig. 2.1A**). Data revealed no significant changes at 24-hours [$F_{(2,43)}$=0.7725, p=0.4682] (**Fig. 2.1B**), however, a significant group effect was found at 1-week post-irradiation [$F_{(2,45)}$=8.059, p=0.001] (**Fig. 2.1C**). A significant increase in total blood vessel volume was observed after CONV-RT when compared to control ($p \leq 0.01$), whereas no modifications in volume were observed after FLASH-RT 1-week post-25 Gy irradiation.

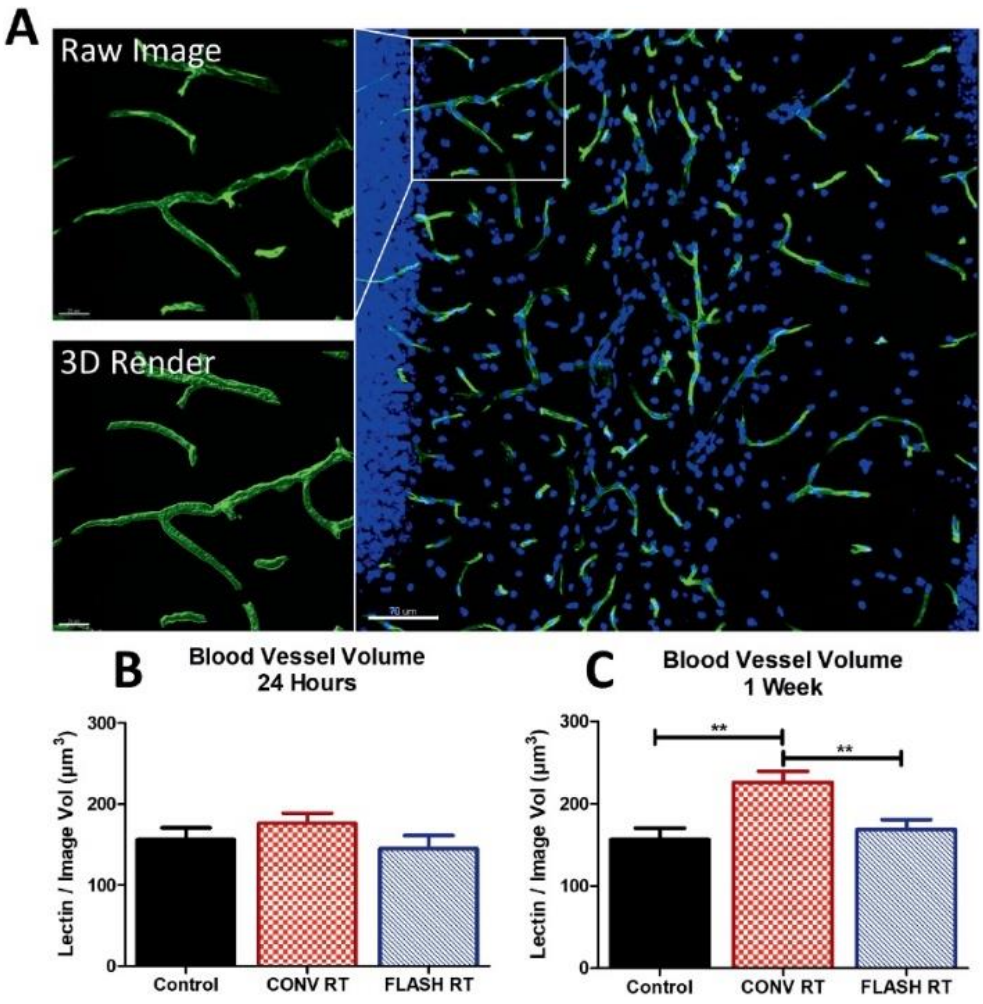

Figure 2.1: FLASH-RT does not induce vascular dilation within the brain microvasculature.

Animals were injected with tomato lectin 30 minutes prior to sacrifice and volumetric analysis was performed. **A**, Representative images of lectin volume quantification at 1-week post irradiation (Scale bars: 20 and 70 μm). **B-C**, Quantification of lectin volume at 24-hour and 1-week after a 25 Gy dose. CONV-RT increased the total volume of lectin at 1-week when compared to Control and FLASH-RT. Data is shown as the mean ± SEM (n=4 per group, 4 images analyzed per animal). P-values were calculated using an ANOVA with Bonferroni's multiple comparisons test (* = $p<0.05$, ** = $p\leq0.01$).

Expression of eNOS has been demonstrated to induce vasogenic dilation and/or edema by production of NO[126,208]. To investigate eNOS's contribution to the vasogenic edema shown in Fig. 1, we measured eNOS production in the molecular layer and stratum radiatum within the hippocampus (**Fig. 2.2)**. Representative images show eNOS expression throughout these regions of the hippocampus (**Fig. 2.2A**). Consistent with previous observations, eNOS was also expressed within the dentate gyrus, pyramidal cells, and astrocytes[209–211]. eNOS was found to be expressed in cells lining the lectin-stained lumen of the microvasculature, therefore eNOS expression was quantified within the nearby vicinity of lectin stained vessels to focus on proximal "paracrine" cellular regulation. This allowed for quantification of protein levels within support cells of the microvasculature. No change in eNOS immunoreactivity was observed at 24-hour post-irradiation in both CONV and FLASH-RT groups (**Fig. 2.2B**). Nevertheless, a significant group effect was observed at 1-week post-irradiation [$F_{(2,31)}$= 5.753, p=0.0075] (**Fig. 2.2C**). CONV-RT was responsible for increased eNOS immunoreactivity when compared to control ($p \leq 0.05$), whereas FLASH-RT produced no increase in eNOS expression ($p \leq 0.05$).

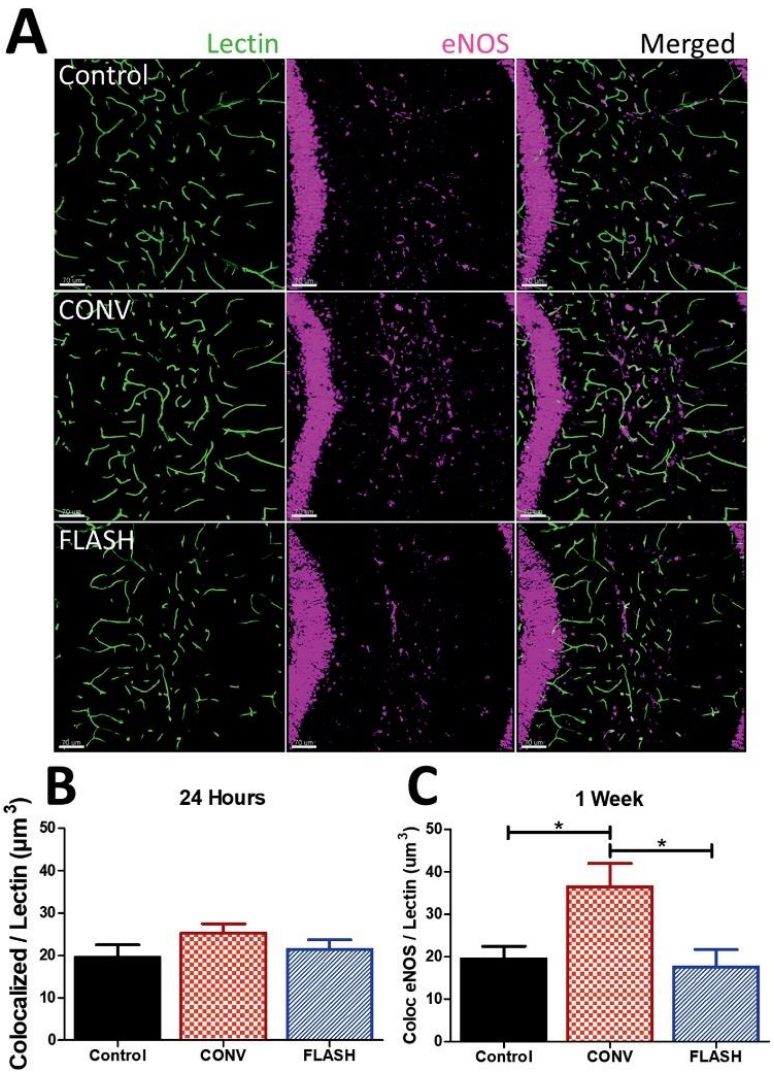

Figure 2.2: FLASH-RT did not elevate vascular eNOS in the brain.

Volumetric analysis of eNOS colocalized with lectin were performed. **A**, Representative images of eNOS immunoreactivity converted to 3-D renderings using IMARIS at 1-week post irradiation (Scale Bars: 70 µm). **B-C**, Quantitative analysis of eNOS colocalized within 5µm of lectin stained microvasculature at 24-hours and 1-week. CONV-RT increased levels of eNOS-lectin at 1-week when compared to control and FLASH-RT. Data is shown as the mean ± SEM (n=6 per group, 2 images analyzed per animal). P-values were calculated using an ANOVA with Bonferroni's multiple comparisons test (* = $p<0.05$).

FLASH irradiation does not induce tight junction protein degeneration.

Prior studies designed to interrogate the blood brain barrier utilized CLDN5 and OCLN as markers of the efficacy of epithelial cell adhesion[212,213]. To determine the effect of CONV and FLASH-RT on the integrity of the blood brain barrier, measurements of tight junction proteins colocalized with lectin+ blood vessels were performed. Representative images of microvasculature and tight junction colocalization are shown (**Fig. 2.3A**). No significant modifications in occludin expression were observed 24-hour post-irradiation (**Fig 2.3B)**. However, analysis of OCLN/lectin colocalization at 1 week showed a significant group effect within the hippocampus [$F_{(2,31)}$=12.12 , p <0.0001] (**Fig. 2.3B**) and the SVZ [$F_{2,31)}$=11.92, p = 0.0002] (**Fig. 2.3B**). Multiple comparisons analysis indicates significant drop in occludin expression after CONV-RT in both subregions ($p< 0.05$ and $p < 0.001$, hippocampus and SVZ respectively), whereas occludin expression was preserved in FLASH-irradiated brains. A significant group effect for Claudin 5 immunoreactivity was observed 24-hour post-25 Gy irradiation within the hippocampus [$F_{(2,29)}$ = 7.219, p=0.0029] (**Fig. 2.3C**). Multiple comparisons test showed an increased level of CLDN5 colocalized to lectin in the hippocampus after FLASH-RT when compared to control ($p\leq0.05$) and CONV ($p\leq0.01$) groups. Within the SVZ, 25 Gy at either dose rate failed to induce any significant changes in the CLDN5 immunoreactivity (**Fig 2.3C**). However, by 1-week significant group effects were found within the hippocampus [$F_{(2,30)}$ =13.43, p<0.0001] (**Fig. 2.3C**) and the SVZ [$F_{(2,29)}$=5.418, p=0.01] (**Fig. 2.3C**). Within the hippocampus, a significant drop in CLDN5 expression colocalized with lectin was observed after CONV-RT when compared to controls ($p\leq0.001$), and FLASH-RT ($p\leq0.01$). No change was observed after FLASH-RT compared to control. Within the SVZ, CLDN5 expression in the CONV-RT group was reduced compared to control ($p\leq0.01$). Altogether, these results suggest

that FLASH-RT does not induce BBB alteration characterized by a decreased expression of tight junction proteins described after CONV-RT at early and late time points post-RT.

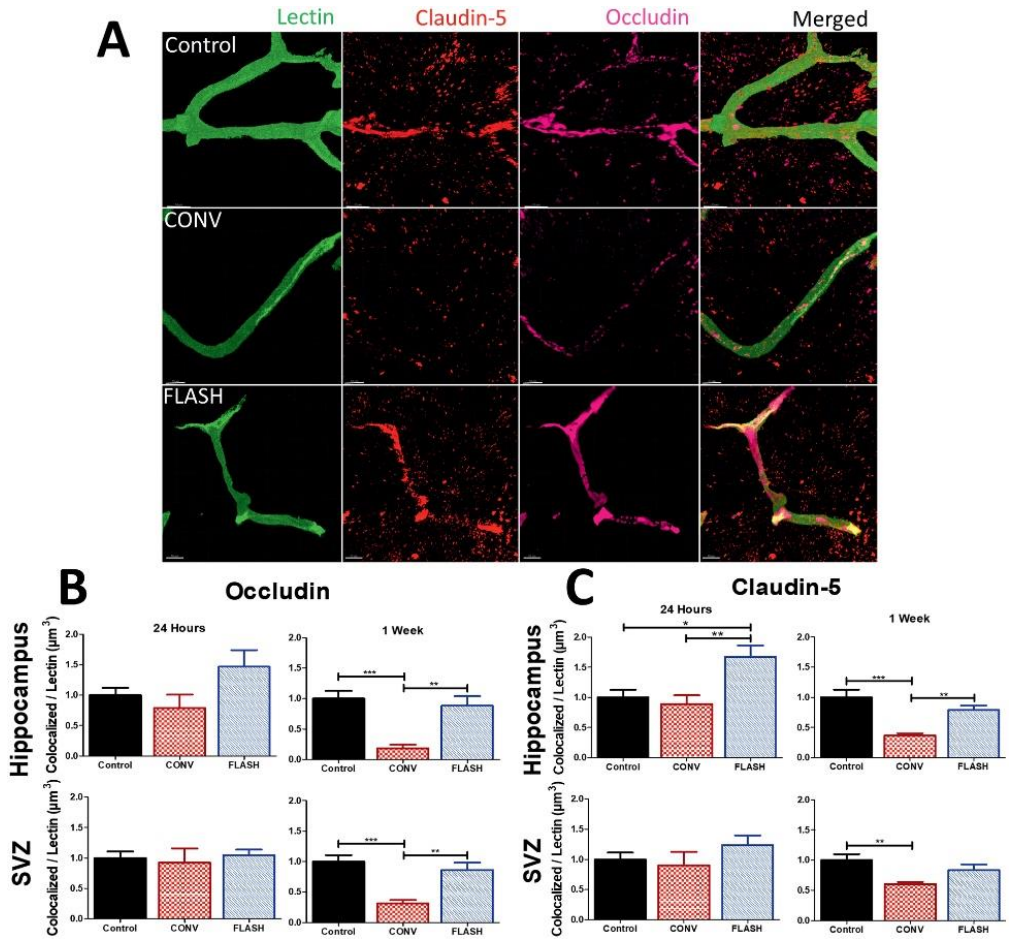

Figure 2.3: FLASH-RT did not reduce immunoreactivity of CLDN5-lectin and OCLN-lectin as CONV-RT did, 1 week after irradiation.

Volumetric analysis of markers CLDN5 and OCLN colocalized to lectin were quantified using IMARIS software. A, Representative images of CLDN5 and OCLN taken at the stratum radiatum of the hippocampus (Scale Bars: 10 µm). B-C, Analysis of OCLN and CLDN5 data at 24-hour and 1-week time points within hippocampus and subventricular zone. CONV-RT showed a significant drop off of tight junction proteins at 1-week post-irradiation when compared to controls and FLASH-RT. Data is shown as the mean ± SEM (n=6 per group, 2 images analyzed per animal). P-values were calculated using an ANOVA with Bonferroni's multiple comparisons test (* = $p \leq 0.05$, ** = $p \leq 0.01$, *** = $p \leq 0.001$).

FLASH irradiation induces less apoptosis in the normal brain after 25 Gy.

To determine if FLASH irradiation protected neurogenic regions (SVZ, DG) of the brain from early apoptosis, a TUNEL assay was performed 24 hours after exposure (**Fig. 2.4**). Representative images of the SVZ (left column) and dentate gyrus (right column) are shown (**Fig. 2.4A**). Data revealed a significant group effect in both the SVZ [$F_{(2,32)}$=32.36, $p<0.0001$) (**Fig. 2.4B**) and DG regions [$F_{(2,28)}$=22.38, $p<0.0001$] (**Fig. 2.4C**). Within the SVZ, a marked increase in Tdt+ cells was observed after exposure to CONV-RT compared to control ($p<0.0001$) and FLASH ($p\leq0.05$). Increased levels of Tdt+ cells were also observed in the FLASH-RT group compared to the controls ($p\leq0.001$) but were significantly lower than observed after CONV-RT ($p<0.05$). Similar results were found in the hippocampal DG. Exposure to CONV-RT increased yields of Tdt+ cells compared to controls ($p<0.0001$) and FLASH ($p\leq0.01$). Differences in the number of Tdt+ cells between control and FLASH irradiated cohorts were not statistically significant. These results indicate that FLASH-RT induced less apoptosis than CONV-RT in the neurogenic regions of the brain.

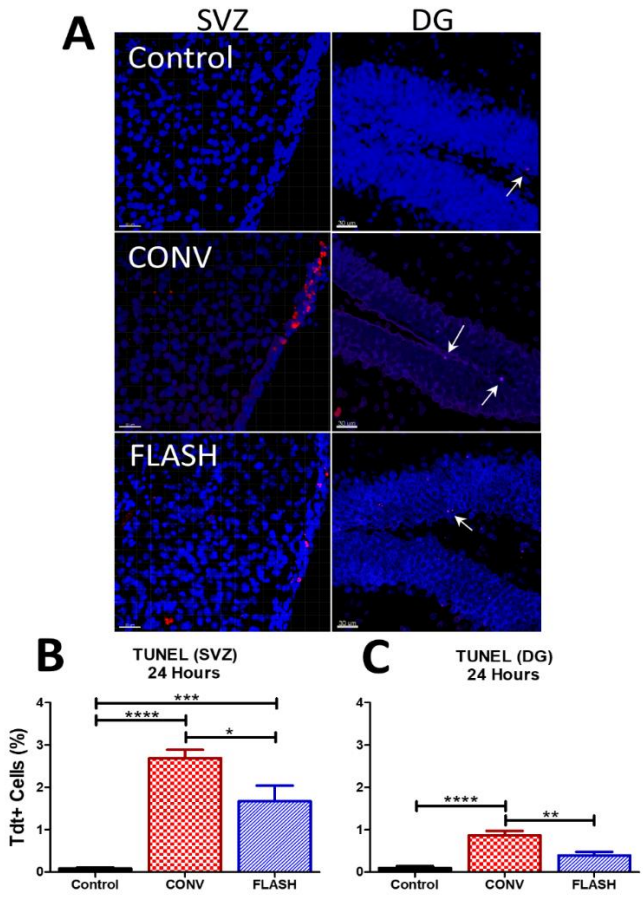

Figure 2.4: FLASH-RT reduces apoptosis compared to CONV-RT within neurogenic regions, 24 hours after irradiation.

A TUNEL assay was performed to determine levels of apoptosis within the dentate gyrus and subventricular zone. CONV-RT irradiated animals exhibited a significant increase when compared to FLASH-RT and control in both the SVZ and DG. Representative images of Tdt+ cells within the SVZ (Left) and DG (Right) (Scale Bars: 30µm). B-C, Analysis of Tdt+ cells within the SVZ and DG at 24-hours post-irradiation. Data is shown as the mean ± SEM (n=6 per group, 2 images analyzed per animal). P-values were calculated using an ANOVA with Bonferroni's multiple comparisons test (* = $p \leq 0.05$, ** = $p \leq 0.01$, *** = $p \leq 0.001$, **** = $p \leq 0.0001$).

FLASH irradiation protects the microvasculature from radiation-induced deficits 1-month after exposure.

To determine if a dose known to induce cognitive deficits (10 Gy) affects the microvasculature, measurements of vascular volume and eNOS vascular dilation were analyzed at 1-month post-irradiation. A significant group effect was found when analyzing total lectin volume [$F_{(2,44)}$= 11.91, $p<0.0001$] (**Fig. 2.5A**). A significant increase in lectin volume was observed after CONV-RT when compared to controls ($p\leq0.001$) and FLASH-RT ($p<0.05$) (**Fig. 2.5A**). While an increase in average lectin volume was measured for FLASH-RT compared to controls ($p=0.075$), no statistically significant change was found (**Fig. 2.5A**). eNOS colocalization was measured to determine if levels coincided with this increase increased vascular volume. Changes in the level of eNOS expression colocalized with the vasculature 1-month after exposure was found to have a significant group effect [$F_{(2,32)}$= 5.075, $p=0.0122$) (**Fig. 2.5B**). Expression of eNOS in the hippocampus after CONV-RT was elevated significantly when compared to control ($p\leq0.05$) and FLASH-RT ($p\leq0.05$) groups, however, no significant change between control and FLASH-RT was observed.

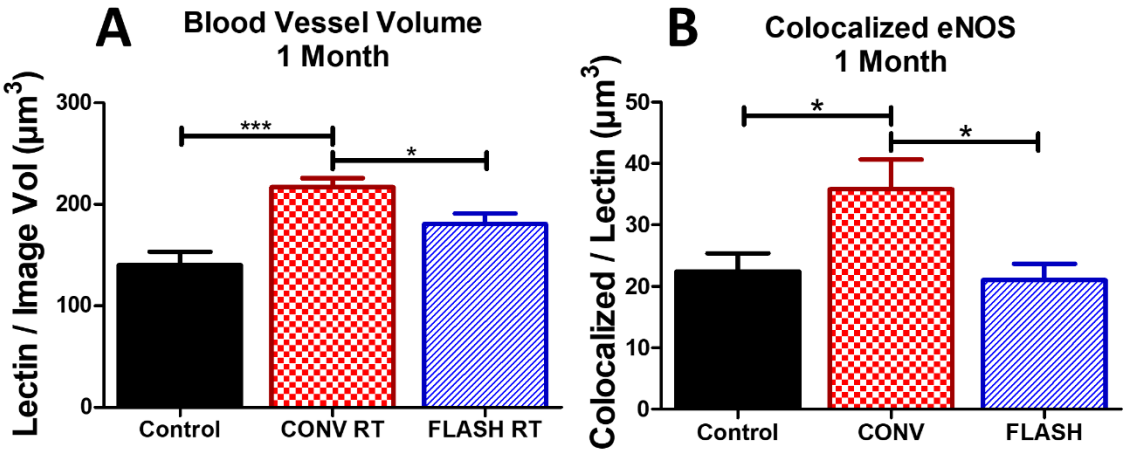

Figure 2.5: FLASH irradiation protects against eNOS induced blood vessel dilation when compared to CONV irradiation after 1-month (10 Gy) in the hippocampus.

Animals were injected with tomato lectin 30 minutes prior to sacrifice and volumetric analysis was performed. A, Quantification of lectin volume at 1-month post irradiation show that CONV dose rates cause an increase in Lectin volume after 10 Gy that is not observed after FLASH ultra-high dose rates. B, Colocalization of eNOS within 5µm of Lectin show that FLASH does not induce an increase in immunoreactivity while CONV does. Blood vessel volume data is shown as the mean ± SEM (n=4 per group, 4 images analyzed per animal). eNOS data is shown as the mean ± SEM (n=6 per group, 2 images analyzed per animal). P-values were calculated using an ANOVA with Bonferroni's multiple comparisons test (* = $p \leq 0.05$, *** = $p \leq 0.001$).

Vascular integrity was also interrogated at 1-month (10 Gy) by measuring levels of tight junction proteins that colocalized with lectin. Analysis of OCLN-lectin immunoreactivity indicates a significant group effect within the hippocampus [$F_{(2,33)}$=4.922, p=0.0139]. Multiple comparison analysis reveal that control animals exhibited higher levels of OCLN-lectin colocalization when compared to CONV-RT ($p \leq 0.05$) and FLASH-RT($p \leq 0.05$) (**Fig. 2.6A**). Within the SVZ, similar albeit non-significant trends were observed.

Analysis of CLDN5-lectin immunoreactivity within the hippocampus uncovered a significant group effect [$F_{(2,30)}$=4.288, p=0.0230], but not in the SVZ [$F_{(2,27)}$=2.226, p=0.1274] (**Fig. 2.6B**). Compared to controls, FLASH-RT exhibited no statistical difference of CLDN5-lectin colocalization in the hippocampus, however, significant decreases were found in cohorts exposed to CONV-RT ($p \leq 0.05$). Within the SVZ, CLDN5-lectin staining was increased significantly after FLASH-RT when compared to control ($p \leq 0.05$) and CONV-RT ($p \leq 0.01$). Decreased immunoreactivity of CLDN5 compared to controls was non-significant. Collectively, these data indicate that FLASH-RT protects against vascular dilation while providing some protection to markers of tight junctions, 1 month after irradiation.

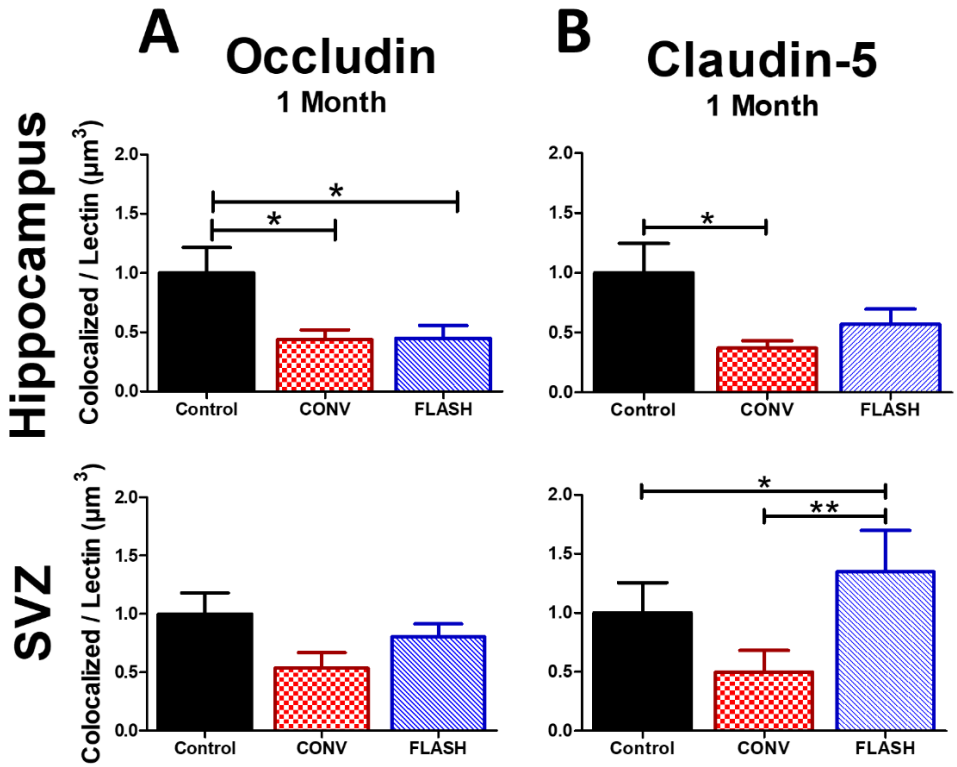

Figure 2.6: FLASH-RT provides some protection against CONV-RT induced tight junction modification at 1-month (10 Gy) post irradiation.

Volumetric analysis of OCLN and CLDN5 colocalization with Lectin were measured using IMARIS software within the stratum radiatum of the hippocampus and subventricular zone. A, Measurements of OCLN indicate that both FLASH and CONV irradiation decreased levels of immunoreactivity within the hippocampus, but do not significantly change levels within the SVZ compared to controls. B, FLASH irradiation does not induce a significant decrease in CLDN5 that CONV dose rates do in the hippocampus. FLASH irradiation causes a significant increase of CLDN5 when compared to both CONV and control. Data is shown as the mean ± SEM (n=6 per group, 2 images analyzed per animal). P-values were calculated using an ANOVA with Bonferroni's multiple comparisons test (* = $p \leq 0.05$, ** = $p \leq 0.01$).

Discussion

Late occurring damage to the brain after radiotherapy is a significant concern for thousands of people who are treated for CNS malignancies each year. Higher doses of cranial irradiation have been shown to temporarily induce microvasculature damage that are part of the initial radiation-induced pathogenic signals[30,214]. In the current study, we have shown that FLASH irradiation can circumvent some of the early and more persistent detrimental effects to the CNS microvasculature when compared to CONV-RT. We assessed key parameters including blood vessel volume, eNOS expression, tight junction morphology and expression to determine the impact of two irradiation modalities on brain microvasculature. Whether this might translate to reduced risk of hemorrhage, microbleeds, vasculopathy and/or stroke in patients subjected to cranial radiotherapy remains to be investigated in detail, but for survivors of pediatric brain malignancies, FLASH-RT provides a potentially new avenue for mitigating additional cerebrovascular complications from their radiotherapy, risks that have been clearly shown to only increase with age[215]. Results from this study corroborate with previous findings that normal tissue damage is reduced within the brain and other tissues[2,5,202]. Other CNS complications such as white matter necrosis[216], hearing loss[215] and vascular abnormalities resulting from larger field or targeted high dose approaches for treating AVM[194,196,197,217] may also benefit from FLASH-RT. These findings have important repercussions for anyone subjected to cranial radiotherapy, known to cause not only cognitive dysfunction but to compromise longer-term cerebrovascular health.

Aberrations to the morphology of the microvasculature have long been implicated in the progression of white matter necrosis likely caused by decreased metabolism stemming from reduced oxygen transfer[198,218]. For the treatment of vascular abnormalities in humans, gamma

knife doses can range around 25 Gy, as they are very focused, and the irradiated volumes are small. In our experiments, we had no access to conformal irradiation and used WBI. In this context, 25 Gy delivered in a single fraction would be lethal, especially after CONV-RT. Therefore, to make vascular analyses feasible, animals were sampled at earlier post-RT times. While one study has reported on the CNS benefits 1-month following a 30 Gy WBI dose of FLASH-RT[219], we opted to focus our study of 25 Gy to the earlier 24-hour and 1-week post irradiation times to ensure survival. We chose to analyze the microvasculature morphology using lectin, as its ability to accurately stain the blood vessels has been found to be more accurate than that of the use of endothelial antibodies[220]. An analysis of the microvasculature indicates that CONV-RT induced a significant increase in vessel volume associated with production of the vasodilator eNOS[221] at both 1-week (25 Gy) and 1-month (10 Gy). This indicates that CONV-RT treatment for vascular malformations as well as doses that are known to induce cognitive deficits induce microvascular disruption that are not observed after FLASH-RT at the same time points. While FLASH-RT prevented significant vessel volume dilation when compared to CONV-RT at 1-month post-exposure, there was a non-significant increase in mean vessel size compared to controls, indicating that some level of vessel disruption does occur after FLASH-RT and could persist over time. While further studies at additional post-irradiation times are clearly needed to expand our findings, present data does point to the capability of FLASH-RT to attenuate changes in vessel volume.

Alterations to microvasculature integrity can lead to debilitating effects in survivors that can develop months to years after treatment manifesting as white matter necrosis and/or edema[222]. Although the exact mechanism of delayed CNS radiation injury is not fully understood, the vascular injury hypothesis attributes many of the these detrimental effects to vascular dilation,

vascular wall thickening, endothelial cell nuclear enlargement and breakdown of tight junctions[223]. Results from this study indicate that FLASH-RT may reduce some of the potential underlying causes of clinically relevant vascular side effects. Additionally, previous studies from our group have shown that FLASH-RT produces a lower level of reactive oxygen species[2] which may explain the decreased levels of eNOS reported in the present work. However, additional mechanisms can be involved. It has been described that HSP90 and ATM phosphorylation induced during DNA repair were responsible for activation of eNOS30, suggesting that the attenuation of DNA damage after FLASH-RT, as recently reported by Fouillade et al[224], could restrain eNOS expression and help maintain a normal vascular morphology.

While the capability of FLASH-RT to reduce ROS production may well account for the observed reduction in apoptotic cells in the neurogenic regions of the SVZ and the DG, disruptions in the microvasculature and subsequent micro-environmental factors could also contribute to cell death. Previous studies have shown that proliferating neural precursor cells cluster around small vessels, suggesting that even small disruptions in homeostasis could negatively impact neurogenesis by altering cell survival and/or later recruitment of neural precursor cells[225]. It has also been shown that radiation-induced microvasculature changes could alter neurogenesis through changes in the microenvironment[226]. These data suggest that damage to the microvasculature could have persistent adverse effects on the regenerative reserve of the brain, an effect that FLASH-RT was able to circumvent, possibly through the preservation of vascular integrity. Further work will be needed to more conclusively link the underlying causes impacting cerebrovascular and neurocognitive outcomes in the irradiated brain.

Expression of tight junction proteins have been known to coincide with the overall integrity and permeability of the blood brain barrier[30,212]. We found that FLASH preserved the integrity of the

BBB when compared to CONV irradiation. Using markers for CLDN5 and OCLN, a stark difference between FLASH and CONV-RT 1-week after irradiation was observed. Interestingly, FLASH-RT caused a significant increase in CLDN5 and an upward trend in OCLN 24-hour compared to CONV-RT and control in the hippocampus, post-RT. While further work is required to pinpoint the molecular basis of this transient increase (transcriptional, post-translational, reduced turnover etc.) FLASH irradiation is clearly engaging different signaling pathways in the irradiated brain. Interestingly, previous work has shown that breakdown of CLDN5 and OCLN is directly related to an inflammatory response involving VEGF[62], suggesting that the observed attenuation of neuroinflammation following FLASH-RT[2] may contribute to the preservation of tight junctions.

This study serves to build on the growing body of knowledge supporting the "FLASH effect", operationally defined as the capability of FLASH-RT to spare normal tissue toxicities. As early studies identified the dose rate as the essential parameter[5,202], more recent work and publications emphasize that additional physics parameters such as the instantaneous dose rate, pulse frequency and pulse duration are critical to reach the FLASH effect[2,227,228]. Here, using maximal electron current to produce the highest instantaneous dose rate possible with the eRT6 (**Table 1**), study of the FLASH effect has been extended to the normal vasculature of the irradiated brain. While further work is required to substantiate the potential vascular benefits in the CNS over a larger range of doses and post-irradiation times, our study demonstrates the beneficial impact of FLASH compared to CONV irradiation on important cerebrovascular endpoints. The inclusion of additional functional studies coupled with dose fractionation to more thoroughly evaluate whether FLASH-RT might mitigate cerebral bleeds, stroke and white matter necrosis would also add important insights. Findings here highlight the promising potential of this innovative

irradiation modality to minimize microvasculature complications and related side effects associated with cranial irradiation procedures, as well as other radiotherapeutic treatments tailored to manage head & neck and pancreatic malignancies.

Strengths and Weaknesses

This preliminary project paved the way for future experiments designed to utilize strengths of this strategy while also addressing the goals that were not obtained. Primarily, these series of experiments were the first to address FLASH irradiation's potential protection of the blood brain barrier by mitigating loss of tight junction proteins and reducing eNOS dependent edema. Additionally, use of several different timepoints and doses helped to elucidate the temporal effects on the BBB at 24 hours, 1 week, and 1-month post-irradiation. This study was also the first to find that FLASH protects the hippocampus and subventricular zone; both neurogenic niches that are viewed as vital to maintaining cognition.

While this study helped to expand our understanding of the FLASH effect on the BBB, the limited scope of the project left a considerable number of questions to pursue. First, irradiations were only performed in female mice. Previous data has suggested that female animals are less susceptible to cognitive damage due to irradiation and inducing cognitive damage in conventional animals, we assume that future projects using males will yield similar results. Second, animals were irradiated without the presence of a brain tumor. Protection of the normal tissue is considered crucial in the clinic, but the project does not address the effects of irradiation on a CNS tumor. Third, doses used in this study are not considered to be clinically relevant and were selected for either large dose effect (25 Gy) or for doses that have been known to cause cognitive damage (10 Gy). Given that these data are preliminary, we escalate our dose in later studies to mimic palliative care. Fourth, while this study did indicate that damage was done to the BBB, we produced no functional endpoint that leakage did occur.

Elucidating the neurological mechanism of the FLASH effect in juvenile mice exposed to hypofractionated radiotherapy.

Abstract

Ultra-high dose-rate radiotherapy (FLASH-RT) affords improvements in the therapeutic index by minimizing normal tissue toxicities without compromising anti-tumor efficacy compared to conventional dose rate radiotherapy (CONV-RT). To investigate the translational potential of FLASH-RT to human pediatric medulloblastoma brain tumor, we used a radiosensitive juvenile mouse model to assess adverse long-term neurological outcomes. Three-week-old male and female C57Bl/6 mice exposed to hypofractionated (2×10 Gy) whole brain irradiation underwent behavioral testing to ascertain cognitive status four months post-treatment. Animals were sacrificed 6 months post-irradiation and tissues analyzed for neurological and cerebrovascular decrements. The neurological impact of FLASH-RT was analyzed over a 6-month follow-up. FLASH-RT ameliorated neurocognitive decrements induced by CONV-RT and preserved synaptic plasticity and integrity at the electrophysiological (long-term potentiation), molecular (synaptophysin) and structural (Bassoon/Homer-1 bouton) levels in multiple brain regions. The benefits of FLASH-RT were also linked to reduced neuroinflammation (activated microglia) and a preservation of cerebrovascular structure, by maintaining aquaporin-4 levels and minimizing microglia colocalized to vessels. Hypofractionated FLASH-RT affords significant and long-term normal tissue protection in the radiosensitive juvenile mouse brain when compared to CONV-RT. The capability of FLASH-RT to preserve critical cognitive outcomes and electrophysiological properties over 6-months is noteworthy and highlight its potential for resolving long-standing complications faced by pediatric brain tumor survivors. While care must

be exercised before clinical translation is realized, present findings document the marked benefits of FLASH-RT that extend from synapse to cognition and the microvasculature.

Introduction

Dose-rate modulation has now been recognized as a potential tool in the fight against cancer, as a wealth of recent preclinical data have now demonstrated that increasing the mean dose rate in excess of 100 Gy/s provides significant benefits in terms of reducing normal tissue toxicities without compromising tumor treatment[2,3,181,229–231]. The term FLASH radiotherapy (FLASH-RT) has been coined to distinguish the delivery of radiation at ultra-high dose rates under specific beam parameters from conventional dose rates (CONV) that are commonplace in clinical practice. As a preamble to clinical translation, investigators are now engaged across all interdisciplinary aspects of radiation oncology to elucidate optimal beam parameters, fractionation schedules and tissue-specific dose limiting toxicities and the mechanistic basis of how dose rate modulation discriminates between normal tissue and tumors.

The toxicities associated with standard of care cranial radiotherapy have been well documented, and none are more pressing than the multifaceted and progressive cognitive deficits that manifest over protracted times. This is particularly true for pediatric brain tumor patients, where survival of those afflicted with the most common type of primary brain cancer, medulloblastoma (MB) exhibit a five-year survival rate of 73.7%[24]. Unfortunately, survivors of MB suffer from reductions in IQ, disruptions in mood and up to a 2-fold incidence of cerebral microbleeds and stroke resulting from their intensive cranial-spinal irradiation regimens, all factors that are unmet medical needs that severely compromise long-term quality of life[232,233]

In recognition of these complications, our group previously evaluated the response of the highly radiosensitive juvenile brain to a large single 8 Gy dose of FLASH- or CONV-RT. Cohorts of 3-week-old juvenile mice were evaluated on a variety of behavioral platforms starting 4 months after exposure to FLASH or CONV irradiation. Results confirmed significant learning and

memory deficits in CONV but not FLASH irradiated mice. Corroborating data found that FLASH-RT spared immature neurons and hippocampal neurogenesis, reduced neuroinflammation, and preserved plasma levels of growth hormone, all factors that were contributory if not causal to the beneficial neurocognitive outcomes of FLASH-RT[231]. These encouraging results substantiated many of our past findings in the adult rodent brain and pointed to the feasibility of implementing FLASH-RT in a pediatric clinical setting. To substantiate further the dose tolerances of the juvenile rodent brain under a 2×10 Gy hypofractionated RT protocol and to elucidate the neurological mechanisms underlying normal tissue sparing in tumor free mice, we expanded our neurocognitive testing platform to include a new task termed objects-in-updated-location (OUL). The increased cognitive load (rigor) associated with this task can analyze multiple associative memory traces using a single test and yields outcomes comparable between rodents and humans[234]. Behavioral data were coupled with an electrophysiological assessment of synaptic plasticity and long-term potentiation (LTP) in the hippocampus. With these critical functional outcomes assessed 4-6 months after irradiation, molecular follow up studies were performed on those same mice to define how brain function was maintained. To this end we analyzed synaptic density and structure, neuroinflammation and measures of cerebrovascular integrity. Here we report new findings that shed considerable light on normal tissue sparing in the FLASH irradiated juvenile mouse brain.

Materials and Methods

Experimental Design

To determine if an animal model of juvenile normal tissue damage is able to withstand further dose tolerances under a hypofractionated regiment, 3-week-old, immune competent, C57Bl/6 mice were irradiated (2×10 Gy, FLASH or CONV irradiation, head only). Four months after irradiation, all animals underwent a battery of behavioral tests to assess neurocognitive effects of radiotherapy (n=12/sex/treatment). Six months post-irradiation, animals were sacrificed. Half of the male and female mice were administered tomato lectin (Vector® Laboratories, Burlingame, CA) via retro-orbital injection 30 minutes prior to PFA perfusion and used to assess vasculature and/or cognitive histological endpoints (n=6/sex/treatment). Remaining female mice were sacrificed for electrophysiology and hippocampal slices were prepared as previously described[235] (n=6/treatment). A schematic representation of the experimental design is represented in **Figure 3.1**.

Animals

All animal procedures were conducted in accordance with the Swiss ethics committee (VD3603) and the University of California, Irvine Institutional Animal Care and Use Committee (IACUC, AUP-21-025) for animal experimentation. Pregnant female C57Bl/6 mice were purchased from Charles River Laboratories (France) and pups were aged until 3 weeks at which time they were irradiated. The inbred C57Bl/6 mouse model was chosen for this experiment as it is a multipurpose model that is frequently used for cognitive outcomes.

Irradiation

Two-fraction, whole-brain irradiations were performed on a prototype Oriatron 6e, 6-MeV electron beam linear accelerator (LINAC) at the Lausanne University Hospital (Lausanne, Switzerland), as described elsewhere[203]. Dosimetry has been extensively described and published to ensure reproducible reliable delivery[203–206]. Animals received two whole-brain, head only, doses of 10 Gy, separated by 48 hours using a 17-mm graphite applicator at either CONV dose rate (0.09 Gy/s) or ultra-high-dose-rate FLASH (delivered at $5.6 \cdot 10^6$ Gy/s in a single 1.8 μs pulse) delivered to the whole brain (**Table. 3.1**).

Electrophysiology

Female mice (n=6/treatment, 18 total) were sacrificed for electrophysiology and hippocampal slices were prepared as previously described[235]. Following isoflurane anesthesia, mice were decapitated, and the brain was quickly removed and submerged in ice-cold, oxygenated dissection medium containing (in mM): 124 NaCl, 3 KCl, 1.25 KH2PO4, 5 MgSO4, 0 CaCl2, 26 NaHCO3, and 10 glucose. Coronal hippocampal slices (340 μm) were prepared using a Leica vibrating tissue slicer (Model:VT1000S) before being transferred to an interface recording containing preheated artificial cerebrospinal fluid (aCSF) of the following composition (in mM): 124 NaCl, 3 KCl, 1.25 KH2PO4, 1.5 MgSO4, 2.5 CaCl2, 26 NaHCO3, and 10 glucose and maintained at 31 ± 10°C. Slices were continuously perfused with this solution at a rate of 1.75-2 ml/min while the surface of the slices were exposed to warm, humidified 95% O2 / 5% CO2. Recordings began following at least 2 hr of incubation.

Field excitatory postsynaptic potentials (fEPSPs) were recorded from CA1b stratum radiatum apical dendrites using a single glass pipette filled with 2M NaCl (2-3 MΩ) in response to orthodromic stimulation (twisted nichrome wire, 65 μm diameter) of Schaffer collateral-commissural projections in CA1 stratum radiatum. Pulses were administered 0.05 Hz using a

current that elicited a 50% maximal spike-free response. After establishing a 20 min stable baseline, long-term potentiation (LTP) was induced by delivering 5 'theta' bursts, with each burst consisting of four pulses at 100 Hz and the bursts themselves separated by 200 msec (i.e., theta burst stimulation or TBS). The stimulation intensity was not increased during TBS. Data were collected and digitized by NAC 2.0 (Neurodata Acquisition System, Theta Burst Corp., Irvine, CA) and stored on a disk.

Data in the text are presented as means ± SD, while in the figures as mean ± SEM. The fEPSP slope was measured at 10–90% fall of the slope and data in figures on LTP were normalized to the last 20 min of baseline. Electrophysiological measures were analyzed using a 1-way ANOVA.

Behavioral testing

To evaluate the potential cognitive deficits induced by irradiation of the brain, all animals underwent a battery of behavioral tests four months post irradiation. Cognitive testing was performed over the course of five-weeks and included paradigms designed to interrogate spatial memory, social interactions, anxiety, and extinction memory. Tests include objects in updated location (OUL), novel object recognition (NOR), social interaction (SIT), and light-dark box (LDB). All behavioral testing was conducted as described previously[231]. Video recordings were taken for all arena testing and subsequently hand scored by an individual that was blinded to the treatment groups.

Arena Object Testing

Objects in updated location (OUL) and novel object recognition (NOR) are paradigms intended to interrogate the cognitive capacity of the hippocampus, medial prefrontal cortex, and perirhinal

cortex. Prior to OUL testing, mice were handled for two minutes per day for four days to reduce anxiety. Following this, animals were habituated to the arenas (30×30×30 cm acrylic boxes with a corn cob bedding base) for six consecutive days. OUL testing was performed over the course of five days. A week after the completion of the OUL task, animals were re-habituated to empty arenas for one day before undergoing NOR testing. The discrimination index (DI) for this task was then calculated for each mouse from these values: ((novel/total exploration time) − (familiar/total exploration time)) × 100.

Social Interaction Testing

To interrogate social interaction and social avoidance in irradiated mice, animals were exposed to a novel animal of the same sex and equal or lesser weight. Animals within this experiment were handled and habituated to the previously described arena for five min the day before testing. On testing day, the novel animal was allowed to freely explore the arena for 10 min prior to the test mouse being introduced. Animals were allowed to freely explore, without any barriers for 10 min and video recorded for later analysis. Data were analyzed by someone blinded to treatment groups. Social interactions included any time the test mouse spent sniffing while in active contact with the novel animal's snout, flank or anogenital area, mutual grooming or directed pursuit of the novel mouse. Concurrently, avoidance behavior was characterized as the time that the test mouse spent actively avoiding social interactions initiated by the novel mouse.

Immunofluorescent and pre- and post-synaptic Ultra-High Resolution imaging

To reduce regional sampling bias, two sections per brain were selected from the ventral hippocampus approximately 300-400 µm apart. Brain sections were permeabilized using 0.1% Triton and blocked using bovine serum albumin (BSA). Sections were incubated overnight at

4°C in TBS with 1% BSA, 4% goat serum, 0.1% Triton, and with primary antibodies glial fibrillary acidic protein (GFAP, 1:500, Millipore), aquaporin-4 (AQP4, 1:500, Abcam), ionized calcium binding adaptor molecule (IBA-1, 1:200, Wako), and cluster of differentiation 68 (CD68, 1:500, Biorad), Homer1a (rabbit anti-Homer1a, 1:500, Synaptic Systems) and BSN (mouse anti-BSN, 1:500, Neuromab). Tissues were incubated with the following secondary antibodies: Goat anti-mouse 647 (1:1000, Abcam), goat anti-rabbit 555 (1:1000, Invitrogen), or goat anti-mouse (1:1000, Abcam) before counterstaining with DAPI. Homer1A and BSN were imaged using a ZEISS ELYRA7 with Lattice SIM and post-processed in Zen. AQP4, CD68, GFAP, Lectin and IBA1 were imaged using a Nikon Ti2 fluorescent microscope.

Statistical analysis

All statistical analysis was performed in Prism (Graphpad Software Inc, San Diego California, USA, version 5.04). Averages of individual animal replicates were used to calculate group interactions using a one-way analysis of variance (ANOVA). Upon significant results, Bonferroni's post-hoc testing was performed. Data is presented as Mean ± SEM. Values of $P \leq 0.05$ were considered statistically significant.

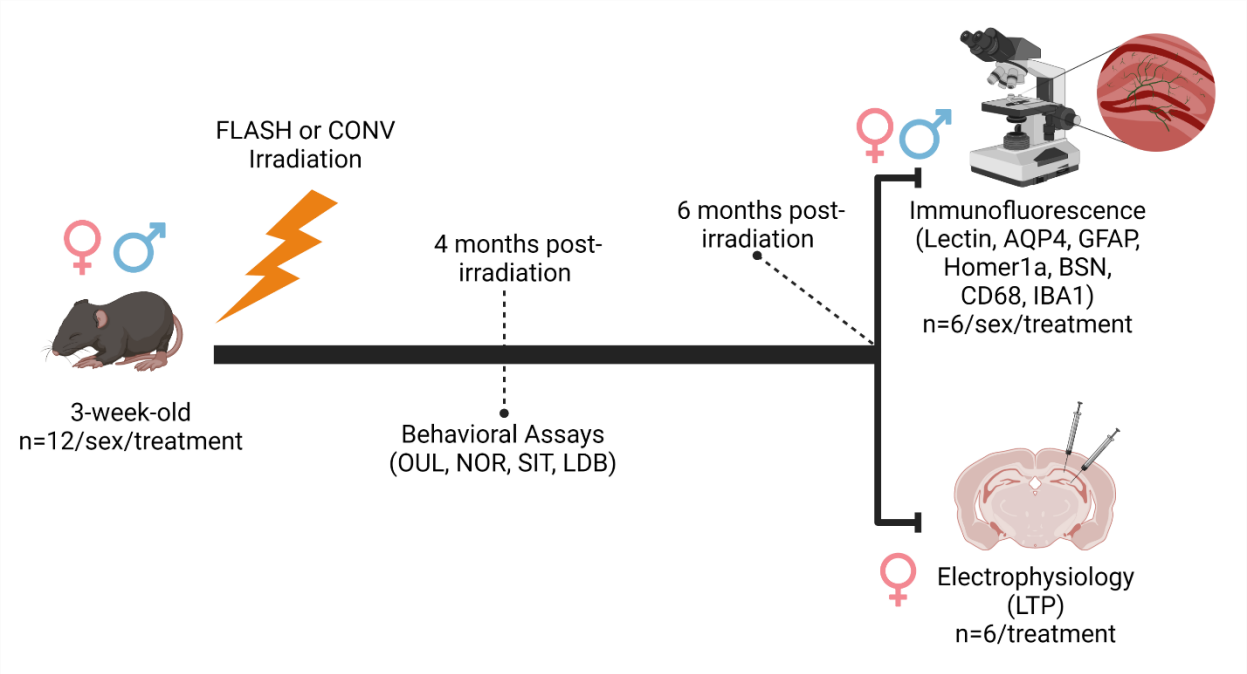

Figure 3.1: Experimental Design.

3-week-old animals received hypofractionated FLASH-RT or CONV irradiation (2×10 Gy). Four months post-irradiation, animals underwent behavioral testing (n=12/sex/treatment). At 6-months post-irradiation, animals were sacrificed, and tissues were prepared for various endpoints. Half of the female animals were randomly assigned for assessment of long-term potentiation (n=6/treatment). Both male and female animals were used for immunofluorescence analysis of various markers (n=6/sex/treatment). Abbrev: OUL = Objects in updated location, NOR = Novel object recognition, SIT = Social interaction testing, LDB = light dark box, AQP4 = Aquaporin4, GFAP = Glial fibrillary acidic protein, BSN = Bassoon, CD68 = Cluster of differentiation 68, IBA1 = Ionized calcium-binding adapter molecule 1.

	Prescribed dose and regimen	
	CONV	FLASH
Beam parameters	2 × 10 Gy	2 × 10 Gy
Graphite applicator type and size (mm)	Hemi-circular Ø17	Hemi-Circular Ø17
Source-to-surface distance (mm)	800	209
Pulse repetition frequency (Hz)	10	100
Pulse width	1.0 µs	1.8 µs
No. of pulses	1170-1180	1
Treatment time (s)	117	$1.8x10^{-6}$
Mean dose rate (Gy/s)	0.1	$5.6x10^{6}$
Instantaneous dose rate (Gy/s)	$8.5x10^{3}$	$5.6x10^{6}$

Table 3.1: Irradiation Parameters, Juveniles

Fractionated whole brain irradiation was performed on the Oriatron 6e, 6MeV electron beam linear accelerator (LINAC) at Lausanne University Hospital. Animals received 2 doses of 10 Gy separated by 48 hours at either CONV (CONV-RT; 0.09 Gy/s) or ultra-high dose rate FLASH (FLASH-RT, delivered at 5.6×10^{6} Gy/sec in a single 1.8 µs pulse).

Results

FLASH-RT does not inhibit hippocampal long-term potentiation (LTP) in mice.

LTP defines a critical functional outcome in the CNS and, we hypothesized that activity-dependent synaptic connections between interconnected hippocampal circuitry involving excitatory neurons and diverse populations of GABAergic interneurons could be maintained in FLASH-irradiated animals. Theta burst stimulation (TBS) applied to the Schaffer collaterals produced an immediate and robust increase in LTP, quantified as the relative change in the slope of evoked field excitatory postsynaptic potentials (fEPSPs) generated by CA1 apical dendrites (**Fig. 2A**). Following TBS, a gradual decay in the fEPSP slope to more stable levels of potentiation were observed in all cohorts, where LTP levels recorded from hippocampal slices 6-months after irradiation were consistent with our prior reports[236]. Importantly, levels of potentiation in the fEPSP slope maintained at 1h post-TBS were reduced significantly in the hippocampus of CONV mice, but not in CONT or FLASH mice (**Fig. 3.2B and 3.2C**; one-way ANOVA: $F_{(2,31)}=32.13$; $P<0.0001$; Bonferroni *post-hoc*: CONTROL vs CONV: $P<0.001$; FLASH vs CONV: $P<0.0001$). Given these findings, it is remarkable that over such protracted times, FLASH mice were statistically indistinguishable from controls, while CONV-RT led to an apparent permanent inhibition of LTP.

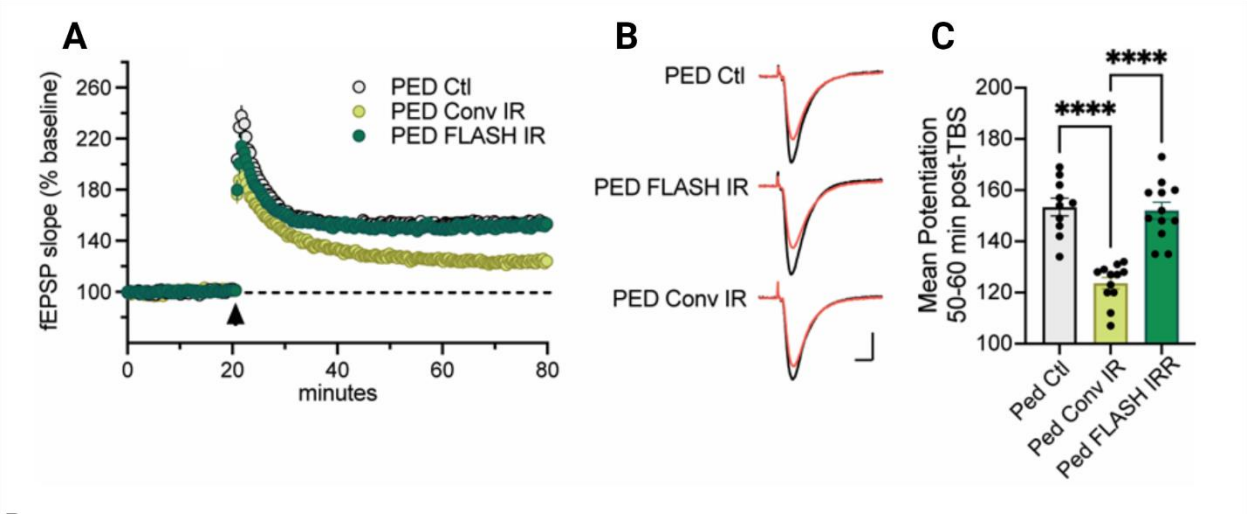

Figure 3.2: FLASH irradiation protects against reductions in long term potentiation (LTP) after CONV irradiation.

(A) Theta burst stimulation (TBS) applied to the Schaffer collaterals produced a robust increase in fEPSP slope (as percent of baseline) in CONTROL and FLASH-RT female animals but reduced in CONV-RT animals 6-months after exposure. (B/C) Levels of potentiation in the fEPSP slope maintained 1h post-TBS was reduced significantly in the hippocampus of CONV-RT mice, but not in control or FLASH irradiated mice. Scale: 1 mV/5 ms. All data were analyzed using a one-way ANOVA followed by Bonferroni's multiple comparison test (n=6/sex/treatment). ****=$P \leq 0.0001$.

FLASH-RT preserves synaptic structure and density in the hippocampus.

To provide deeper insight of our previous findings[2,231] into how dose rate modulation might impact the breakdown or preservation of synaptic connections, we used super resolution microscopy (ELYRA7) to evaluate pre- and post-synaptic junctions on a nanometer scale (**Fig. 3.3A**). Previous studies evaluating synaptic bouton suggested that an analysis of the juxtaposition of pre-synaptic bassoon (BSN) and post-synaptic homer scaffold protein 1a (Homer1a) puncta might shed light on the ultra-structural integrity of the synapse[237]. The average diameter of Homer1a and BSN foci were found to be ~120μm, determined by our IMARIS spot analysis. Analysis quantified only pre- and post-synapses that were within twice the radius of the foci, allowing for an assessment of pre/post-synaptic markers that remained in direct contact. Both male and female mice exhibited similar trends, where FLASH-RT was associated with higher levels of tight association, however, only the male cohort reached statistical significance when comparing CONV mice to CONTROL and FLASH cohorts. (**Fig. 3.3C**; one-way ANOVA: $F_{(2,15)}=16.65$, $P=0.0002$; Bonferroni *post-hoc*: CONTROL vs CONV: $P<0.01$; FLASH vs CONV: $P<0.001$).)

The expression of the major synaptic vesicle protein synaptophysin (**Fig. 3.3B)** was also investigated and similar trends were observed in both male and female mice where FLASH and CONTROL animals maintained similar levels of synaptophysin (**Fig. 3.3D**; one-way ANOVA: Males: $F_{(2,13)}=13.68$, $P=0.0006$; Females: $F_{(2,15)}=14.06$, $P=0.0004$). However male mice exposed to CONV irradiation exhibited a significant reduction in synaptophysin when compared to both CONTROL ($P\leq0.01$) and FLASH ($P\leq0.001$). Analogous results were found in CONV irradiated female mice, exhibiting significant reductions in synaptophysin compared to CONTROL ($P\leq0.05$) and FLASH ($P\leq0.001$) cohorts. Collectively, these data provide significant new

evidence that FLASH-RT does preserve synaptic integrity in the juvenile brain whereas it is altered after CONV irradiation (**Fig. 3.3D**; one-way ANOVA $F_{(2,15)}$=14.06, *P*=0.0004).

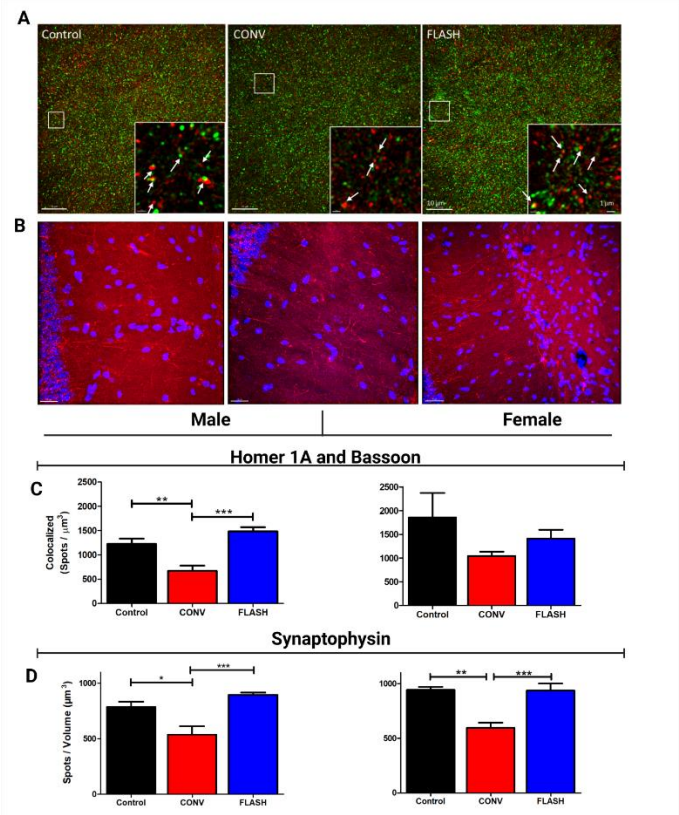

Figure 3.3: FLASH irradiation protects against disruptions to dendritic spine morphology and expression observed after CONV irradiation.

(A) Representative images of Homer1a and Bassoon colocalization in the stratum radiatum. (B) Representative images of synaptophysin expression in the stratum radiatum. (C) Quantification of Homer1a and Bassoon colocalized spots. Male (left) CONT and FLASH-RT animals expressed similar levels of pre- and post-synaptic labeling, while CONV irradiation exhibited significantly less. Female animals (right) exhibited trends similar to that of the males without achieving statistical significance. (D) Quantification of synaptophysin. Male and female synaptophysin were reduced when animals were CONV irradiated but protected in FLASH irradiated animals. All data analyzed using a one-way ANOVA followed by Bonferroni's multiple comparison test (n=6/sex/treatment). *= $P \leq 0.05$, **=$P \leq 0.01$, ***=$P \leq 0.001$.

FLASH-RT ameliorates radiation-induced cognitive impairments in juvenile mice.

The preservation of synaptic integrity at the functional (electrophysiologic) and structural levels (synaptic bouton) found after FLASH-RT suggest that behavioral outcomes should also be differentially affected by dose rate modulation. To evaluate this, male and female juvenile mice were subjected to a comprehensive behavioral testing panel after exposure to hypofractionated-RT. The objects in updated location (OUL) task represents a novel memory updating paradigm, able to assess original and updated information in a single test session. The ability to discriminate between multiple overlapping associative memories with this task provides a deeper dissection of neurocognitive functionality which shows strong cross species correlates. Assessment of intact cognitive function is quantified by the time spent exploring the objects in novel locations compared to familiar locations. After training (**Fig. 3.4A)** in which the mice learned the spatial location of identical objects (A_1, A_2) they were reintroduced the next day into the same familiar context for an update session (Day 4), where an original object was moved to a new location (A_3). While male CONTROL and FLASH-RT cohorts successfully recognized the A_3 location as novel, CONV-RT cohorts did not, exhibiting a lack of preference for the novel location when compared to CONTROL and FLASH mice (**Fig. 3.4B**; one-way ANOVA: $F_{(2,30)}$=7.004; *P*=0.0032; Bonferroni *post-hoc*: *P*=0.0018; *P*=0.046, respectively). These findings were corroborated in the female cohort as CONV animals also lacked preference for the novel A_3 location when compared to CONTROL and FLASH (one-way ANOVA: $F_{(2,30)}$=6.074; Bonferroni *post-hoc*: *P*=0.0061; *P*=0.0073; *P*=0.015, respectively).

Following the update session all groups were given a test session (**Fig. 3.4C, 3.4D**; Day 5). In this phase of OUL testing, memory for the updated information was compared against

exploration of the object in the novel location (A_4) to exploration of the fixed, initial, and updated locations (A_1, A_2 and A_3, respectively). Intact memory for the original training or update sessions is demonstrated by a preference of the object in the novel (A_4) compared to the other prior object locations as indicated by higher scores on the discrimination index (DI). Importantly, male mice exposed to FLASH-RT retained a similar preference as control animals for the object in the novel A_4 location relative to the prior updated (A_3) and fixed (A_1) object locations object (**Fig. 3.4C, 3.4D,** respectively). Male mice exposed to CONV-RT however, exhibited no preference for novelty at the A_4 location compared to the updated A_3 or fixed A_1 locations (**Fig. 3.4C**; one-way ANOVA $F_{(2,30)}$=5.023; *P*=0.013; Bonferroni *post-hoc*: *P*=0.021; *P*=0.015 and **Fig. 3.4D**; one-way ANOVA $F_{(2,32)}$=4.38; *P*=0.021; Bonferroni *post-hoc*: *P*=0.038; *P*=0.023, respectively). Interestingly, neither the CONV nor the FLASH female mice exhibited decrements on the test phase of this task, indicating intact hippocampal pattern separation and the capability to retain novelty discrimination even after irradiation (**Fig. 3.4C**; one-way ANOVA $F_{(2,31)}$=0.097; **Fig. 3.4D**; one-way ANOVA $F_{(2,32)}$=1.151).

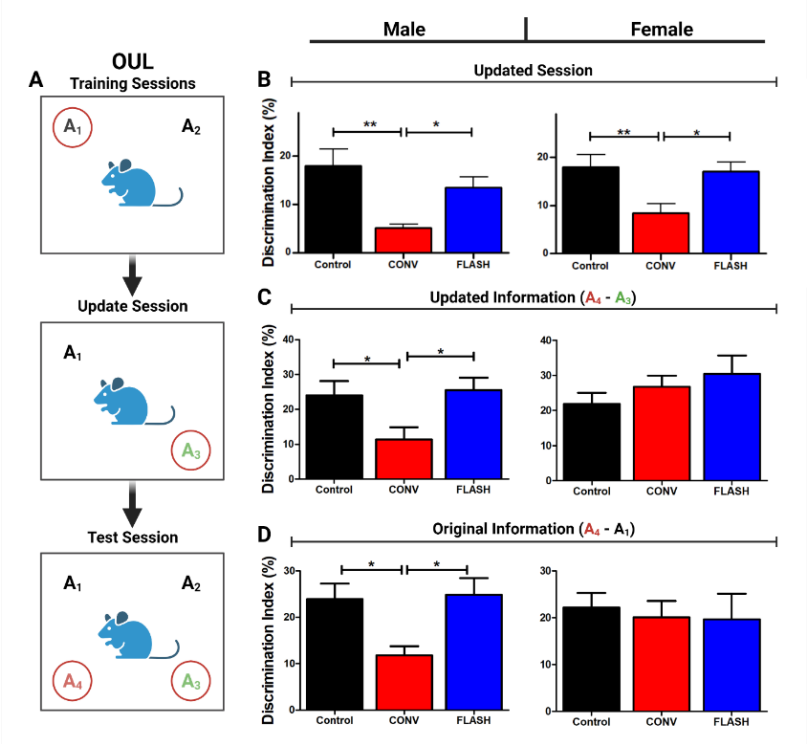

Figure 3.4: Animals exposed to FLASH-RT performed similar to controls in hippocampal dependent learning and memory tests objects in updated location (OUL) while conventionally irradiated (CONV-RT) animals did not. (A) Objects in updated locations testing experimental design. (B) Update session behavior. At 4 months post-irradiation, FLASH and control animals showed preference for the novel toy and location in both males (left) and females (right) while CONV did not. (C) Updated information test session. CONV irradiated male animals failed to learn the updated novel (A_4) object over its predecessor (A_3) when compared to FLASH and control animals. No differences were observed in female mice. (D) Original information test session. CONV irradiated male mice were unable to differentiate between the updated novel location (A_4) and the original location (A_1) while FLASH and control performed similarly. No changes in female mice were observed. All data were analyzed using a one-way ANOVA followed by Bonferroni's multiple comparison test (n=12/sex/treatment). * = $P \leq 0.05$, ** = $P \leq 0.01$.

After OUL testing, mice were subjected to a standardized Novel Object Recognition (NOR) task (**Fig. 3.5A**) as described previously [181,231]. Here, both male and female mice exposed to FLASH were statistically indistinguishable from CONTROL, whereas CONV mice exhibited significant impairments in the ability to discriminate novelty (**Fig. 3.5A**). For males, CONV animals were impaired compared to CONTROL and FLASH-RT mice (one-way ANOVA: $F_{(2,32)}$=4.6; *P*=0.017; Bonferroni *post-hoc*: *P*=0.016 and *P*=0.035, respectively). In females, CONV irradiated mice showed impairments compared to CONTROL (one-way ANOVA: $F_{(2,32)}$=6.84; *P*=0.0034; *P*=0.0038) and FLASH mice (*P*=0.083).

Social interaction test (SIT) and light-dark box (LDB)

Following the NOR task, animals were tested sequentially on the social interaction test (SIT) to test approach and avoidance of a novel animal and the light-dark box (LDB) to interrogate unconditioned anxiety associated with spontaneous exploration. For the social interaction test (SIT), male CONT- and FLASH-RT mice behaved similarly, with trends toward increased interaction and less avoidance compared to CONV although these differences did not reach significance (**Fig. 3.5B, 3.5C**; one-way ANOVA: $F_{(2,32)}$ = 2.51; *P* = 0.098). Female mice behaved similarly to the males, but differences between FLASH and CONV experimental groups were significant, where FLASH females showed increased interaction and reduced avoidance compared to CONV (**Fig. 3.5B**; one-way ANOVA: $F_{(2,32)}$ = 6.809; *P* = 0.0034); **Fig. 3.5C**; one-way ANOVA: $F_{(2,32)}$ = 6.81; *P* = 0.0034 respectively). Despite differences found on the SIT, experimental cohorts analyzed here did not show significant differences in the LDB task (**Fig. 3.5D**; Males; one-way ANOVA: $F_{(2,32)}$ = 2.001; *P* = 0.1517. Female; one-way ANOVA: $F_{(2,31)}$ =1.143; *P*=0.3319). Collectively, behavioral outcomes corroborated electrophysiological and

synaptic protein measures pointing to the widespread capability of FLASH-RT to minimize adverse radiation-induced sequelae in the juvenile mouse brain.

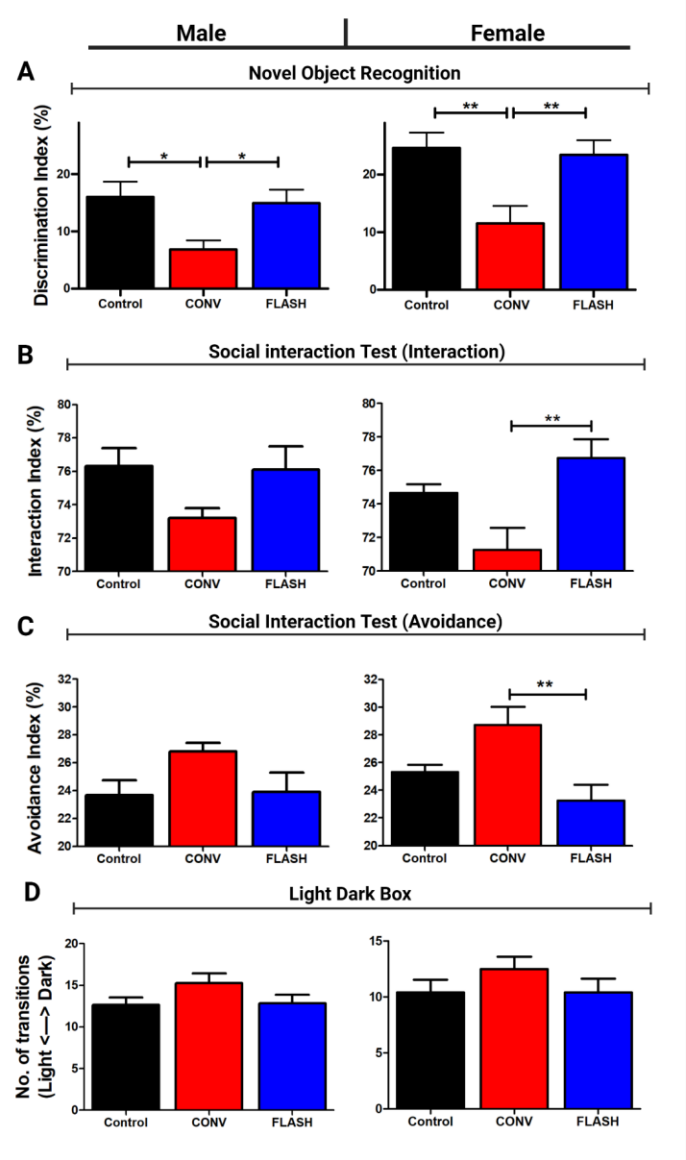

Figure 3.5: Animals exposed to FLASH-RT performed similar to controls in learning and memory as well as anxiety-like behavior while conventionally irradiated (CONV) animals did not.

(A) Novel object recognition testing (NOR). Male and female mice control and FLASH animals performed similar while animals exposed to CONV irradiation were unable to differentiate the novel toy. (B/C) Social interaction/avoidance testing (SIT). Four months post-irradiation animals were exposed to a novel mouse and measured for avoidance and interaction behaviors and

presented as a percentage of total time interacting. Female FLASH animals exhibited reduced anxiety when compared to CONV animals. Male animals performed the same as controls, while CONV irradiated exhibited anxiety, albeit in a non-significant way. (D) Light dark box testing (LDB). Male and Female mice performed similar to control regardless of treatment. All data were analyzed using a one-way ANOVA followed by Bonferroni's multiple comparison test (n=12/sex/treatment). * = $P \leq 0.05$, ** = $P \leq 0.01$.

FLASH-RT does not induce persistent inflammation as observed after CONV irradiation.

Previous publications demonstrate that radiotherapy-induced microglial activation contributes to cognitive impairments[238–240] and blood brain barrier (BBB) damage[241]. To assess the effect of FLASH-RT on neuroinflammation through the activation of CD68 in microglia of juvenile animals, immunofluorescence of IBA1 and CD68 co-labeling were analyzed (**Fig. 3.6A**). While resting microglia volumes were not altered by either irradiation modality, data indicate that a significant increase in activation persists in both male and female animals (**Fig. 3.6B;** one-way ANOVA $F_{(2,33)}$=4.952, P=0.0132, $F_{(2,32)}$=36.70, P<0.0001, respectively) . Consistent with past results[239,242], an elevated level of CD68 volume colocalized with IBA1 at this protracted time was found in CONV irradiated females ($P \leq 0.0001$) with a similar trend in male mice that neared significance. When comparing CONV-RT activation of microglia to FLASH-RT, no late term activation of microglia was found in males and was greatly reduced in females ($P \leq 0.05$, $P \leq 0.0001$, respectively). A sex specific increase in persistent inflammation was observed in female mice as both CONV and FLASH induced activation of microglia that far surpassed the male animal response and an increase in CD68/IBA colocalization in FLASH animals ($P \leq 0.01$) was higher than controls.

It is estimated that a large portion of all microglia directly interact with the microvasculature of the BBB and assist in vasculature repair[239,243]. Correlation between an increase in $CD68^+$ microglia colocalized to the BBB has been associated with vasculature leakage[243,244]. Using lectin to highlight microvasculature colocalized with $CD68^+$ microglia, we assessed whether the decrease in activated microglia that was observed in FLASH-RT treated animals extended regionally to the BBB. Analysis of colocalization of lectin and CD68 indicated reduced inflammatory recruitment to the BBB in both male juvenile mice (**Fig. 3.6C;** one-way ANOVA

$F_{(2,15)}$=10.79, P=0.0013; $F_{(2,14)}$=21.49, P<0.0001, respectively). Male CONV irradiated animals had significantly more CD68 colocalized with lectin than that of either FLASH-RT or CONTROL ($P \leq 0.01$). Female animals exposed to CONV-RT had significantly elevated levels of CD68/lectin colocalization when compared to CONTROL and FLASH-RT ($P \leq 0.0001$ and $P \leq 0.05$, respectively). Female FLASH animals did however exhibit levels of CD68/lectin colocalization significantly higher than controls ($P \leq 0.01$). These data taken together indicate that FLASH-RT does not produce prolonged microglia activation, which likely contribute to the neurological benefits of this irradiation modality.

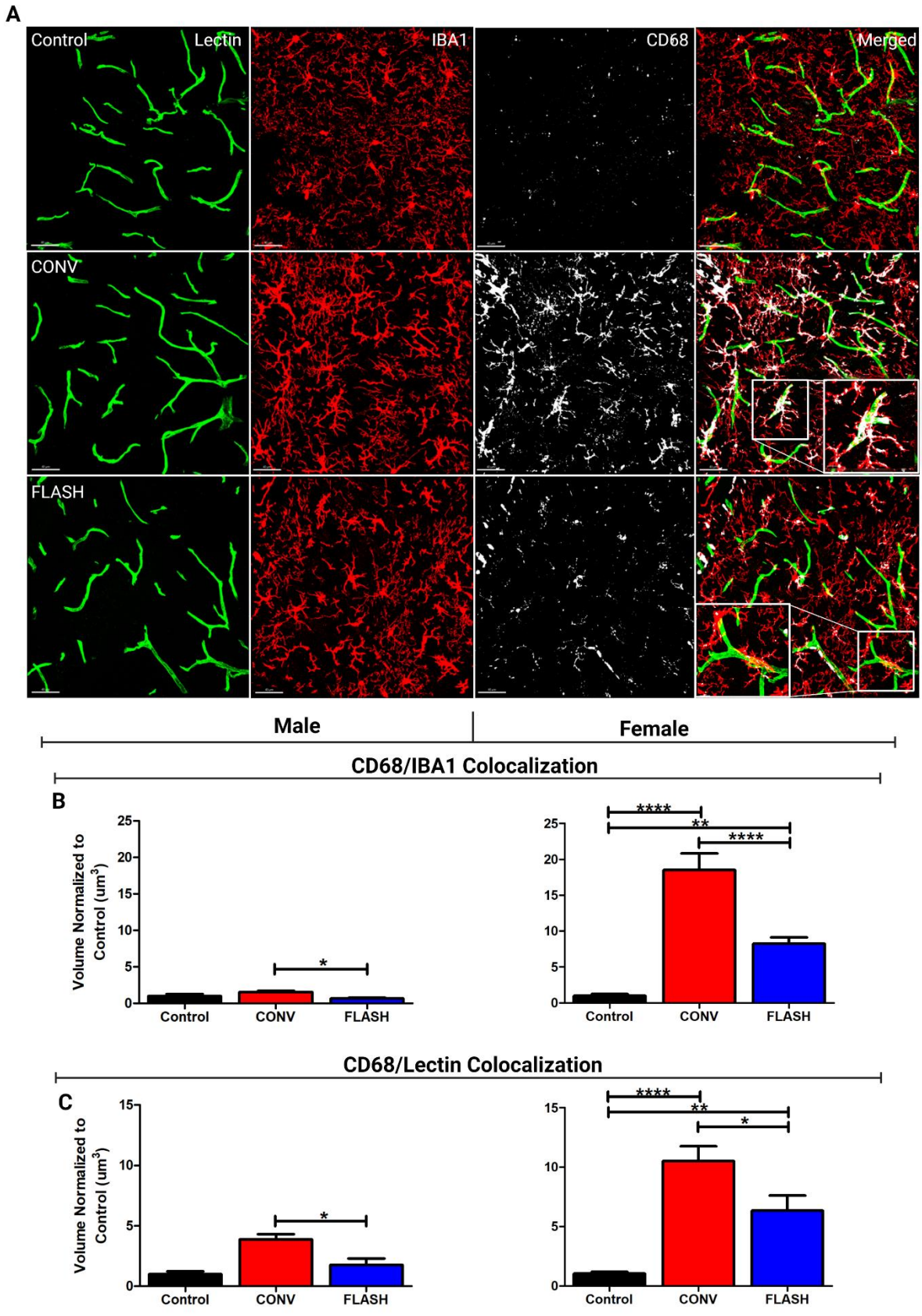
A
Control
Lectin
IBA1
CD68
Merged
CONV
FLASH
Male
Female
CD68/IBA1 Colocalization
B
Volume Normalized to Control (um3)
Control
CONV
FLASH
*
****
**
CD68/Lectin Colocalization
C

Figure 3.6: FLASH irradiation does not contribute to prolonged inflammation observed in CONV animals six-months post-irradiation.

(A) Representative images of activated microglia (CD68/IBA1) and vasculature in female mice. (B) Quantification of CD68/IBA1 colocalization. Male (left) animals exposed to FLASH exhibit significantly less microglial activation that CONV irradiated animals. Female (right) animals exposed to FLASH irradiation exhibited significantly less microglial activation than CONV irradiated animals. (C) Quantification of CD68/lectin colocalized within 5 µm. Male animals exposed to FLASH irradiation had significantly fewer activated microglia enveloping the microvasculature compared to CONV. Female animals exposed to FLASH irradiation exhibited less CD68-activated microglia associated with the vasculature yet both FLASH-RT and CONV-RT animals were significantly higher than controls. All data analyzed using a one-way ANOVA followed by Bonferroni's multiple comparison test (n=6/sex/treatment). *=$P \leq 0.05$, **=$P \leq 0.01$, ****=$P \leq 0.0001$.

FLASH preserves the microvasculature of the BBB through protection of Aquaporin 4.

To determine if FLASH-RT would protect the BBB of juvenile mice at protracted times we analyzed the neurovascular unit (NVU). Astrocytic end-feet cover microvessels where they act as intermediaries between neurons and the vasculature and are known to mediate the flow of fluid and ions from blood vessels into the parenchyma through AQP4 channels (**Fig. 3.7A)**. Globally, similar trends were found in both male and female mice, six-months post-irradiation independent of the modality of irradiation (**Fig. 3.7B, 3.7C**; one-way ANOVA $F_{(2,17)}$=4.823, *P*=0.0219 and $F_{(2,19)}$=13.54, *P*=0.0002, respectively). FLASH-RT did not induce any modification AQP4 immunoreactivity when compared to CONTROL whereas CONV-RT animals exhibited significantly reduced AQP4 immunoreactivity than that of control male and female animals ($P \leq 0.05$ and $P \leq 0.001$, respectively) animals and FLASH-RT male and female animals ($P \leq 0.05$). Astrocytic coverage of the microvasculature was found to be reduced after CONV-RT ($P \leq 0.01$) in female mice (**Fig. 3.7E**; one-way ANOVA $F_{(2,19)}$=6.842, *P*=0.0058), however, no significant differences were found in males (**Fig. 3.7D**; one-way ANOVA $F_{(2,17)}$=0.8118, *P*=0.4606). While FLASH-RT did appear to reduce GFAP/lectin colocalization in females, no significant differences were found when compared to control or CONV-RT in males. To determine if AQP4 expression was reduced overall in astrocytes, we measured colocalization of AQP4 to GFAP and found trends that CONV-RT did reduced immunoreactivity compared to control and FLASH-RT, but no significance was found in males or females (**Fig. 3.7F/G**).

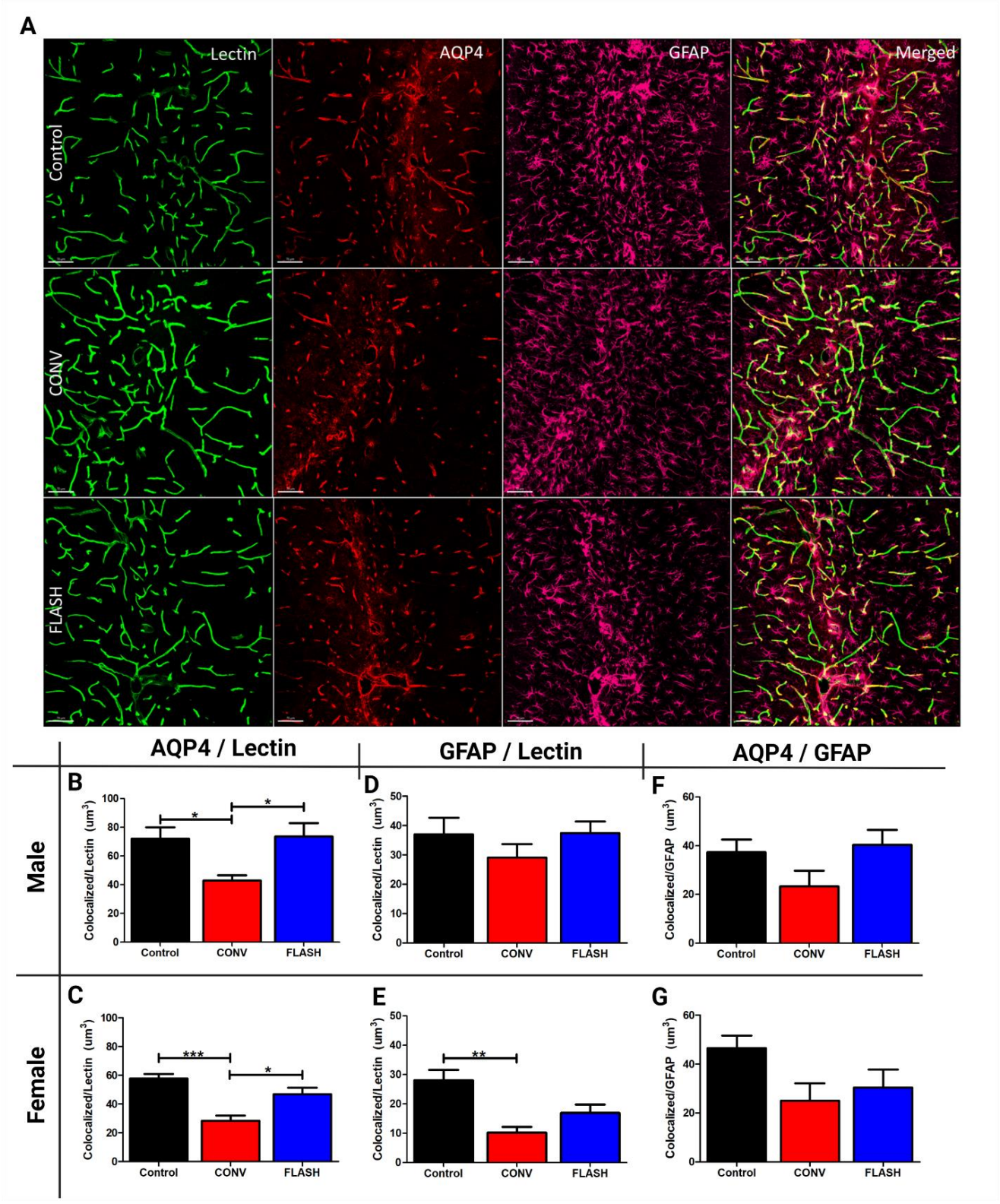
A
Lectin
AQP4
GFAP
Merged
Control
CONV
FLASH
AQP4 / Lectin
GFAP / Lectin
AQP4 / GFAP
Male
Female
B
C
D
E
F
G
Colocalized/Lectin (um3)
Colocalized/GFAP (um3)
Control
CONV
FLASH
*
**
***

Figure 3.7: FLASH irradiation protects against late-modification of the BBB through protection of fluid channel AQP4 and astrocytic coverage.

(A) Representative images of lectin-coated microvasculature, Aquaporin 4 (AQP4), and astrocytes (GFAP) in the hippocampus of male mice. (B/C) Quantification of AQP4/lectin colocalization. At six months post-irradiation, FLASH-RT protectedmale and female animals from reduced AQP4 expression along blood vessels while CONV-RT did not. (D) Male FLASH-RT animals did not display any deviation from CONTROL or CONV irradiated animals. (E) FLASH-RT and CONTROL female mice exhibited no significant deviations in astrocytic coverage of the microvasculature compared to CONV-RT. (F/G) No significant changes were observed in AQP4 expression in GFAP labeled astrocytes after FLASH-RT or CONV-RT irradiation. All data analyzed using a one-way ANOVA followed by Bonferroni's multiple comparison test (n=6/sex/treatment). *=$P \leq 0.05$, **=$P \leq 0.01$, ***=$P \leq 0.001$.

Discussion

The current study was designed as a proof of concept, to demonstrate the potential benefit of hypofractionated FLASH-RT in the tumor free juvenile mouse brain, in order to substantiate the translational promise of this new modality for improving outcomes for medulloblastoma patients. Here we provide novel insights into how FLASH-RT preserves critical functional outcomes and protects structural elements of the synapse and vasculature in the radiosensitive juvenile mouse brain over extended post-irradiation times, defining global benefits that are compromised after CONV-RT.

It has been established that synaptic inputs from CA3 to CA1 pyramidal neurons through the Schaffer collateral pathway can attenuate and increase firing activity, known as LTP, thereby constituting a cellular basis of memory[244,245]. Learning and memory formation in the brain are attributed by changes in synaptic connectivity (Hebb, 1949). Long-term potentiation (LTP) is a synaptic mechanism underlying learning and memory in that it produces long-lasting increases in synaptic strength and an increase in signal transmission in the brain. This substrate for memory has been studied extensively in laboratory animals over the past 50 years, and recently in intact humans (Clapp et al., 2012). The key evidence shows that; LTP is synapse specific, rapidly induced, and extremely persistent; all important characteristics that explain the capacity, rapid acquisition, and stability of memory. Past work has shown that irradiation can compromise LTP, where homeostatic plasticity mechanisms normally enabling neuronal networks to cope with specific insults remain disrupted[246] This apparent "permanent" disruption could reflect an inability to properly regulate other cellular properties, such as ion channel expression function, translocation of presynaptic vesicles, or stabilizing the post-synaptic density to facilitate to

proper re-integration of "normal" synaptic connectivity and overall homeostasis. In this light, it is noteworthy that six months after FLASH-RT, LTP remains essentially unchanged and identical to controls, in marked contrast to what is observed after CONV-RT. The differential response of LTP to dose-rate modulation defines a robust functional outcome in the irradiated brain and may well provide a reliable and reproducible *ex vivo* validation of the FLASH effect useful for future investigations.

Plasticity is reliant on multiple mechanisms and one key component of these signaling pathways is the proper pairing of pre- and post-synaptic structures to facilitate efficient neurotransmission[247–249]. Therefore, to evaluate whether FLASH-RT might preserve critical neuronal connections in the hippocampus we quantified levels of pre- and post-synaptic bouton through ultra-high resolution (ELYRA7) microscopy. Homer1A (post) and BSN (pre) synaptic proteins were selected due to their high binding specificity at the synaptic cleft as shown in other studies[237]. Measuring regional proximity on a nanometer scale presumes a scrutiny of tight synaptic binding, since only pre- and post-synaptic fluorescent puncta colocalizing within 120 µm were quantified. Whereas CONV irradiation decreased the yield of colocalized puncta, FLASH-RT preserved these "tighter" connections, consistent with LTP preservation as opposed to the brain exposed to CONV-RT. To further evaluate synaptic integrity, we quantified the total fluorescent intensity of pre-synaptic synaptophysin vesicles known to be downregulated after irradiation [250,251]. Immunofluorescent analysis confirmed past results[251] and CONV irradiation significantly reduced synaptophysin levels, whereas FLASH-RT preserved these levels equivalent to those observed in controls. The synapse is a complex and dynamic structure subject to plasticity-induced changes that facilitate translocation of presynaptic vesicles and receptor subunits to attenuate excitatory and inhibitory neurotransmission[252,253]. Dissecting the details of

how dose rate modulation impacts synaptic plasticity is beyond the scope of the present manuscript. Nonetheless, these new and provocative results support the hypothesis that the stability of synaptic connections and/or the preservation of synaptic density are contributory if not causal to the beneficial cognitive and LTP functional outcomes in the FLASH irradiated brain.

In considering the quality of life for brain cancer survivors, no functional outcome holds more importance to than the preservation of cognitive function, regardless of the myriad of mechanisms potentially responsible. Herein lies the true benefit of FLASH-RT, where the behavioral testing conducted in this study provides evidence that FLASH-RT ameliorates radiation-induced damage to hippocampal, prefrontal, and amygdala circuitry known to be involved and disrupted following CONV-RT[2,5,231]. Our extensive behavioral testing platform suggests undeniable benefits of FLASH-RT in juvenile animals, where both sexes were similarly (albeit not identically) protected.

Implementing a higher dose fractionated FLASH-RT paradigm, we showed that juvenile male and female mice exhibited significant reductions in activated microglia compared to CONV irradiated mice, thereby providing valuable information regarding dose tolerances in both sexes. Interestingly, past reports documenting differences in basal and radiation-induced inflammation between the sexes was not found here, possibly reflecting differences in radiation modality, mouse strain, age at time of irradiation, or post-irradiation time of analysis[254,255]. Juxtavascular microglia also play an intricate role in BBB integrity. As they encapsulate the vasculature in areas of low astrocytic coverage, modulating neuronal signaling, regulating angiogenesis, modify tight junction expression, and rapidly migrating to areas of vasculature damage[243,256,257]. Activation of microglia has been shown to lead to increased permeability of the BBB, likely

through reduction of zona occluden-1, claudin-5, and occludin tight junction proteins[244,258]. Importantly, current findings indicate that juxtavasculature microglia remain activated 6 months after CONV irradiation but to a significantly lesser extent than those treated with FLASH-RT. The association of these key pro-inflammatory cells with the vasculature could well compromise the integrity of the BBB over prolonged periods and elevate the risk for other complications such as white matter necrosis and stroke[259]. Our new findings couple the vascular and parenchymal components of radiation-induced brain injury though microglial mediated BBB damage and suggest that FLASH-RT exerts global benefits in irradiated tissue by attenuating chronic inflammation.

Cranial irradiation can damage the BBB and lead to short term vascular leakage, edema, and inflammation[9,19,30,260]. Additionally, persistent damage to the microvasculature can cause irregularities within the NVU leading to white matter necrosis, increased risk of stroke, fibrinoid necrosis, and telangiectasis all of which are relevant to survivors of pediatric CNS tumor treatments[261,262]. At these latter times (>3 months) irregularities may reflect variations in oxygen and ion transfer across the vasculature and/or cell senescence that led to a prolonged inflammatory footprint. Previous reports from our lab have documented that FLASH-RT spares the BBB at early time points (≤ 1month) by mitigating tight junction protein loss and reducing vasculature dilation, which may reduce the risk of edema[9]. In addition to microvasculature associated inflammation, we focused on astrocytic end-feet and concomitant fluid channels (AQP4) that not only support and regulate the BBB but are also associated with synaptic plasticity, learning, and memory[263]. GFAP and astrocytic end-feet wrap around the vasculature and express high levels of AQP4 to regulate fluid and ion levels in a bi-directional manner within the parenchyma, indicating a role in parenchymal homeostasis. Emerging evidence also points to

AQP4 as a regulator of synaptic plasticity, LTP, and amygdala-hippocampal dependent cognitive outcomes attributed to GFAP/AQP4 expression found at the synaptic cleft[263]. Our current findings indicate that after CONV-RT, AQP4 levels associated with, and covering the vasculature are reduced, effects that are not observed after FLASH-RT. Collectively, these data indicate that FLASH-RT likely protects key components required to maintain the "normal" cerebrovascular homeostasis, factors that are presumed to promote and hasten the recovery of the irradiated juvenile brain.

This paper is the first to demonstrate the benefits of hypofractionated FLASH-RT in the highly radiosensitive juvenile mouse brain. Strengths of the present findings include a robust and longitudinal assessment of functional neurocognitive and electrophysiological outcomes in radiosensitive juvenile mice exposed to hypofractionated radiotherapy at protracted post-irradiation times. Deficits found in each these functional outcomes after CONV-RT are not observed after FLASH-RT, where FLASH irradiated cohorts are consistently and statistically similar to controls. While certain sexual dimorphisms were found (OUL test session) which warrant further directed studies, in no instance was FLASH-RT found to be more toxic than CONV-RT for any of the CNS endpoints analyzed or between the sexes. Cognitive sparing in FLASH irradiated cohorts was linked to the preservation of LTP, a validated measure of synaptic plasticity. Other measures of synaptic structure and density and aquaporin-4 levels along the vasculature were also spared by FLASH-RT, which was associated with significant reduction in inflammatory microglia. Maintenance of BBB integrity was likely instrumental in sustaining a steady supply of nutrients and oxygen and reducing neuroinflammation.

While these promising results portend potential benefits for clinical translation, caution must be exercised in extrapolating these findings to human patients. For one, human tumors involve

much larger treatment volumes which may limit the extent of the normal tissue benefits observed in mice. Further, the present study was conducted in tumor free mice, and while challenging, ongoing work in mouse models of medulloblastoma will help define more realistic long-term outcomes. Nonetheless, the capability to minimize radiation-induced toxicities might provide the rationale for using FLASH-RT without combined chemotherapy, another potential benefit that may spare systemic toxicity that requires further exploration at the pre-clinical level. These studies find significance in the context of pediatric brain tumor survivors, where favorable survival is inevitably associated with lifelong impairments in cognition and cerebrovascular complications. Herein lies the potential benefit of FLASH-RT, and if safely translated to the clinic, may provide equal efficiency in eradicating malignancies such as medulloblastoma, but without the adverse normal tissue complications that severely compromise quality of life.

Strengths and Weaknesses

This project was designed to interrogate the normal tissue sparing effects of FLASH-RT on a particularly radiosensitive population while also address questions from our previous studies. Building upon our latest experiments on female juvenile mice that received 8 Gy, we opted to irradiate both males and females. at an escalated dose that is closer to palliative care, to investigate potential sex differences. Additionally, we looked to determine what neurological mechanisms could have been altered after irradiation by using electrophysiology to measure changes in long-term potentiation, and using ultra-high resolution microscopy to see changes in dendritic binding, a first in the field of FLASH. This study was also the first to look at late vasculature protection of FLASH measuring reactive microglia and Aquaporin4 levels.

This study played an important role in defining the normal tissue protection of FLASH-RT; however, the scope of this project left many more questions. First, these animals were irradiated without the presence of a medulloblastoma. While previous experiments show that FLASH-RT is equal to CONV-RT in its ability to control tumor growth, the presence of a tumor could modify the surrounding normal tissue in ways that are unknown. Additionally, tumors are highly vascularized, albeit a modified version of the BBB, and we have not address how the BTB would react to FLASH-RT. Second, This study continued to escalate the dose given to these animals; however, we have not reached the same total dose as palliative care which can reach > 30 Gy delivered in 20 fractions. Our method of 20 Gy delivered in 2 fractions has the potential to deliver a higher amount of damage in a shorter period of time. Third, we have yet to develop a working protocol for a functional endpoint of vascular damage. A small cohort of male mice from this study were used in a preliminary MRI study to measure vasculature health, however, no data was produced by the team leading the experiment. A second experiment was also

performed to measure cerebral microbleeds using a Prussian Blue stain for iron within the brain. While positive controls indicated that the stain worked, no evidence of microbleeds were present in the tissues of animals who had received CONV- or FLASH-RT at this time point. This left us uncertain as to whether cerebral microbleeds is an attainable outcome due to the lack of literature evidence in irradiated rodent models.

Uncovering the protective neurological mechanisms of hypofractionated FLASH radiotherapy

Abstract

Implementation of ultra-high dose-rate FLASH radiotherapy (FLASH-RT) is rapidly gaining traction as a unique cancer treatment modality able to dramatically minimize normal tissue toxicity while maintaining anti-tumor efficacy compared to standard of care radiotherapy at conventional dose rate (CONV-RT). The resultant improvements in the therapeutic index have sparked intense investigations in pursuit of the underlying mechanisms. As a preamble to clinical translation, we exposed non-tumor bearing male and female mice to hypofractionated (3x10 Gy) whole brain FLASH- and CONV-RT to evaluate differential neurological responses using a comprehensive panel of functional and molecular outcomes over a 6-month follow up. In each instance, extensive and rigorous behavioral testing showed FLASH-RT to preserve cognitive indices of learning and memory that corresponded to a similar protection of synaptic plasticity as measured by long-term potentiation (LTP). These beneficial functional outcomes were not found after CONV-RT and were linked to a preservation of synaptic integrity at the molecular (synaptophysin) level and to reductions in neuroinflammation (CD68+ microglia) throughout specific brain regions known to be engaged by our selected cognitive tasks (hippocampus, medial prefrontal cortex). Ultra-structural changes in pre/post-synaptic bouton (Bassoon/Homer-1 puncta) within these same regions of the brain were not found to differ in response to dose rate. With this clinically relevant dosing regimen, we provide a mechanistic blueprint from synapse to cognition detailing how FLASH-RT reduces normal tissue complications in the irradiated brain.

Introduction

Standard radiotherapy (RT) at conventional dose rate (CONV-RT) is routinely used to control malignant growth, typically involving photon modalities delivered at mean dose rates in the range of ~0.03 Gy/sec. Improvements in conformality and stereotactic approaches have greatly improved certain patient outcomes, however curative intent is still hampered by radioresistant tumor recurrence and resultant normal tissue toxicities that define dose tolerances. For decades these fundamental limitations have been tackled by tailoring fractionation schedules combined with technological improvements in imaging and beam delivery to squeeze out relatively incremental gains in the therapeutic index. Ultra-high dose rate FLASH-RT has been shown to afford marked normal tissue sparing while maintaining anti-tumor efficacy, *in vivo* outcomes that define the "FLASH effect"[201,264,265].

Recent work has substantiated the broad ranging capability of FLASH-RT using electrons, photons, and protons to alleviate normal tissue toxicities in the brain, lung, gut, blood, bone, muscle and skin without compromising the tumoricidal activity of ionizing radiation4. Importantly, these findings regarding normal tissue sparing have been validated in fish, mice, cats, dogs, and mini-pigs as well as in multiple preclinical mouse tumor models[266]. The global scope of these far-reaching benefits coupled with the diversity of the normal tissues and tumor types involved has in large part, confounded efforts aimed at elucidating a unifying mechanistic hypothesis able to account for the FLASH effect. Notwithstanding, extensive data derived from the normal mouse brain and mice bearing orthotopic brain tumors has substantiated the promise of FLASH-RT at ameliorating many of the long-lasting neurocognitive and cerebrovascular complications caused by cranial radiotherapy that severely compromise the quality of life of adult and pediatric brain tumor survivors[2,5,9,181,231,267]. In this light, the focus of this study was to

advance our mechanistic understanding of how FLASH-RT forestalls (if not eliminates) the progressive onset of the neurological decrements observed routinely with CONV-RT. The temporal development of normal tissue toxicities associated with standard of care cranial radiotherapy for glioblastoma (GBM, 30fx at 2 Gy +/- temozolomide) have been well documented[268]. Despite promising trials implementing the N-methyl-D-aspartate receptor (NMDAR) antagonist memantine and/or hippocampal sparing[269,270], multifaceted cognitive deficits are inadequately resolved, in part, since these functional outcomes are readouts of network level disruptions not restricted to perturbations of NMDAR signaling or damage to the temporal lobes.

The foregoing provides the rationale for pursing the mechanistic basis of the FLASH sparing effect in the brains of adult male and female mice exposed to hypofractionated cranial FLASH- and CONV-RT previously validated to control GBM and spare cognition[267]. Mice were evaluated on a rigorous behavioral platform beginning 10-weeks after exposure, designed to discriminate the extent of radiation-induced cognitive deficits between the cohorts. In each instance and regardless of sex, FLASH and control cohorts were statistically indistinguishable, whereas CONV cohorts exhibited significant learning and memory impairments on each of the behavioral paradigms administered (Objects in Updated Locations, OUL; Novel Object Recognition, NOR; Light/Dark Box, LDB and Fear Extinction, FE). Cognitive deficits coincided with impaired synaptic plasticity, as electrophysiological assessments of LTP conducted in the hippocampus and/or medial prefrontal cortex showed that CONV-RT inhibited LTP significantly, whereas FLASH-RT did not. Sparing of these critical functional outcomes in the FLASH irradiated brain was investigated at the molecular and structural levels of the synapse. Results show that FLASH preserved synaptic density (synaptophysin), whereas the

structural integrity of pre- and post-synaptic bouton (Bassoon/Homer-1) remained unchanged 6-months post-RT. The beneficial neurobiological effects of FLASH-RT extended to microglia, where a significant increase in the levels of activated CD68+ microglia found after CONV-RT were not evident in FLASH irradiated brains, confirming the relative absence of this key marker of neuroinflammation. Collectively, these new data highlight structural, molecular and functional endpoints that link the neurological benefits of FLASH-RT from synapse to cognition.

Materials and Methods

Animals

Animal procedures were conducted in accordance with the Swiss ethics committee (VD3603) and the University of California, Irvine Institutional Animal Care and Use Committee (IACUC, AUP-21-025) for animal experimentation. Male and female C57Bl/6J mice (n=8/treatment/sex) were purchased from Charles River Laboratories (France, strain code 632) and were allowed to acclimate. Mice were 10-weeks of age at the time of irradiation.

Irradiation

Whole-brain irradiations were performed on a prototype Oriatron 6e, 6-MeW electron beam linear accelerator (LINAC) at the Lausanne University Hospital (Lausanne, Switzerland), as described previously[206]. Extensive description of this prototype Oriatron dosimetry have been previously described[203,204]. Mice received three whole-brain, head only, doses of 10 Gy, separated by 48 hours using a 17-mm graphite applicator at either CONV dose rate (0.09 Gy/s) or ultra-high-dose-rate FLASH delievered in a single 1.8 μs pulse (5.6×10^6 Gy/s). Details of the irradiation parameters are listed in **Table 4.1**.

Experimental design

To determine the neuro-mechanistic basis of the FLASH effect, we exposed adult (10-week-old) male and female mice to a hypofractionated dose (3 x 10 Gy, 48 hours apart) of either FLASH or CONV radiotherapy. Four months post-irradiation, mice performed in a series of behavior assays to assess radiation associated cognitive damage. After six months, mice were sacrificed, and tissues removed/prepared for assessment of endpoints listed below. Visual representation of the experimental design is presented in **Figure 4.1**. Prior to sacrifice, mice were randomly assigned

to either immunohistochemical endpoints (n=4/treatment/sex), molecular (n=5-8 males/treatment) (Fig. 4.1A) or for electrophysiology (n=10-11 females/treatment) (Fig. 4.1B). Mice designated for immunohistochemical analysis were intracardially perfused using 25 mL of heparinized saline followed immediately by 4% paraformaldehyde. Preparation for electrophysiology is described below.

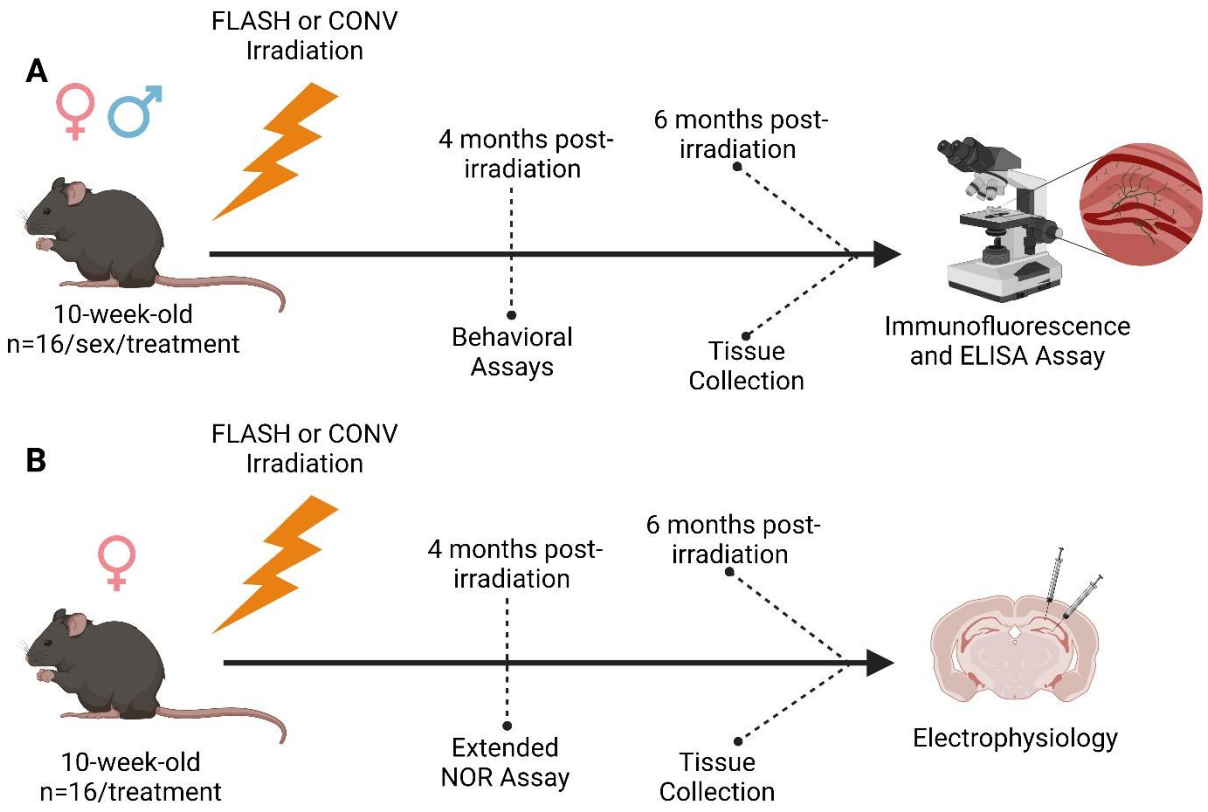

Figure 4.1: Study design.

10-week-old mice received hypofractionated FLASH or CONV irradiation (3 × 10 Gy). (A) Male and female mice underwent behavioral testing 4-months post-irradiation. At 6-months post-irradiation, mice were sacrificed, and tissues were prepared for either immunohistochemical analysis (n=4/sex/treatment) or ELISA (n=5-8/sex/treatment). (B) Female mice were used to assess long-term potentiation. At 4-months post-irradiation, animals performed in the extended NOR behavioral assay (n=16/treatment). At 6-months post-irradiation, mice were sacrificed and prepared for electrophysiological analysis of long term potentiation (n=10-11/treatment).

	Prescribed dose and regimen	
	CONV	FLASH
Beam parameters	3 × 10 Gy	3 × 10 Gy
Graphite applicator type and size (mm) Source-to-surface distance (mm) Pulse repetition frequency (Hz) Pulse width No. of pulses Treatment time (s) Mean dose rate (Gy/s) Instantaneous dose rate (Gy/s)	Hemi-Circular Ø17 800 10 1.0 ms 1170-1180 117 0.1 $8.5x10^{3}$	Hemi-Circular Ø17 209 100 1.8 ms 1 $1.8x10^{-6}$ $5.6x10^{6}$ $5.6x10^{6}$

Table 4.1: Irradiation Parameters, Adults

Fractionated whole brain irradiation was performed on the Oriatron 6e, 6MeV electron beam linear accelerator (LINAC) at Lausanne University Hospital. Mice received 3 doses of 10 Gy separated by 48 hours using a 17mm graphite applicator at either CONV (CONV-RT; 0.09 Gy/s) or ultra-high dose rate FLASH (FLASH-RT, delivered at 5.6×10^{6} Gy/sec in a single 1.8 μs pulse).

Behavioral testing

Behavior apparatus

All behavior was conducted in a dimly lit room inside an arena (30×30×30 cm) lined with a layer of fresh corncob bedding. During Object Updated Location (OUL) testing a thin blue strip of duct-tape was placed on one of the walls of the arena, to serve as an orientating mark. All plastic toys used for OUL and Novel Object Recognition (NOR) were cleaned prior to testing. Sessions were recorded offline using IC Capture for the purpose of offline exploration analysis via an overhead camera.

Objects in Updated Locations Test (OUL)

Mice were handled for two minutes per day for a period of four days prior to a period of habituation inside the empty arenas lasting six consecutive days. After habituation, mice were trained with two identical plastic toys in specific locations (A1, A2) for 3 days. Toys were magnetically fixed 16 cm apart from one another, and the mice were allowed to explore the context for 5 minutes. 24 hours later, one toy was moved to an updated location (A3), and mice were allowed to explore for 5 minutes. Finally, mice were given a retention test, where identical toys were placed in all three previous locations (initial and updated locations (A1, A2, A3)), as well as a fourth toy in a novel location (A4) (n=16/sex/treatment). Preference for the various locations was calculated as a Discrimination Index (DI), ((novel/total exploration time) − (familiar/total exploration time)) × 100.

Novel Object Recognition (NOR)

Mice were habituated for 5 minutes in empty plastic arenas for 1-day post-OUL testing. 24 hours later, mice were then allowed to explore the arena for 5 minutes with identical plastic toys. Mice

were removed from the arena and were placed back into their home cage for 5 minutes. Mice were returned to the arena containing one original and one novel toy and allowed to explore for 5 minutes. Minutes 1-3 were used in the analysis to allow animals a chance to habituate to the toys and arenas (n=13-16/sex/treatment). Additionally, female mice used for electrophysiology performed the long-term NOR test which extended the period of time between the training and testing phase from 5 mins to 24 hours (n=15-16/treatment).

Light-Dark Box (LDB)

Anxiety behavior was evaluated using the LDB test. The LDB arena comprised of an exposed light section (30×20×27 cm) connected to a covered dark section (15×10×27 cm) via a small opening. Mice were allowed to explore the arena for 5 mins; amount of time spent in each section as well as the number of transitions between the two sections were recorded (n=16/treatment).

Fear Extinction (FE)

To test the impact of the treatments on the ability of the mice to learn and extinguish fear responses, we conducted a series of FE experiments. Testing occurred in 2 similar yet different contexts within a behavioral testing chamber (17.5×17.5×18 cm, Coulbourn Instruments) consisting of a steel slat floor (3.2 mm diameter slats, 8 mm spacing). In context A mice were exposed to a vinegar scent, comprised of a solution of 10% vinegar sprayed within the chamber. In context B, metal slats were covered with a plastic tile and mice were exposed to a new scent comprised of a solution of 10% almond extract in a chamber equipped with modified lighting. Fear conditioning was performed in context A, where mice were habituated for 2 minutes; three pairings of a tone (16KHZ, 80dB, 120 secs) with a foot shock (0.6mA, 1 sec) were applied to the

mice. For the following 3 days, the mice underwent extinction training in context B. Mice underwent 2 mins of habituation, before a series of 20 unpaired tones (16KHZ, 80dB, 120 secs) was applied to the mice. Freezing behavior was recorded by an overhead camera and analyzed using an automated motion detection program (FreezeFrame, Cobourn Instruments). Tones 2 – 12 were used for extinction training analysis to allow animals a brief habituation to the chamber and reduce false freezing behavior when animals stop near the end of the 45 min long trial (n=16/sex/treatment).

Mice were then finally tested again in context B with 2 minutes of habituation, followed by a series of 3 unpaired tones (16KHZ, 80dB, 120 secs). Data was recorded using the overhead camera setup and freezing behavior was analyzed using FreezeFrame. A threshold separating values for freezing behavior and motion was set by an investigator, based on identifying a trough separating low and high mobility behaviors.

Electrophysiology

Female mice (n=10-11/treatment, 31 total) were sacrificed for electrophysiology and hippocampal slices prepared as described previously[271]. The uteri of female mice were dissected and weighed prior to LTP assessments, confirming that none of the subjects were in estrus. Mice were anesthetized, decapitated, and the brains rapidly removed into ice-cold, oxygenated dissection medium containing (in mM): 124 NaCl, 3 KCl, 1.25 KH2PO4, 5 MgSO4, 0 CaCl2, 26 NaHCO3, and 10 glucose. Hippocampal slices (340 µm, coronal) were cut from a vibratome (Leica, Model:VT1000S) before transfer to an interface recording containing prewarmed (31 ± 10C) artificial cerebrospinal fluid (aCSF) composed of (in mM): 124 NaCl, 3 KCl, 1.25 KH2PO4, 1.5 MgSO4, 2.5 CaCl2, 26 NaHCO3, and 10 glucose. Slices were perfused

continuously at a rate of 1.75-2 ml/min while the surface of the slices were exposed to warm, humidified 95% O2/5% CO2. Recordings began following at least 2 hr of incubation.

Field excitatory postsynaptic potentials (fEPSPs) were recorded from CA1b stratum radiatum apical dendrites using a glass pipette filled with 2M NaCl (2-3 MΩ) in response to orthodromic stimulation (twisted nichrome wire, 65 µm diameter) of Schaffer collateral-commissural projections in CA1 stratum radiatum. Pulses were administered 0.05 Hz using a current that elicited a 50% maximal spike-free response. After maintaining a stable baseline (20 min), long-term potentiation (LTP) was induced by delivering 5 'theta' bursts, with each burst consisting of four pulses at 100 Hz separated by 200 msec (i.e., theta burst stimulation or TBS). The stimulation intensity was not increased during TBS. Data were collected and digitized by NAC 2.0 (Neurodata Acquisition System, Theta Burst Corp., Irvine, CA) and stored on a disk.

Data in the text are presented as means ± SD, while in the figures as mean ± SEM. The fEPSP slope was measured at 10–90% fall of the slope and data in figures on LTP were normalized to the last 20 min of baseline. Electrophysiological measures were analyzed using a 1-way ANOVA.

Immunofluorescence imaging

Two 30-um thick sections per brain were selected from the ventral hippocampus and the medial prefrontal cortex (mPFC), roughly 300-400 µm apart. Tissues were washed and permeabilized using 0.1% triton in TBS and blocked using 10% goat serum prior to overnight incubation with the following primary antibodies: cluster of differentiation 68 (CD68, 1:500, Biorad), Homer1a (1:500, Synaptic Systems), Bassoon (BSN; 1:500, Neuromab), Synaptophysin (Syn, 1:500, Sigma), Toll-like receptor 4 (TLR4, 1:500, Novus). Tissues were incubated for 1 h at room

temperature with the following secondary antibodies: Donkey anti- rabbit 488 (1:1000, Invitrogen) Goat anti-mouse 647 (1:1000, Abcam) and goat anti-rabbit 555 (1:1000, Invitrogen), before counterstaining with DAPI and being slide mounted. Homer1a and BSN were imaged at 63× using a ZEISS ELYRA7 with Lattice SIM and post processed in Zen and quantified using IMARIS software. CD68 and Syn were imaged on a Nikon Ti2 microscope at 40x magnification.

IMARIS 3d Rendering

All Z-stack images were imported into Imaris version 9.7.0 and deconvoluted using an adaptive, theoretical PSF batch processing. Deconvoluted images were then processed for spot analysis for CD68 and Synaptophysin. To evaluate the mature synaptic binding, Homer1a and BSN super resolution images were analyzed using spot analysis that confirmed any spot larger than 180 nm, but no larger than 300 nm, as positive. A spot-to-spot analysis was performed to only include Homer1a and BSN spots that were within 180 nm of each other, confirming that the spots were touching and interlocked.

Enzyme-linked Immunosorbent Assay (ELISA)

Immediately after fresh dissection, hippocampal tissue from male animals were flash frozen and stored at -80°C. Tissues were lysed in RIPA buffer and supernatant prepared for ELISA testing. Protein concentrations of lysates were determined using a Bradford assay (Bio-Rad). A cytokine panel ELISA kit (Biolegend LEGENDPLEX) was used to detect IL-1β, TNFα, and IL-1α from lysates. Results are presented as fluorescent intensity/µg protein and normalized to controls.

Statistical analysis

All statistical analysis was performed in Prism (Graphpad Software Inc, San Diego California, USA, version 5.04). For all endpoints, averages of individual animal replicates were used to calculate group interactions using a one-way analysis of variance (ANOVA) except for fear extinction group analysis where a two-way ANOVA was performed. Upon significant results, Bonferroni's post-hoc testing was performed to determine statistical significance. For behavioral testing, outliers were removed from the statistical analysis. These outliers are defined as scoring outside 2 standard deviations of the mean. Data are presented as Mean ± SEM. Values of $P \leq 0.05$ were considered statistically significant.

Results

FLASH-RT does not elicit cognitive impairments

To date, the long-term impact of hypofractionated FLASH-RT on neurocognitive function has not been reported using an extensive battery of behavioral testing over protracted post-irradiation times. While past reports have documented cognitive sparing after single dose exposures or in tumor bearing mice with a single task[2,219,231,267], it was uncertain whether such benefits would manifest across multiple tasks under the current dosing regimen and between the sexes. Here we also implemented a more rigorous cross-species relevant (meaning that performance metrics share a commonality between rodents and humans) task, namely the Objects in Updated Locations (OUL)[272]. The OUL task can be used to evaluate if/how irradiation interferes with prior associative recognition memories, proving a more rigorous assessment of how animals respond to increasing cognitive load.

Our behavioral battery was started by assessing performance of male and female mice on the OUL task. A representative image of this test is presented in **Figure 4.2A**. Days 1-3 involved training mice to two identical objects and location, while on day 4 mice were tested on their updated location memory. Control and FLASH irradiated male mice recognized the A_3 location as novel while CONV irradiated mice did not (**Fig. 4.2B**; one-way ANOVA: $F_{(2,38)} = 8.616$; $P = 0.0008$). These data were corroborated in female mice (**Fig. 4.2B**; one-way ANOVA: $F_{(2,42)} = 7.336$; $P = 0.0019$). Following the updating session, mice performed in the testing session (Day 4) where exploration of toy in a novel location was compared to updated information memory (A4 vs A3) and the original fixed toy (A4 vs A1). Male mice exposed to FLASH-RT performed similar to controls, and exhibited DI values that were significantly higher than CONV irradiated male mice (**Fig. 4.2C**; one-way ANOVA: $F_{(2,36)} = 4.448$; $P = 0.0188$). Female mice exhibited

similar but more significant differences than males after exposure to FLASH-RT (**Fig. 4.2C**; one-way ANOVA: $F_{(2,39)}$=12.57; $P < 0.0001$). When comparing novel location to original information (A4 vs A1), male mice exhibited similar albeit non-significant trends, (**Fig. 4.2D**; one-way ANOVA: $F_{(2,36)} = 1.929$; $P = 0.16$). However, FLASH irradiated female mice performed the same as controls while CONV irradiated female mice performed significantly worse (**Fig. 4.2D**; one-way ANOVA: $F_{(2,39)} = 7.236$; $P = 0.0021$).

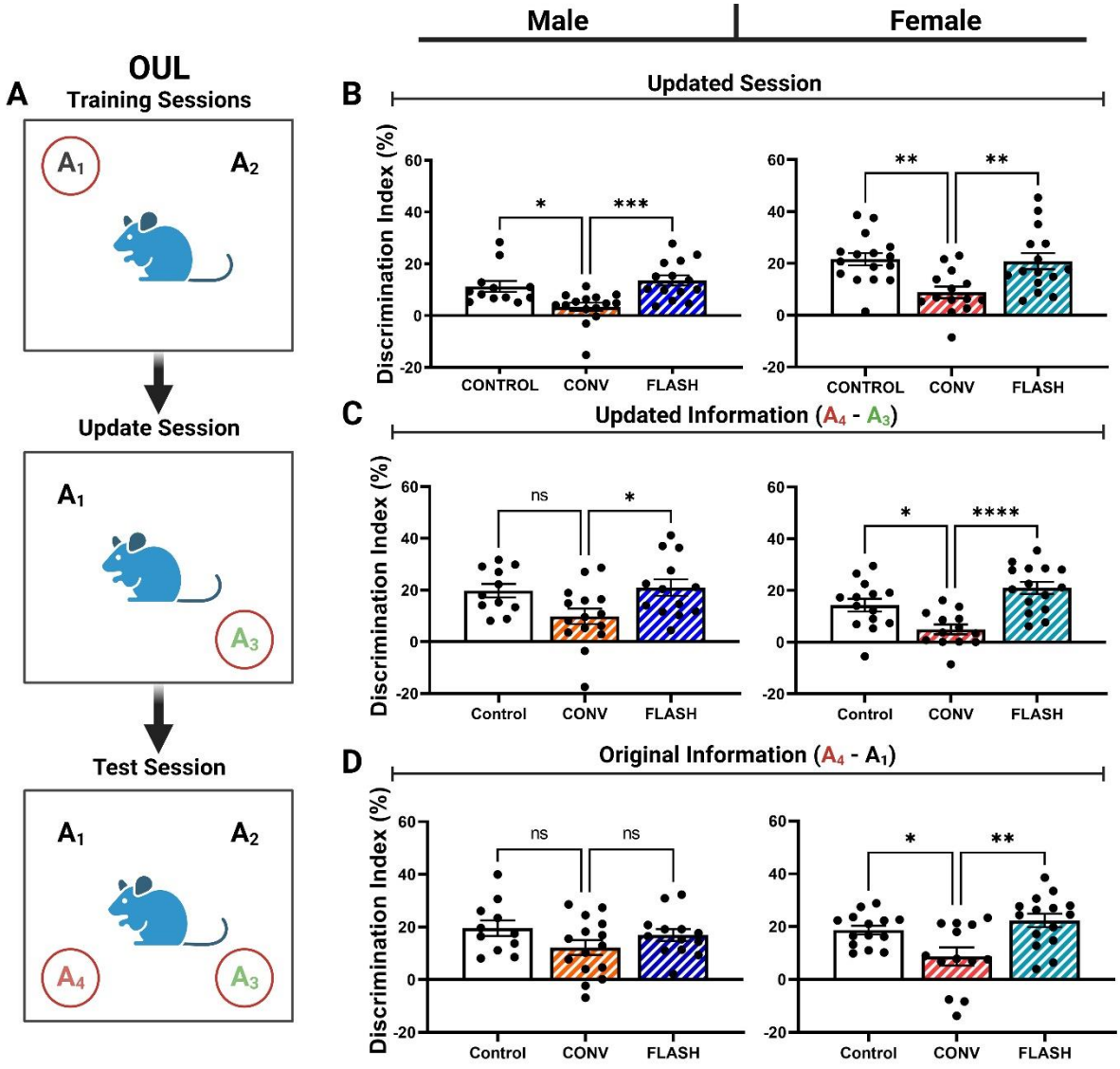

Figure 4.2: Mice exposed to FLASH-RT performed similar to controls in hippocampal dependent learning and memory tests objects in updated location (OUL) while CONV-RT mice did not.

(A) Objects in updated locations testing experimental design. (B) Update session behavior. At 4 months post-irradiation, FLASH and control mice showed preference for the novel toy and location in both males (left) and females (right) while CONV did not. (C) Updated information test session. CONV irradiated female mice failed to learn the updated novel (A_4) object over its

predecessor (A_3) when compared to FLASH and control mice. CONV irradiated male mice performed significantly worse than FLASH mice. (D) Original information test session. CONV irradiated female mice were unable to differentiate between the updated novel location (A_4) and the original location (A_1) while FLASH and control performed similarly. No significant changes in male mice were observed. All data **were analyzed using a one-way** ANOVA followed by Bonferroni's multiple comparison test (n = 11-16/sex/treatment). * = $P \leq 0.05$, ** = $P \leq 0.01$, ns = no significance.

Following OUL testing, mice were analyzed on the novel object recognition task (NOR) to evaluate episodic memory. Male mice exposed to FLASH-RT were indistinguishable from control mice while CONV irradiated mice performed significantly worse than either (**Fig. 4.3A**; one-way ANOVA: $F_{(2,35)}$= 6.403; P = 0.0043). Female mice exposed to FLASH-RT performed similar to controls, however, the CONV-RT cohort did not show a decrement post-irradiation (**Fig. 4.3A**; one-way ANOVA: F(2,42) = 2.922; P = 0.0648).

After completion of the NOR test, mice were evaluated in the light/dark box (LDB) arena. Anxiety is assessed by the number of transitions made between the light and dark areas. Results from this test indicate that control mice performed better than CONV-RT and FLASH-RT in both males (**Fig. 4.3B**; one-way ANOVA: $F_{(2,38)}$=4.603; P=0.0162) and females (**Fig. 4.3B**; one-way ANOVA: $F_{(2,41)}$=6.548; P=0.0034).

The behavioral battery was concluded by assessing freezing behavior of mice in the fear extinction test. Fear extinction refers to the dissociation of a learned response to a prior adverse effect. Both male and female mice learned to associate a tone and mild foot shock during the conditioning phase of the trial. During extinction training (days 2-4), mice were repeatedly exposed to the tone in a new environment and freezing behavior was measured, providing time for mice of both sexes and treatment to dissociate the learned response in a new hippocampal-dependent context. In males, a group effect was found during training (**Fig 4.3C;** Two-way ANOVA: $F_{(2,40)}$ = 3.376, P = 0.0442) and extinction training (**Fig 4.3C;** Two-way ANOVA: $F_{(2,40)}$ = 4.121, P = 0.0236) indicating that CONV irradiation caused animals to increase freezing behavior. A group effect was also found in female animals during the extinction training phase (**Fig 4.3D;** Two-way ANOVA: $F_{(2,45)}$ = 3.287, P = 0.0465) indicating that CONV irradiated animals were unable to reduce freezing behavior when shock stimulus was removed. On the final

day of testing, mice are returned to the original environment where they received a mild foot shock followed by a tone. CONV irradiated mice exhibited higher levels of freezing than control or FLASH in both males (**Fig 4.3E**; One-way ANOVA: $F_{(2,38)} = 5.982$, $P = 0.0055$) and females (**Fig 4.3F**; One-way ANOVA: $F_{(2,41)} = 4.145$, $P = 0.0229$), indicating that FLASH-RT preserved extinction memory in both sexes of mice.

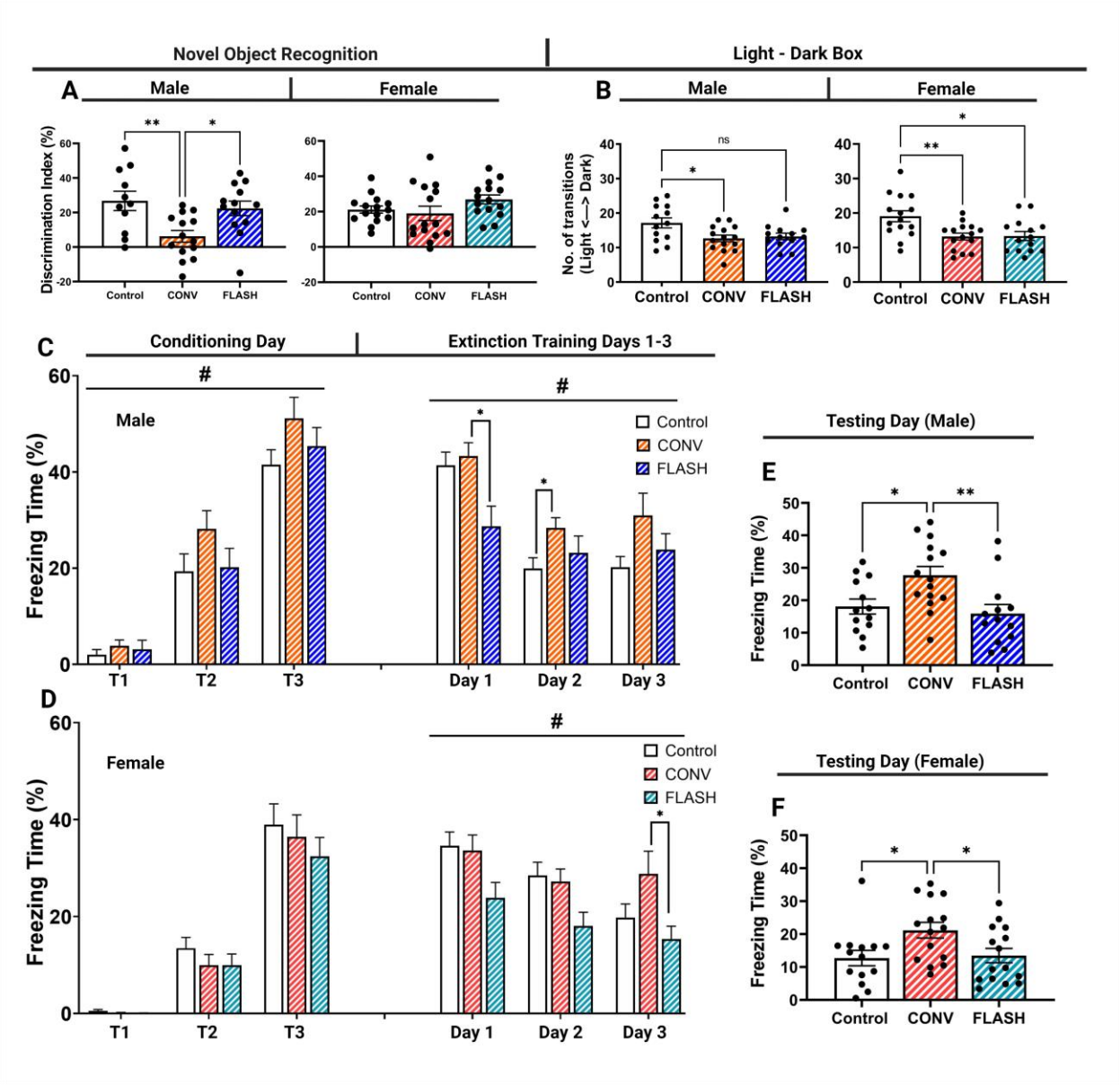

Figure 4.3: Mice exposed to FLASH-RT performed similar to controls in the novel object recognition (NOR), light – dark box (LDB) and fear extinction tests.

(A) NOR testing. Male mice exposed to FLASH-RT performed similar to controls, while CONV-RT were unable to differentiate between the familiar and novel object. Female mice exposed to FLASH-RT and CONV-RT exhibited no significant difference between controls. (B) Measurement of transition between light and dark environments in LDB testing. Male and

female mice exposed to CONV-RT performed significantly worse than controls. Male FLASH-RT mice were not significantly different than controls, however, female mice did not transition between arenas as controls did. (C-D) Fear extinction training and extinction days. Exposure to CONV-RT caused male mice to exhibit increased freezing during training, while this was not observed in FLASH-RT or females. Exposure to CONV-RT also inhibited mice ability disassociate the tone/shock pairing as well as FLASH and controls in males and females. Group effects (#) were found in training days indicate that CONV irradiated animals exhibited increase freezing behavior. (E-F) Fear extinction testing. FLASH and control mice greatly reduced their tone/shock associations while CONV male (left) and female (right) mice did not. Data were analyzed using a one-way or two-way ANOVA followed by Bonferroni's multiple comparison test (n=11-15/sex/treatment). * = $P \leq 0.05$, ** = $P \leq 0.01$, # = $P \leq 0.05$, ns = no significance.

Electrophysiological evaluation reveals the capability of FLASH-RT to preserve long-term potentiation (LTP).

Electrophysiology provides for direct and functional measures of neurotransmission, which can clearly impact behavioral outcomes, and to date, no such measurements have been recorded from the brains of FLASH irradiated mice. Due to the nature of these experiments, prior exposure to mild electrical shock (FE task) could confound such measurements, which necessitated the analysis of a separate cohort of mice (female) subjected to the same hypofractionated regimen. As LTP provides a validated method for assessing synaptic plasticity[273], we hypothesized that this measure of activity-dependent synaptic connections between interconnected hippocampal circuitry might be preserved after FLASH- versus CONV-RT at protracted time points.

To test this, we irradiated a cohort of female mice at 10 weeks of age and tested them 4 months later on an extended (1 day between exploration and testing) NOR task to confirm neurocognitive sparing before LTP assessment. Mice exposed to FLASH-RT performed similar to controls, while CONV irradiated mice were unable to differentiate between the novel and familiar toy (**Fig 4.4A**; One-way ANOVA: $F_{(2,44)}=9.711$, $P=0.0003$). Interestingly, and opposed to the short-term version of this assay on female mice (Fig. 4.3A), the extended NOR assay was able to validate the FLASH effect in this cohort. Following NOR testing, female animals were subjected to the measurement of hippocampal LTP along the Schaffer collaterals.

Theta burst stimulation (TBS) applied to the Schaffer collaterals produced a rapid and robust increase in LTP, quantified as the relative change in the slope of evoked field excitatory postsynaptic potentials (fEPSPs) generated by CA1 apical dendrites (**Fig. 4.4B**). Following the TBS, the fEPSP slope gradually decayed to more stable levels of potentiation for all cohorts. Notably, mean potentiation levels in the fEPSP slope maintained at 1h post-TBS were reduced

significantly in the hippocampus following CONV-RT, but not in control or following FLASH-RT (**Fig. 4.4C**; one-way ANOVA: $F_{(2,28)}$=56.99, P<0.0.0001; Bonferroni *post-hoc*: CONTROL vs CONV: P<0.001; FLASH vs CONV: P<0.0001). Moreover, the fact that these data were collected at protracted post-irradiation times (6 months), suggests that CONV-RT elicits a relative permanent inhibition of LTP, whereas unirradiated controls and FLASH irradiated mice were remarkably, statistically indistinguishable. Such robust functional readouts demonstrate that FLASH-RT can protect the normal tissue structure function relationships of the mouse brain such that synaptic plasticity that underlies critical learning and memory processes can be preserved.

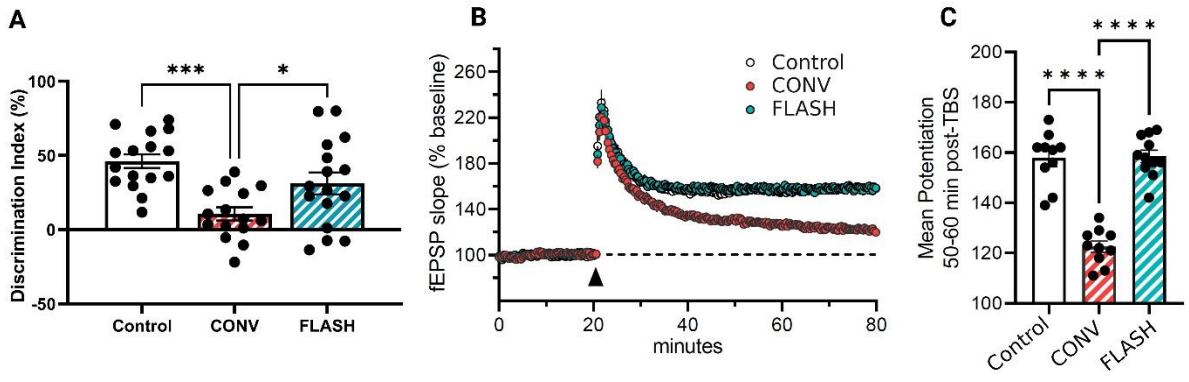

Figure 4.4: FLASH irradiation protects against reductions in long term potentiation (LTP) after CONV irradiation, six months after irradiation.

(A) Extended novel object recognition testing, four months post-irradiation. Female mice that exposed to FLASH-RT performed significantly better than those who received CONV-RT. (n=15-16/treatment) (B) Theta burst stimulation (TBS) applied to the Schaffer collaterals produced a robust increase in fEPSP slope (as percent of baseline) in control and FLASH irradiated female mice but reduced in CONV mice six months after exposure. (C) Levels of potentiation in the fEPSP slope maintained 1h post-TBS was reduced significantly in the hippocampus of CONV-RT mice, but not in control or FLASH irradiated mice. Scale: 1 mV/5 ms. Data were analyzed using a one-way ANOVA followed by Bonferroni's multiple comparison test (n=10-11/treatment). * = $P \leq 0.05$, *** = $P \leq 0.001$, **** = $P \leq 0.0001$.

FLASH irradiation preserves synaptic density in the hippocampus and medial prefrontal cortex (mPFC)

Expression of the major synaptic vesicle protein synaptophysin was evaluated to quantify pre-synaptic vessel density in both the hippocampus and mPFC (**Fig. 4.5A**). A significant decrease in pre-synaptic synaptophysin density after CONV-RT was observed in the hippocampus that was not found after FLASH-RT, 6-months post-irradiation in both males (**Fig. 4.5C**; One-way ANOVA: $F_{(2,9)}$=15.82 , P=0.0011) and females (**Fig. 4.5C**; One-way ANOVA: $F_{(2,8)}$=98.95, P=0.0001). This data was further corroborated in the mPFC finding similar significant differences in females (**Fig. 4.5D**; One-way ANOVA: $F_{(2,9)}$=23.55, P=0.0003), but not in FLASH irradiated males (**Fig. 4.5D**; One-way ANOVA: $F_{(2,9)}$=6.458, P=0.0182). Taken together, these data indicate that FLASH-RT spared synaptophysin density in two distinct regions of the brain, in stark contrast to CONV-RT.

In our previous studies we have shown that FLASH-RT preserved spine density and dendritic complexity after irradiation8. To further scrutinize synaptic connections, we used an ELYRA7 super resolution microscope to evaluate pre- and post- synaptic connectivity (**Fig. 4.5B**). Previous studies evaluating synaptic bouton suggested that an analysis of the juxtaposition of pre-synaptic bassoon (BSN) and post-synaptic homer scaffold protein 1a (Homer1a) puncta would provide a robust analysis of synaptic connections[237]. Our results indicate that no significant changes were found after either irradiation modality in either the male (**Fig. 4.5E**; One-way ANOVA: $F_{(2,9)}$=0.1032, P=0.9030) or female (**Fig. 4.5E**; One-way ANOVA: $F_{(2,9)}$=3.744, P=0.0656) hippocampus, or the male (**Fig. 4.5F**; One-way ANOVA: $F_{(2,9)}$=0.07531, P=0.928) or female (**Fig. 4.5F**; One-way ANOVA: $F_{(2,9)}$=0.4298, P=0.6633) mPFC.

Figure 5

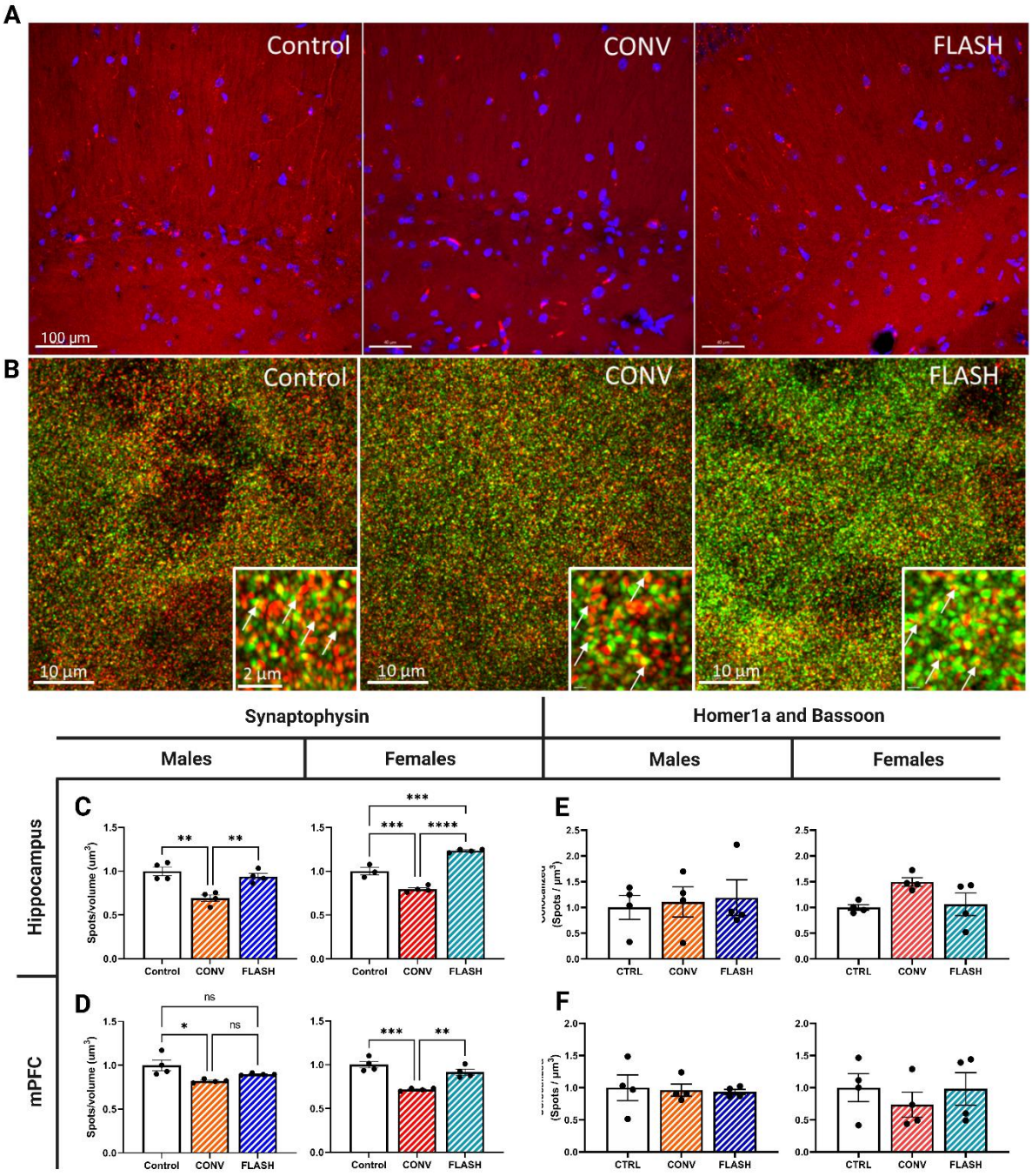

Figure 4.5: FLASH irradiation protects synaptic density and spine morphology, six months after irradiation.

(A) Representative images of synaptophysin (red), DAPI (blue) (Scale bar = 100 μm). (B) Representative image of Homer1a (red)/Bassoon (green), respectively (Scale bar = 10 μm and 2 μm in the zoomed image). (C/D) Quantification of synaptic density using synaptophysin found that FLASH did not induce dendritic disruptions that were observed in mice exposed to CONV-RT in both the Hippocampus and mPFC. (E/F) Quantification of Homer1a and Bassoon spots within 120nm of each other. Male and female mice exhibited no differences between pre- and post- synaptic binding after FLASH or CONV irradiation in the hippocampus or mPFC. All data were analyzed using a one-way ANOVA followed by Bonferroni's multiple comparison test (n=4/sex/treatment, 2 sections analyzed/region/animal). * = $P \leq 0.05$, ** = $P \leq 0.01$, *** = $P \leq 0.001$, **** = $P \leq 0.0001$, ns = no significance.

FLASH-RT does not elicit an inflammatory response after hypofractionation at a protracted time.

Previous work has documented a robust inflammatory response associated with cognitive impairments occurring after radiotherapy[240]. To assess if FLASH-RT induced long-lasting neuroinflammation, measurements of reactive microglia (CD68) (**Fig. 4.6A**) and quantification of IBA1 (microglia) and TLR4 colocalization (**Fig. 6B**) were analyzed using immunofluorescent staining. Data indicated that a robust inflammatory response was found in the hippocampus of mice exposed to CONV-RT, however, FLASH-RT animal expressed levels similar to control in males (**Fig. 4.6B**; One-way ANOVA: $F_{(2,9)}=75.49, P<0.0001$) and females (**Fig. 4.6B**; One-way ANOVA: $F_{(2,9)}=63.31, P<0.0001$). These findings were corroborated in the mPFC in males (**Fig. 4.6C**; One-way ANOVA: $F_{(2,9)}=11.21, P=0.0036$); however, FLASH irradiated females also expressed higher levels of inflammation that controls, though significantly less than CONV (**Fig. 4.6C**; One-way ANOVA: $F_{(2,9)}=153.7, P<0.0001$).

Toll-like receptor 4 (TLR4) is known as a mediator of inflammation which can trigger pro-inflammatory cytokines. Data from IBA1 and TLR4 colocalization analysis found that CONV-RT induced an inflammatory response while FLASH-RT protected the brain, similar to our previous findings of reactive microglia (CD68) in both the male (Fig. 4.6D; One-way ANOVA: $F_{(2,9)}=11.96$, $P=0.0029$) and female (Fig. 4.6D; One-way ANOVA: $F_{(2,9)}=23.91$, $P=0.0003$) hippocampus. These findings were corroborated within the mPFC in both males (Fig. 4.6D; One-way ANOVA: $F_{(2,9)}=18.16$, $P=0.0007$) and females (Fig. 4.6D; One-way ANOVA: $F_{(2,9)}=7.804$, $P=0.0108$). Because TLR4 is known to induce pro-inflammatory cytokines we assessed tissues of male mice using ELISA. Our results indicated that CONV-RT elevated levels of IL-1α when compared to controls while FLASH-RT caused no change (Fig. 4.6E; One-way ANOVA:

$F_{(2,14)}$=4.554, P=0.03). While similar trends of elevated IL-1β and TNFα after CONV-RT were observed, these did not reach significance. These results are consistent with previous findings that co-evaluated neuroinflammation with neurological damage and cognitive impairment[2,231].

Figure 6

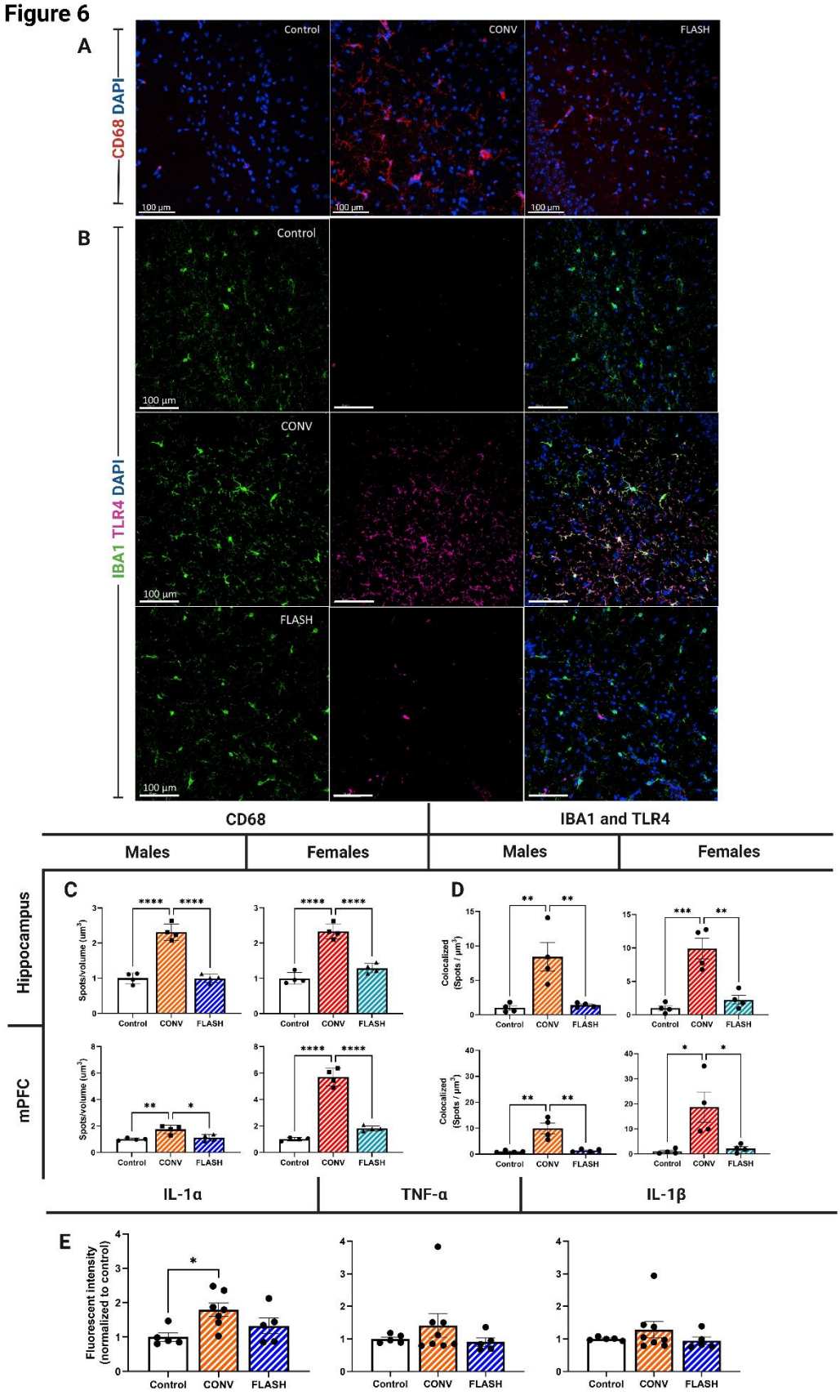
A
CD68 DAPI
Control
CONV
FLASH
100 µm
B
IBA1 TLR4 DAPI
Control
CONV
FLASH
100 µm
CD68
IBA1 and TLR4
Males
Females
Males
Females
Hippocampus
mPFC
C
D
Spots/volume (um³)
Colocalized (Spots / µm³)
Control
CONV
FLASH
IL-1α
TNF-α
IL-1β
E
Fluorescent intensity (normalized to control)

Figure 4.6: FLASH irradiation protected against prolonged inflammation found in CONV mice, six months post-irradiation.

(A) representative images of reactive microglia CD68 (Red) and DAPI (Blue) in the male mouse hippocampus and (B) representative images of IBA1 (Green), TLR4 (Red), and DAPI (Blue) (Scale bar = 100 μm). (C) Quantification of CD68 immunofluorescence in the hippocampus and medial prefrontal cortex. Male (left) and female (right) mice exposed to FLASH-RT exhibit no significant change in CD68 expression while CONV mice expressed a neuroinflammatory response. (D) Quantification of IBA1 and TLR4 colocalization in the hippocampus and medial prefrontal cortex. Male and female mice were protected from increased levels of the neuroinflammatory mediator TLR4 when compared to CONV irradiation. (E) Inflammatory cytokines measured using ELISA. IL-1α exhibited elevated expression after CONV-RT exposure when compared to controls while FLASH induced no changes. No significant changes were observed in TNF-α or IL-1β. All data were analyzed using a one-way ANOVA followed by Bonferroni's multiple comparison test (n=4/sex/treatment, 2 sections analyzed/region/animal). * = $P \leq 0.05$, ** = $P \leq 0.01$, **** = $P \leq 0.0001$.

Discussion

Here we describe the first comprehensive and long-term assessment of critical functional, cellular, and molecular outcomes in the hypofractionated FLASH irradiated mouse brain. The fact that control and FLASH cohorts exhibited outcomes that were statistically similar (if not indistinguishable) across such a varied series of endpoints is remarkable, considering the protracted times of follow-up. In nearly every instance, CONV-RT led to significant disruptions in each endpoint measured that was not observed after FLASH-RT. Neurocognitive benefits tracked with the preservation of synaptic plasticity and integrity through multiple measures that were coincident with reductions in neuroinflammation.

To safely implement FLASH-RT into the clinic the convergence of multiple expertise and continued research is needed. To that end we have focused on delivering a high total fractionated dose to the brain, close to the standard of care currently used for the treatment of brain metastasis[274,275] in efforts to establish a link between critical functional outcomes and key cellular, molecular, and structural mediators of neurotransmission. Our initial focus was to critically evaluate the long-term capability of hypofractionated FLASH-RT to spare neurocognition using an expanded behavioral battery by the inclusion of a cross-species relevant OUL task and an extended (24 h) NOR task in tumor-free animals. It was noteworthy, especially after a total dose of 30 Gy, that data derived from 4 distinct tasks conducted 4-6 months after irradiation, routinely showed that FLASH tracked control cohorts and did not exhibit the significant deficits observed after CONV-RT. Interesting too was that the cognitive benefits of FLASH-RT extended (for the most part) across both sexes, and in no instance was FLASH observed to be more deleterious than CONV-RT. FLASH may not elicit the same level of radiolytic change to preexisting structural elements critical for synaptic transmission. Whether

reduced damage to certain normal tissue targets favors faster tissue repair or remodeling cannot be formally ruled out, however, we have found similar normal tissue sparing in the brain (albeit after different irradiation regimen) from 1-6 months post-exposure. In the end, whatever FLASH damage was produced appears to be below the threshold required to elicit or manifest functional change in the CNS. Such results portend favorable new treatment options for those suffering with brain tumors, where the use of hypofractionated radiosurgery or SBRT-FLASH (brain metastasis) or whole brain FLASH-RT (unresectable glioma, palliative care) may help remediate mid- and longer-term neurocognitive complications.

The fact that indices of learning and memory remained relatively intact after a 30 Gy hypofractionated dose of FLASH-RT points to the preservation of certain synaptic elements involved in neurotransmission. In this regard, electrophysiological assessments provide direct measures of electrical activity within the brain, and long-term potentiation has remained a reliable standard in the field for assessing synaptic plasticity[276,277]. Past work from our lab (albeit using distinctly different irradiation paradigms) has found that paired cell recordings are able to uncover subtle yet significant radiation-induced changes in the excitability profiles of principal cells in select cortical and hippocampus subfields[246,278]. These changes become more significant when excitability is assessed over larger networks involving multiple synapses, suggesting that LTP measures within the hippocampal CA1 might reveal dose rate dependent effects[246,279]. Indeed, FLASH-RT preserved hippocampal LTP identically compared to control cohorts, whereas CONV-RT inhibited LTP significantly. Interestingly, data also suggest that LTP may serve as a biomarker of the FLASH effect, and ongoing studies will confirm the time course of dose-rate dependent changes in LTP at earlier post-irradiation times. In addition, preservation (FLASH) and inhibition (CONV) of LTP appear permanent after irradiation, but

additional studies may identify synaptic substrates able to potentiate or reverse LTP shortly after TBS, in efforts to further evaluate the plasticity of molecular events involved in consolidation of LTP after irradiation. The fact that FLASH-RT preserved this measure of synaptic function corroborates our cognitive data and suggests that FLASH-RT does not perturb the underlying circuit firing along a pathway (Schaffer collaterals) in a hippocampal region evaluated in our cognitive testing. These data suggest that even after hypofractionated FLASH-RT, synaptic functional integrity and neurotransmission can be spared, effects that are clearly perturbed after CONV irradiation.

To assess more formally what components of synaptic architecture might be preserved or disrupted after FLASH- or CONV-RT, we utilized immunohistochemistry to quantify levels of the pre-synaptic marker synaptophysin in the hippocampus and mPFC. The capability of FLASH-RT to preserve the density of pre-synaptic synaptophysin vesicles, which was compromised significantly after CONV-RT suggest a potential underlying mechanism for the preservation of synaptic plasticity assessed by out LTP measurements. To provide a higher resolution analysis of synaptic structures, we utilized super-resolution microscopy to quantify the extent of colocalization between pre- and postsynaptic bouton[237]. The close association ($\leq$ 100 nm) of Bassoon in the pre-synaptic active zone and Homer-1 in the postsynaptic density presumes "tight binding" and provides an indication of whether the structural interaction between these integral synaptic scaffolding proteins was maintained (or not) after FLASH-RT. Colocalization data indicated that the association between Bassoon and Homer-1 in the hippocampus and medial pre-frontal cortex was not changes significantly by irradiation whereas LTP was spared by FLASH-RT only. These results suggest that FLASH preserves synaptic function and the release of neuromediators required for neurocognitive function.

While the precise mechanism by which FLASH limits toxicity in the brain remains difficult to pinpoint, it was not the aim of this study, which focused on later biological events. Our data has provided considerable evidence linking the beneficial effects of FLASH-RT from synapse to cognition. Other publications have however, focused on possible primary events in efforts to rationalize how FLASH might spare normal tissue toxicity which have invoked differential free radical cascades and reduced secondary yields of ROS after FLASH vs CONV[2,265] in addition to the striking absence lipid peroxidation after FLASH vs CONV[280]. These factors likely limit neuroinflammation, in addition to other mechanisms as proposed in our recent review[266] . Here we can speculate that a "certain as yet unidentified" preexisting structural motif may define a target unique to normal tissue that is not as susceptible to radiolytic change. Whether this target is either absent or altered in tumors that renders them equally susceptible to dose rate modulation is uncertain, but based on all available data to date, the FLASH effect likely involves multiple complex responses that are distinct between normal tissue and tumors[266].

Microglia play pleiotropic roles in maintaining the health of the CNS, effects that depend on the specific context (age, disease, endo/exogenous stressor) in which they exist. As the innate macrophages of the CNS, they participate in gliovascular and synaptic remodeling through process motility, secretion of soluble factors and their capacity for phagocytosis[281]. In the irradiated CNS, microglia likely operate though a "sensome" that facilitates their capability to transition between dynamic reactive states able to survey, detect and quickly respond to changes in their local environment[281]. This enables multifunctionality, where microglia can preserve synaptic and vascular integrity (FLASH) or enact opposite responses (CONV) depending on the local cues in which they respond[282–284]. Precisely how these local cues differ in response to dose-rate modulation is uncertain at present but might involve different free radical cascades, as

suggested above. Nonetheless, evidence clearly indicates that the sustained microglial response is sensitive to dose rate-induced changes, where the preservation of a more "normal" unirradiated homeostatic state is more readily achieved when a toxic dose is delivered at FLASH dose rates. Indeed, past work has delineated a variety of important roles they have in directly mediating the radiation response of the CNS[240,285], and how they can modulate information processing important for cognition by potentiating or suppressing inflammation in the brain[286,287]. In response to CONV-RT and other higher LET modalities, reactive microglia have been linked to impaired cognition through the complement signaling cascade[288], reactive astrogliosis and microgliosis that elevate inflammatory cytokines[2]. Many of these pro-inflammatory signatures can be attenuated by microglial depletion[240,289], inhibition of adenosine kinase[290] and the HMGB1/TLR4 signaling axis[291] or in the case of past[2,181,231] and present findings FLASH-RT. The marked capability of FLASH-RT to suppress (if not prevent) persistent elevations in microglial activation after a high dose, hypofractionated regimen point to one of the more significant outcomes of this new cancer treatment modality that should hasten clinical translation.

Using a well characterized FLASH beam (eRT6, Oriatron), this work now provides a proof of concept that hypofractionated FLASH irradiation is beneficial over protracted post-exposure times. While this device is clearly not suitable for clinical radiotherapy of brain tumors, proton FLASH does currently have the beam characteristics more favorable for immediate to mid-term clinical translation. Notwithstanding *in vivo* validation of normal tissue sparing in the brain with pencil beam scanning of larger volumes treated with proton FLASH, the development of very high energy electron (VHEE) and photon FLASH beams may provide suitable solutions in the future. On the topic of mechanism, a topic of intense interest in the field, we can pro-offer 2

ideas. As alluded to above, we suspect that normal cells have certain pre-exiting structural elements that are resistant to radiolytic change at ultra-high dose rates, but one might simply surmise that FLASH and CONV kill tumors the same way. In the second idea, FLASH may induce a metabolic switch in normal cells that promotes a state of quiescence, one that normal tissues can tolerate but tumors cannot. Reduced transcriptional, translational stress and lower macromolecular synthesis may alleviate normal tissue toxicities but may be more consequential to tumors that are more reliant on such processes for growth and survival. We have discussed many of these possibilities among others in further detail in a recent review[266].

As the landscape of modern radiotherapy continues to evolve and improve, so too have patient outcomes. Technological and biological advancements have ushered in a new era of stereotactic conformality that can be coupled with more tumor selective agents that are clearly extending overall survival for nearly every cancer, especially those diagnosed before oligometastatic dissemination[292]. The challenge of targeting malignant subpopulations of cancer cells within our most structurally complex and important organ cannot be overstated, and while the eventual eradication of brain cancer remains a challenge, it is perhaps the target organ that stands to benefit the most from FLASH-RT. While neurosurgery remains the standard, the capability of ionizing radiation to non-invasively penetrate the protective structures of the brain provides FLASH-RT coupled with SBRT and radiosurgery to pursue curative intent while maintaining acceptable long-term normal tissue toxicities for the benefice of patients with brain tumors.

Strengths and Weaknesses

This project was designed to build upon the growing evidence of normal tissue sparing observed after FLASH-irr and which neurocognitive mechanisms are protected that are otherwise altered after CONV-irr. This experiment is the first to test clinically relevant doses of FLASH irradiation (30 Gy total dose) in an animal model of CNS radiotherapy in both male and female mice. While we have not matched clinical palliative care protocols that require 20 or more fractions, we have delivered a biologically equivalent dose that aligns with patient care. While experiments measuring long-term potentiation and dendritic binding are not new to our experiments, this was the first time we have measured the adult brain in a model of GBM. This data gives us new insight to the long-term cognitive benefits that are afforded by using FLASH-RT.

While this study helped expand our knowledge of the neurocognitive protection of FLASH-RT in the adult brain, several aspects of the study were limited in scope. First, this study did not interrogate vasculature endpoints due to several complications. Primarily this was due to animals not being lectin injected, and while other methods of vasculature staining are available, our experience has found that paraformaldehyde fixed tissues are overly cross-linked and unable to bind antibodies. Additionally, this study does not examine a functional endpoint of vascular damage. Second, like previous chapters, we lack animals with GBMs in this study. Protection of the normal tissue is considered crucial in the clinic, but the project does not address the effects of irradiation on a CNS tumor. Our lab devised several studies to address both the lack of vasculature (Chapter 5) and GBM; however transportation of FLASH irradiated tissues with tumors failed to reach UCI and were destroyed in transit, leaving questions regarding tumor vascular changes unanswered. Third, this study had a limited number of animals and required some endpoints to only assess male or female endpoints. This led to assessment of only female

LTP and male inflammation cytokines. Additional cohorts of male animals are being assessed for LTP, however in the past we have found differences in basal inflammation levels based on sex.

Acknowledgements:

This work was supported by NCI grants P01CA244091 (MCV and CLL), R01CA2544892 (MC-V and CLL), SNFS grants Synergia-MAGIC- FNS CRS II5_186369 and Spirit IZSTZ0_198747/1 (MCV and PBZ). We also acknowledge support from the the Optical Biology Core Facility of the Developmental Biology Center, a shared resource supported by the Cancer Center Support Grant (CA-62203) and Center for Complex Biological Systems Support Grant (GM-076516) at the University of California, Irvine. The authors would like to thank V. Grilj and C. Bailat for their assistance in dosimetry and irradiation. This study was made possible in part through access to the Optical Biology Core Facility of the Developmental Biology Center, a shared resource supported by the Cancer Center Support Grant (CA-62203) and Center for Complex Biological Systems Support Grant (GM-076516) at the University of California, Irvine.

Initial results – Cerebral blood flow and oxygen metabolism in mice exposed to FLASH measured by high-speed quantitative optical imaging.

Abstract

Vasculature abnormalities can persist after radiotherapy leading to a host of issues, including microbleeds, edema, and an increased risk of stroke. Conventional (CONV) dose rates used by clinicians are delivered at ~ 0.03 Gy/Sec to balance normal tissue and tumor damage. While modern advancements in cancer treatment include dose fractionation, imaging, and stereotactic approaches, secondary effects of radiotherapy are of concern. Strategies to reduce normal tissue damage are critical to improve treatment as it would allow for escalated doses to be delivered to the target of interest. Ultra-high dose rate FLASH radiotherapy (RT) has a proven record of normal tissue damage mitigation including vasculature and cognitive effects in the CNS when compared to CONV-RT in pre-clinical trials while maintaining tumor control. While this normal tissue sparing effect extends to many different tissue types and species, more work needs to be done to determine the mechanism of action that causes the "FLASH effect." In this light, our group has previously published extensively on the cognitive sparing effects seen after FLASH-RT. The CNS relies heavily on the vasculature to deliver oxygen and glucose to fuel the brain while also removing metabolic waste to reduce neurotoxic effects from buildup. This preliminary experiment is designed to interrogate the CNS vasculature system by utilizing adult mice exposed to 3 x 10 Gy fractions at either FLASH- or CONV-RT dose rates and imaged 10 weeks after irradiation using spatial frequency domain imaging (SFDI) or laser speckle contrast imaging (LSCI). Our finding, while not conclusive, indicates that FLASH-RT protects the cerebellum from vasculature damage but did indicate that oxygen levels were decreases in the skin. Further analysis of data, as well as a larger cohort of animals are likely necessary to tease out significance.

Introduction

Radiotherapy is commonly prescribed to treat malignancies and vascular abnormalities in the central nervous system (CNS). While recent advancements in conformality and stereotactic delivery have improved cancer treatment, increased risk of stroke, microbleeds, and edema continue to be of concern to clinicians, albeit secondary to survival. Recent discoveries utilizing ultra-high dose rate FLASH-radiotherapy (FLASH-RT) have demonstrated tumor control while mitigating early and late blood brain barrier damage in preclinical studies[9,11]. Whether this protection of the microvasculature translates to larger vessels that directly affect cerebral blood flow (CBF) remains unknown.

The complexity of normal brain function is critically dependent on CBF to meet metabolic demands by delivering oxygen and glucose, while simultaneously clearing waste. While the brain only constituents a small fraction of mass relative to the rest of the body, it demands 20% of cardiac output and available systemic oxygen, largely in part to the high metabolic demands and lack of energy storage in the CNS. Additionally, the vasculature of the CNS is designed to maintain blood flow during frequent systemic physiological changes to heart rate and blood pressure through a process known as autoregulation, driven by myogenic tone, metabolic input, and neurogenic mediation[293,294]. The capacity of the cerebral vasculature to maintain homeostasis during fluctuations protects the brain from hypoxia, ischemia, hyperemia, vascular leakage, stroke, and edema[294].

Homeostasis in the brain can be hindered as late radiation effects cause capillary collapse, thickening of basement membranes, and alterations to the blood brain barrier's (BBB) integrity, likely a factor in chronic radiation diseases[260,295]. In addition to these vascular morphological changes come modification to cerebral blood flow after radiotherapy. Both animal and clinical

studies have reported that radiotherapy causes a dose dependent decrease in CBF that correlate with an increase in edema[296297,298]. Additionally, correlation between decreases in CBF post-irradiation have been associated with elevated risk of stroke and ischemia[299]. Considering these secondary sequelae of normal tissue damage cause by radiotherapy, many would stand to benefit from treatment that reduced vascular damage of the normal tissue.

In this light, FLASH-RT potential to persevere the CBF should be considered given the plethora of pre-clinical findings that find minimized vascular and cognitive damage while simultaneously maintaining tumor control. In this study, we seek to utilize two in vivo imaging techniques, Spatial Domain Frequency Imaging (SFDI) and Laser Speckle Imaging (LSI) to measure CBF in mice that received 30 Gy (3 x 10 Gy, CONV or FLASH dose rates) to determine if FLASH-RT modifies blood flow. Additionally, animals underwent a test of functional hyperemia to determine if autoregulation of the vasculature was impacted by irradiation. Unfortunately reverberations in the data and imaging collection did not allow us to analyze the functional hyperemia data, leaving us with only baseline levels of skin and cerebellum vasculature, hemoglobin and oxygenation.

Materials and Methods

Animals

All animal procedures were conducted in accordance to and Swiss ethics committee (VD3241) and the University of California, Irvine Institutional Animal Care and Use Committee (IACUC) for animal experimentation.

To determine if adult animals exposed to FLASH-RT were protected from reduced cerebral blood flow that is normally observed after CONV-RT, 8-week-old female C57Bl/6J mice were irradiated (3×10 Gy, FLASH or CONV irradiation, head only). Animals were shipped to the University of California, Irvine where they were acclimated for 10 weeks before undergoing imaging.

Irradiation

Whole-brain irradiations were performed on a prototype Oriatron 6e, 6-MeW electron beam linear accelerator (LINAC) at the Lausanne University Hospital (Lausanne, Switzerland), as described previously[206]. Extensive description of this prototype Oriatron dosimetry have been previously described[203,204]. Mice received three whole-brain, head only, doses of 10 Gy, separated by 48 hours using a 17-mm graphite applicator at either CONV dose rate (0.09 Gy/s) or ultra-high-dose-rate FLASH delivered in a single 1.8 μs pulse (5.6 × 106 Gy/s).

	Prescribed dose and regimen	
	CONV	FLASH
Beam parameters	3 × 10 Gy	3 × 10 Gy
Graphite applicator type and size (mm) Source-to-surface distance (mm) Pulse repetition frequency (Hz) Pulse width No. of pulses Treatment time (s) Mean dose rate (Gy/s) Instantaneous dose rate (Gy/s)	Hemi-Circular Ø17 800 10 1.0 ms 1170-1180 117 0.1 $8.5x10^{3}$	Hemi-Circular Ø17 209 100 1.8 ms 1 $1.8x10^{-6}$ $5.6x10^{6}$ $5.6x10^{6}$

Table 5.1: Irradiation Parameters, Adult Cerebral Blood Flow

Animal Surgeries and Anesthesia

Just prior to imaging animals were anesthetized using isoflurane/room air [2%(vol/vol) induction, 1.5% (vol/vol) maintenance; Dechra]. Initial Spatial Frequency Domain Imaging were performed (as described below) and then Lidocaine (Lidocaine Hydrochloride Jelly USP, 2%; AKORN) was liberally applied for 2 minutes before removal. A small incision was made between the bregma and lambda points on the skull and fascia was removed. Saline was frequently used to prevent the skull from drying. Once bleeding stopped, a coverslip was used over the skull with saline used to reduce light refraction. Animals underwent an additional SFDI and then LSCI. Five minutes after LSCI began, animals underwent a hypercapnia challenge as CO2 was added to the anesthesia for an additional 5 min before returning animals to room air and isoflurane. An additional 5 minutes of recovery were recorded using LSCI. Animals' wounds were closed using sterile staples and were then injected with buprenorphine (0.03 mg/kg).

Spatial Frequency Domain Imaging

For SFDI, LEDs at three different wavelengths (655, 730, and 850 nm) were used as light sources. The light was directed to a spatial light modulator that projected square-wave patterns onto the brain. Backscattered light was captured using a scientific complementary metal-oxide-semiconductor (sCMOS) camera (Hamamatsu Photonics). An Arduino Due microcontroller board was used to synchronize the camera acquisition, spatial light modulator, and LEDs. For each wavelength, four patterns were projected onto the tissue in sequence. The first pattern was nonmodulated (i.e., DC illumination), and the three subsequent patterns were modulated at spatial frequency $\sim 0.3\ \text{mm}^{-1}$ with three distinct spatial phases to enable demodulation. Thus, there were a total of (3 wavelengths × 4 frames) = 12 frames of SFDI data for each measurement

time point. The detected square wave pattern could be approximated as a sinusoid, allowing demodulation in the manner described previously by our group. Using this acquisition scheme, reconstruction of tissue hemodynamics and CMRO2, at an effective imaging rate of $\sim$14 Hz$\sim$14 Hz was possible. A figure including the layout of equipment for the SFDI is included in **Figure 5.1.**

Laser Speckle Contrast Imaging

For LSI, a light source consisting of an 809 nm laser with long coherence length (Ondax, Monrovia, California) was used. To increase uniformity of illumination over the imaged region of interest (ROI), a ground-glass diffuser (ThorLabs, Inc., Newton, New Jersey) was placed between the laser and the brain. A CCD camera (Point Grey Research Inc., Richmond, BC, Canada) detected the backscattered light with a 10-ms exposure time, resulting in image acquisition at a frame rate of 60 Hz. Using a 5×5 sliding spatial window filter, the equation $K=\sigma/\langle I\rangle$ was employed to calculate the local speckle contrast K at each pixel, where $\langle I\rangle$ is the mean intensity within the filter and σ is the standard deviation within the filter. Then, the speckle flow index (SFI) was determined from the values of K and the exposure time T via a simplified speckle imaging equation SFI=1/(2TK2). Time-resolved SFI curves were generated by taking the mean of the SFI over a selected ROI at each time point. A figure of the LSCI is included in **Figure 5.1**.

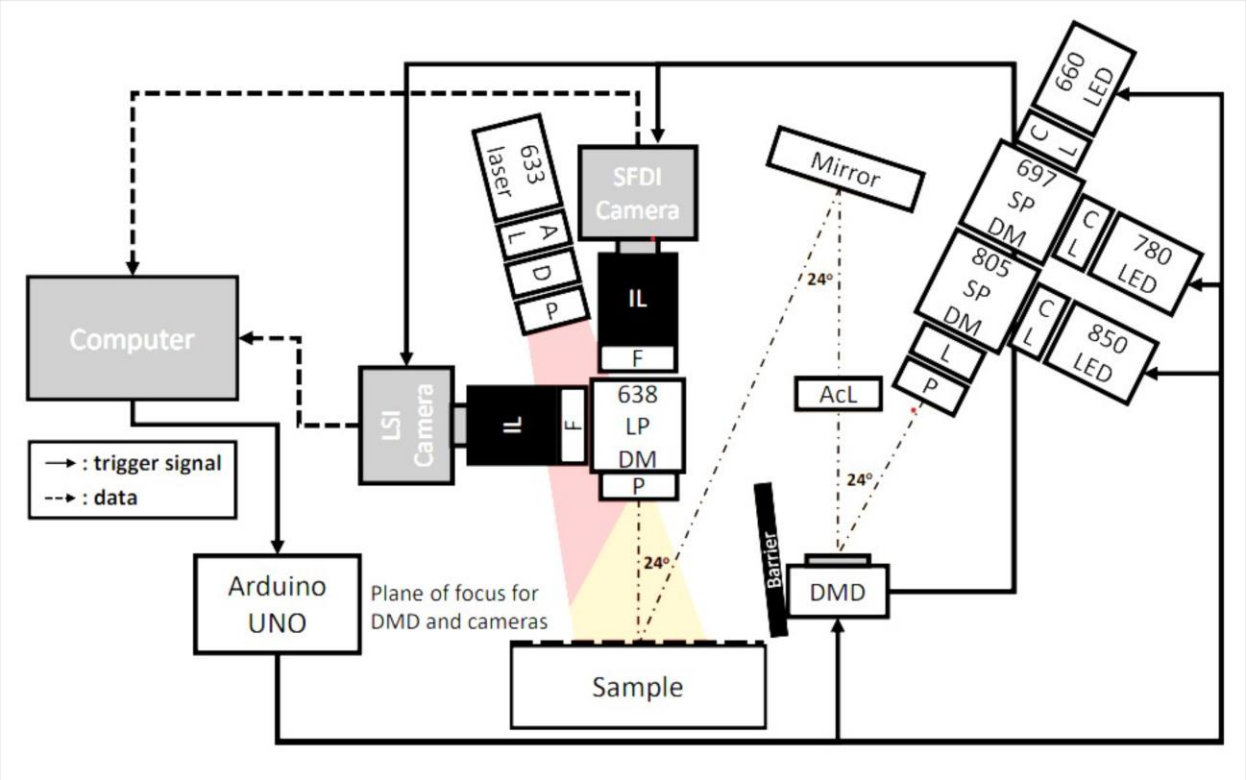

Figure 5.1: Spatial Frequency Domain Imaging and Laser Speckle Contrast Imaging layout

Results

Preliminary results indicate that FLASH protects skin oxygenation levels

Intact vasculature of normal tissue is critical to perfusion of oxygen to tissue. To determine if FLASH-RT protects normal tissue oxygenation, we used LSCI to measure oxygen levels from the head of mice exposed to radiation 5 months prior. Data indicated that conventionally irradiated mice had a reduction in percentage of oxygenation, however this was not significant [**Fig. 5.2:** $F_{(2,3)}=5.166$, $p=0.1067$], likely due to the low animal number (n=2/treatment). This data justified further applications of these imaging techniques with additional animals with clinically relevant doses.

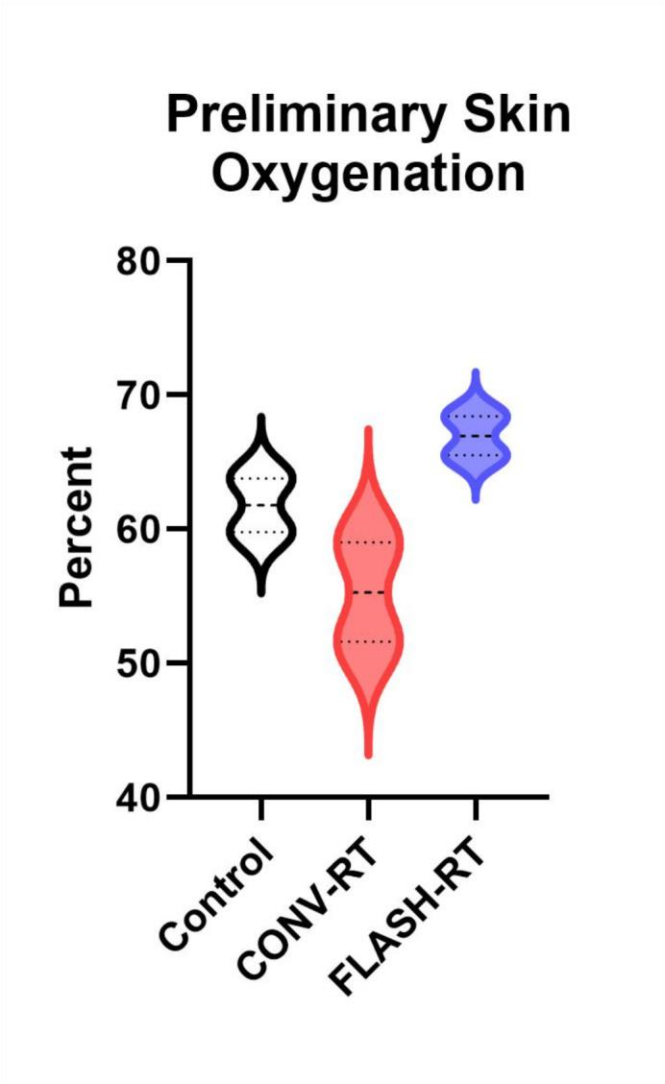

Figure 5.2: Preliminary data suggests that FLASH irradiation protects against radiation induced oxygen depletion from skin, 5 months after irradiation. Oxygenation percentage of the tissue was measured and found a non-significant decrease in CONV irradiated animals, 6 months after irradiation. One-way ANOVA was used to measure variance followed by a Bonferroni post hoc test.

Preliminary results hint that FLASH protects blood flow but reduces oxygen levels in the skin

Building upon the early study results, we utilized animals that received 3 x 10 Gy CONV- or FLASH-RT for further study. Representative images of skin endpoint are shown (**Fig.** 5A) Imaging animals with an intact scalp found no significant between control and FLASH-RT; however CONV-RT is slightly reduced, albeit non significantly in the first minute of imaging [**Fig. 5.3B;** $F_{(2,14)}$=1.242, p=0.3187]. Measurements of hemoglobin concentration (HbT) indicated a slight decrease in both CONV- and FLASH-RT in the first minute of imaging; however this data only bordered significance [**Fig. 5.3C;** $F_{(2,14)}$=3.591, p=0.0551]. Imaging also revealed that there was a significant drop in the percent of oxygenation (StO_2) of the skin when either CONV- or FLASH-RT was used [**Fig. 5.3 D;** $F_{(2,14)}$=11.80, p=0.001]. These findings remain inconclusive and indicate that further analysis of collected data are needed, and potentially additional animals to extract significant data.

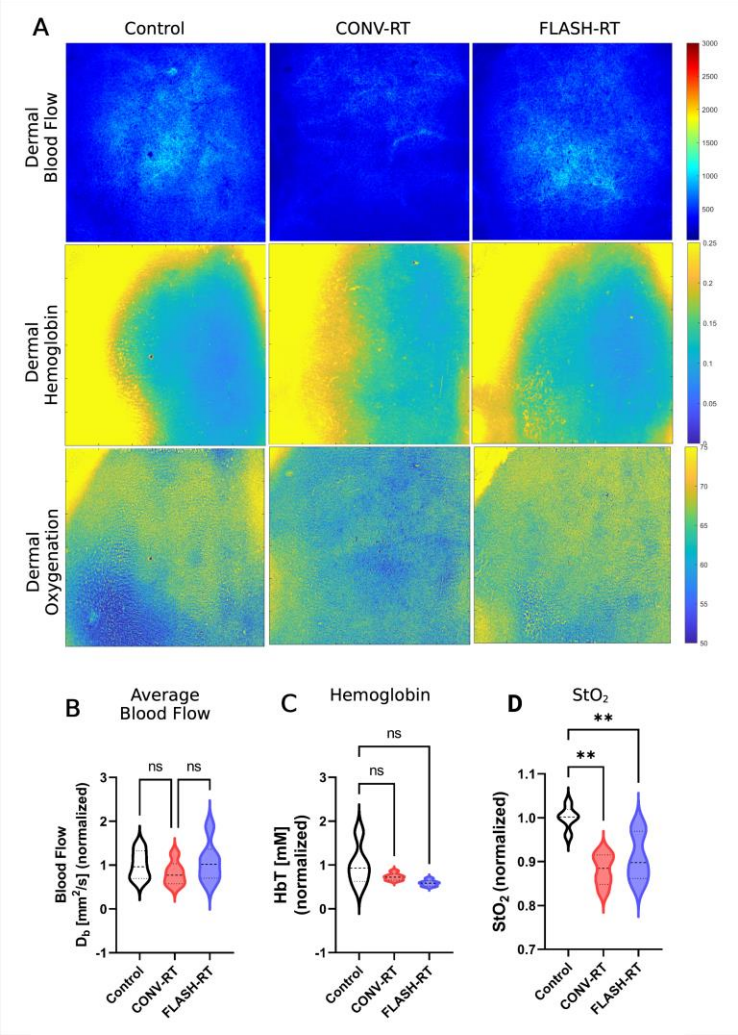

Figure 5.3: Modifications to cerebral blood flow, hemoglobin and oxygenation of the dermis after irradiation using FLASH or CONV dose rates.

(A) Representative images of cranial skin after hair removal for blood flow, hemoglobin, and oxygenation. (B) Measurements of average blood flow found no significant differences between Control, FLASH-RT, or CONV-RT. (C) Hemoglobin levels were not significantly altered after FLASH-RT or CONV-RT. (D) Oxygenation of dermal tissue was significantly lowered after irradiation when compared to controls. All data were analyzed using a one-way ANOVA analysis followed by Bonferroni post-hoc testing (n=5-6 animals/treatment). ** = $P \leq 0.01$.

Preliminary results indicate that no significant changes to baseline levels of blood flow, hemoglobin or oxygen saturation occurred after FLASH- or CONV-RT.

Previous work has indicated that vasculature of the hippocampus is compromised by CONV irradiation but protected by FLASH. To determine if this vasculature protection protects cerebral blood flow and tissue oxygenation levels, we utilized SFDI and LSCI on animals that had had skin and fascia removed from the skull. Representative images of the cerebral endpoints are shown (**Fig. 5.4A**). Initial results indicate a slight drop in cerebral blood flow after irradiation by CONV or FLASH, but variance in the data lead to a lack of significance [**Fig. 5.4B;** $F_{(2,14)}$=0.5390; P = 0.5968]. Additionally, levels of hemoglobin were reduced in both CONV- and FLASH-RT [**Fig. 5.4C;** $F_{(2,14)}$=3.198; P = 0.077], but lacked significance. However, this did not translate into reduced oxygenation within the tissue as FLASH- and CONV-RT did not differ from control [**Fig. 5.4D;** $F_{(2,14)}$=0.0318; P = 0.9687]. Data taken together suggests that some underlying differences may exist; however, use of a limited data set harbored our ability to determine some differences that may be minute.

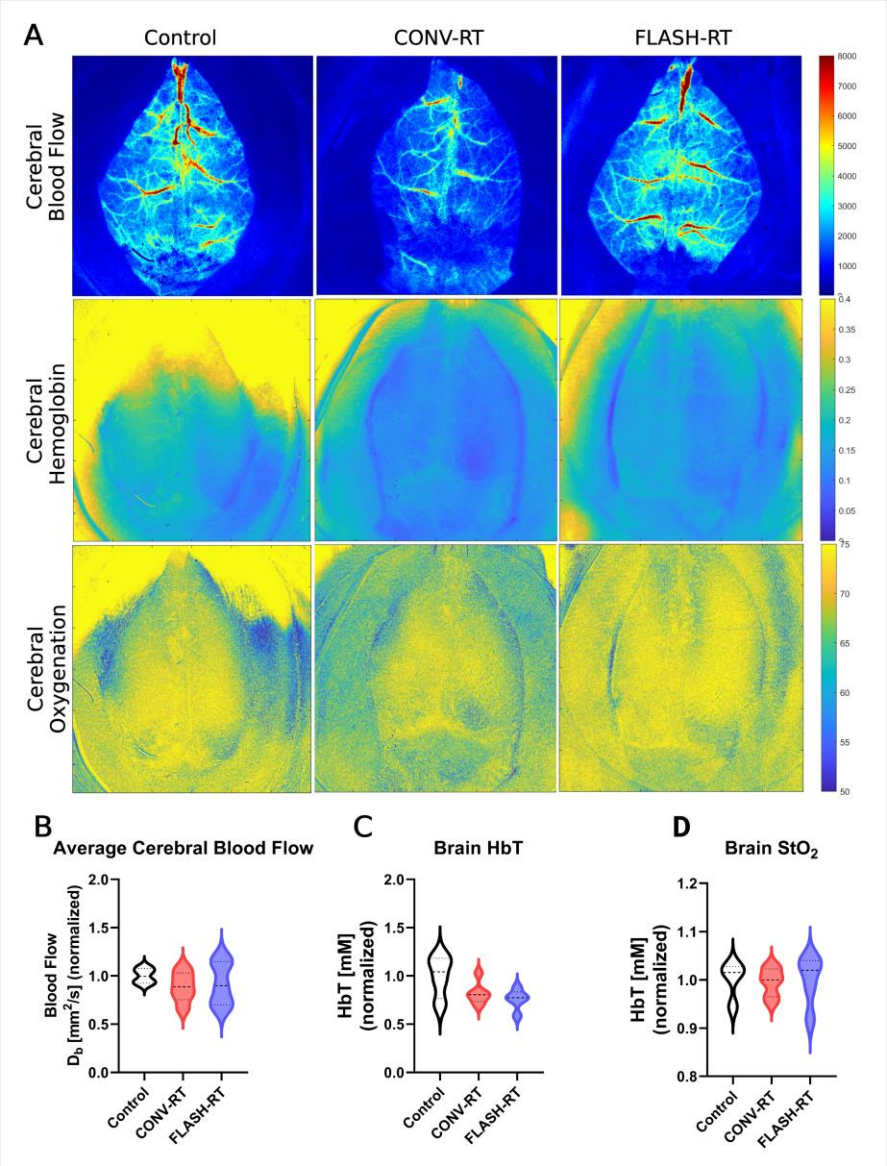

Figure 5.4: Modifications to cerebral blood flow, hemoglobin and oxygenation of the cerebellum after irradiation using FLASH or CONV dose rates.

(A) Representative images of cerebral blood flow, hemoglobin, and oxygenation after irradiation. (B) FLASH- and CONV-RT had no significant decreases in cerebral blood flow after irradiation. (C) Hemoglobin levels in the cerebellum were reduced compared to control, but did not significantly differ. (D) Oxygenation of the cerebellum indicated no significant changes after irradiation. Data was analyzed using a one-way ANOVA analysis followed by a Bonferroni post-hoc test to determine significance (n=4-6).

Discussion

This current study was the first to evaluate FLASH irradiation's effects on cerebral blood flow and oxygenation of the tissue after irradiation, and what potential benefits for patients who receive radiotherapy might exist. Higher doses of radiation are typically used to treat glioblastomas have been shown to reduce blood flow[296,298,299], inhibiting nutrient delivery and metabolic waste removal, potentially causing neurotoxic conditions. In previous pre-clinical studies, clinically relevant doses of FLASH-IRR protected against detrimental damage to vasculature homeostasis[11]. In this study we assessed key aspects of vasculature health including cerebral blood flow, hemoglobin levels, and tissue oxygenation as well as functional hyperemia under conditions of hypercapnia utilizing two novel imaging techniques. Data from this report indicates that FLASH-RT did not induce vasculature damage in the cerebellum; however, our limited data collection from this study did not support that CONV-RT induced significant damage either. Additionally, data collection from the hypercapnia remains under collection, but may lead to limited findings due to a low number of animals and imaging complications.

Aberrations to the vasculature after irradiation have been shown to lead to increases in white matter necrosis, likely stemming from reduced oxygen transfer and removal of metabolic waste that can lead to neurotoxic conditions[198]. Additionally, microbleeds, stroke and cavernous malformation are of concern for patient care[300]. For the treatment of glioblastomas, clinicians frequently use large doses, totaling upwards of 60 Gy delivered in smaller 2 Gy fractions to reduce toxicity; however, these detrimental effects are still observed. By delivering larger doses at less intervals (3 fractions of 10 Gy) we are able to effectively impose the same amount of damage to the brain that routinely observes these detrimental effects in the clinic.

New breakthroughs in the field of in vivo optical imaging techniques[301] have found new and insightful ways to assess vasculature health in patients. By measuring light scattering and doppler scanning, our team has worked to assess blood flow dynamics of animal scalp and cerebellum of animals that received clinically relevant doses of radiation. While we did not achieve significance in the results as hoped for, we did observe trends that average blood flow could be reduced after CONV-RT but maintained in FLASH-RT. Additionally this trend was observed in measurements of cerebral StO_2; however, the opposite was observed in skin. Data regarding the skin oxygenation is not entirely in line with other studies assessing FLASH-RT's dermal protection after irradiation[3], however, these assessments have major key differences, including assessment techniques and species differences. While this is purely speculative at this point, it is clear during the analysis that not enough animals were assessed and warrants further work.

Radiotherapy techniques continue to evolve to improve treatment which benefits both survival and secondary sequelae. While these modifications have predominately focused on different sources of radiation, imaging, and conformality improvements, none have significantly increased the dismal five-year survival rate of glioblastoma patients. Ultra-high dose rate FLASH-RT continues to perform better than CONV-RT in nearly every pre-clinical challenge and the significance of these findings cannot be understated. While there will always more studies to perform and data to interrogate, FLASH continues to prove its worth as a tool in the fight against cancer.

Strengths and Weaknesses

This project was designed to build upon all of the previous chapters by examining a functional endpoint of vasculature integrity after irradiation. We utilized two imaging techniques to determine vasculature regulation and normal tissue hemoglobin/oxygenation levels in animals that received clinically relevant levels of FLASH and CONV irradiation. In addition to these measurements, we interrogated a unique property of cerebral blood flow by exposing animals to a hyperemia CO_2 challenge that measures how well autoregulation of the vasculature response to maintain homeostasis in the brain.

This study was initially designed to interrogate multiple time points and methods of imaging, however, due to several circumstances, not all of our endpoints were realized. First, our largest weakness in the study is that we failed to keep our animals alive long enough to test for multiple time points. Animals that receive a large dose of irradiation that historically cause animals to lose weight and require constant monitoring to keep them alive. In combination with surgery recovery, we unfortunately lost the majority of our irradiated animals over a weekend reducing our n-value to ≥ 2, leading us to cull remaining animals as no further endpoints would be statistically significant/relevant. Second, we only measure CBF in the normal tissue, and do not include tumors as an aim in this study. Tumors are highly vascularized and are shown to have increased blood flow rate when compared to normal tissue. Measurements of oxidation and hypoxia could be of great interest; however, transportation of irradiated, tumor bearing animals from Switzerland (the source of our FLASH irradiator) has proved complicated and imaging techniques may not have yield results due to the penetrative power of the lasers. Third, due to significant animal loss, we were unable to measure molecular endpoints of micro-vasculature health that may have revealed insight into measurements of larger arterial health performed by the LSI and SFDI imaging. Fourth, the hypercapnia portion of the experiment failed to yield relevant data due to large fluctuation that were not previously observed.

References

1. DeAngelis L, Delattre J, Posner J. Radiation-induced dementia in patients cured of brain metastases. *Neurology*. 1989;39(6):789-796. doi:10.1212/WNL.39.6.789

2. Montay-gruel P, Acharya MM, Petersson K, et al. Long-term neurocognitive benefits of FLASH radiotherapy driven by reduced reactive oxygen species. *Proc Natl Acad Sci U S A*. 2020;117(41):25946-25947. doi:10.1073/pnas.2019057117

3. Vozenin MC, De Fornel P, Petersson K, et al. The Advantage of FLASH Radiotherapy Confirmed in Mini-pig and Cat-cancer Patients. *Clinical Cancer Research*. 2019;25(1):35-42. doi:10.1158/1078-0432.CCR-17-3375

4. Bourhis J, Sozzi WJ, Jorge PG, et al. Treatment of a first patient with FLASH-radiotherapy. *Radiotherapy and Oncology*. 2019;139:18-22. doi:10.1016/j.radonc.2019.06.019

5. Montay-Gruel P, Petersson K, Jaccard M, et al. Irradiation in a flash: Unique sparing of memory in mice after whole brain irradiation with dose rates above 100 Gy/s. *Radiotherapy and Oncology*. 2017;124(3):365-369. doi:10.1016/j.radonc.2017.05.003

6. Montay-Gruel P, Bouchet A, Jaccard M, et al. X-rays can trigger the FLASH effect: Ultra-high dose-rate synchrotron light source prevents normal brain injury after whole brain irradiation in mice. *Radiotherapy and Oncology*. 2018;129(3):582-588. doi:10.1016/j.radonc.2018.08.016

7. Vozenin MC, de Fornel P, Petersson K, et al. The Advantage of FLASH Radiotherapy Confirmed in Mini-pig and Cat-cancer Patients. *Clinical Cancer Research*. 2019;25(1):35-42. doi:10.1158/1078-0432.CCR-17-3375

8. Velalopoulou A, Karagounis I v, Cramer GM, et al. FLASH proton radiotherapy spares normal epithelial and mesenchymal tissues while preserving sarcoma response. Published online 2021. doi:10.1158/0008-5472.CAN-21-1500

9. Allen BD, Acharya MM, Montay-Gruel P, et al. Maintenance of Tight Junction Integrity in the Absence of Vascular Dilation in the Brain of Mice Exposed to Ultra-High-Dose-Rate FLASH Irradiation. *Radiat Res*. 2020;194(6):625-635. doi:10.1667/RADE-20-00060.1

10. Allen BD, Limoli CL. Breaking barriers: Neurodegenerative repercussions of radiotherapy induced damage on the blood-brain and blood-tumor barrier. *Free Radic Biol Med*. 2021;178(October 2021):189-201. doi:10.1016/j.freeradbiomed.2021.12.002

11. Allen BD, Alaghband Y, Kramár EA, et al. Elucidating the neurological mechanism of the FLASH effect in juvenile mice exposed to hypofractionated radiotherapy. *Neuro Oncol*. 2022;(November):1-13. doi:10.1093/neuonc/noac248

12. Patel MM, Patel BM. Crossing the Blood–Brain Barrier: Recent Advances in Drug Delivery to the Brain. *CNS Drugs*. 2017;31(2):109-133. doi:10.1007/s40263-016-0405-9

13. Sanchez-Covarrubias L, Slosky LM, Thompson BJ, Davis TP, Ronaldson PT. Transporters at CNS Barrier Sites: Obstacles or Opportunities for Drug Delivery? *Curr Pharm Des*. 2014;20(10):1422. Accessed July 7, 2021. /pmc/articles/PMC3913737/

14. Quail DF, Joyce JA. The Microenvironmental Landscape of Brain Tumors. *Cancer Cell*. 2017;31(3):326-341. doi:10.1016/j.ccell.2017.02.009

15. Jain RK, di Tomaso E, Duda DG, Loeffler JS, Sorensen AG, Batchelor TT. Angiogenesis in brain tumours. *Nat Rev Neurosci*. 2007;8(8):610-622. doi:10.1038/nrn2175

16. Arvanitis CD, Ferraro GB, Jain RK. The blood–brain barrier and blood–tumour barrier in brain tumours and metastases. *Nat Rev Cancer*. 2020;20(1):26-41. doi:10.1038/s41568-019-0205-x

17. Teng F, Tsien CI, Lawrence TS, Cao Y. Blood–tumor barrier opening changes in brain metastases from pre to one-month post radiation therapy. *Radiotherapy and Oncology*. 2017;125(1):89-93. doi:10.1016/j.radonc.2017.08.006

18. Rubin P, Gash DM, Hansen JT, Nelson DF, Williams JP. Disruption of the blood-brain barrier as the primary effect of CNS irradiation. *Radiotherapy and Oncology*. 1994;31(1):51-60. doi:10.1016/0167-8140(94)90413-8

19. Nordal RA, Wong CS. Molecular targets in radiation-induced blood-brain barrier disruption. In: *International Journal of Radiation Oncology Biology Physics*. Vol 62. Elsevier Inc.; 2005:279-287. doi:10.1016/j.ijrobp.2005.01.039

20. Demeule M, Régina A, Jodoin J, et al. Drug transport to the brain: Key roles for the efflux pump P-glycoprotein in the blood-brain barrier. *Vascul Pharmacol*. 2002;38(6):339-348. doi:10.1016/S1537-1891(02)00201-X

21. Stamatovic S, Keep R, Andjelkovic A. Brain Endothelial Cell-Cell Junctions: How to “Open” the Blood Brain Barrier. *Curr Neuropharmacol*. 2008;6(3):179-192. doi:10.2174/157015908785777210

22. Ayloo S, Gu C. Transcytosis at the blood–brain barrier. *Curr Opin Neurobiol*. 2019;57:32-38. doi:10.1016/j.conb.2018.12.014

23. Pardridge WM. Drug transport across the blood-brain barrier. *Journal of Cerebral Blood Flow and Metabolism*. 2012;32(11):1959-1972. doi:10.1038/jcbfm.2012.126

24. Ostrom QT, Cioffi G, Gittleman H, et al. CBTRUS Statistical Report: Primary Brain and Other Central Nervous System Tumors Diagnosed in the United States in 2012-2016. *Neuro Oncol*. 2019;21(S5):V1-V100. doi:10.1093/neuonc/noz150

25. Fortin D. The Blood-Brain Barrier: Its Influence in the Treatment of Brain Tumors Metastases. *Curr Cancer Drug Targets*. 2012;12(3):247-259. doi:10.2174/156800912799277511

26. Arvanitis CD, Ferraro GB. The blood – brain barrier and blood – tumour barrier in brain tumours and metastases. *Nat Rev Cancer*. 2020;20(January). doi:10.1038/s41568-019-0205-x

27. Lockman PR, Mittapalli RK, Taskar KS, et al. Heterogeneous blood-tumor barrier permeability determines drug efficacy in experimental brain metastases of breast cancer. *Clinical Cancer Research*. 2010;16(23):5664-5678. doi:10.1158/1078-0432.CCR-10-1564

28. Groeneveld GJ, Hay JL, van Gerven JM. Measuring blood–brain barrier penetration using the NeuroCart, a CNS test battery. *Drug Discov Today Technol*. 2016;20:27-34. doi:10.1016/j.ddtec.2016.07.004

29. Appelboom G, Detappe A, LoPresti M, et al. Stereotactic modulation of blood-brain barrier permeability to enhance drug delivery. *Neuro Oncol*. 2016;18(12):1601-1609. doi:10.1093/neuonc/now137

30. Fauquette W, Amourette C, Dehouck MP, Diserbo M. Radiation-induced blood-brain barrier damages: An in vitro study. *Brain Res*. 2012;1433:114-126. doi:10.1016/j.brainres.2011.11.022

31. Wang JB, di Ianni T, Vyas DB, et al. Focused Ultrasound for Noninvasive, Focal Pharmacologic Neurointervention. *Front Neurosci*. 2020;14. doi:10.3389/fnins.2020.00675

32. Abrahao A, Meng Y, Llinas M, et al. First-in-human trial of blood–brain barrier opening in amyotrophic lateral sclerosis using MR-guided focused ultrasound. *Nat Commun*. 2019;10(1):1-9. doi:10.1038/s41467-019-12426-9

33. Lajoie JM, Shusta E v, Engineering B. HHS Public Access. 2016;(608):613-631. doi:10.1146/annurev-pharmtox-010814-124852.Targeting

34. S S, W Z. ABC transporters and drug efflux at the blood-brain barrier. *Rev Neurosci*. 2010;21(1):29-53. doi:10.1515/REVNEURO.2010.21.1.29

35. Miller DS. Regulation of P-glycoprotein and other ABC drug transporters at the blood-brain barrier. *Trends Pharmacol Sci*. 2010;31(6):246. doi:10.1016/J.TIPS.2010.03.003

36. Lankford J, Butler IJ, Koenig MK. Glucose Transporter Type I Deficiency Causing Mitochondrial Dysfunction: *http://dx.doi.org/101177/0883073811426503*. 2011;27(6):796-798. doi:10.1177/0883073811426503

37. Ben-Zvi A, Lacoste B, Kur E, et al. Mfsd2a is critical for the formation and function of the blood-brain barrier. *Nature*. 2014;509(7501):507-511. doi:10.1038/nature13324

38. Alakbarzade V, Hameed A, Quek DQY, et al. A partially inactivating mutation in the sodium-dependent lysophosphatidylcholine transporter MFSD2A causes a non-lethal microcephaly syndrome. *Nature Genetics 2015 47:7*. 2015;47(7):814-817. doi:10.1038/ng.3313

39. Guemez-Gamboa A, Nguyen LN, Yang H, et al. Inactivating mutations in MFSD2A , required for omega-3 fatty acid transport in brain, cause a lethal microcephaly syndrome. *Nature Genetics 2015 47:7*. 2015;47(7):809-813. doi:10.1038/ng.3311

40. Martínez-Estrada OM, Villa A, Breviario F, Orsenigo F, Dejana E, Bazzoni G. Association of Junctional Adhesion Molecule with Calcium/calmodulin-dependent Serine Protein Kinase (CASK/LIN-2) in Human Epithelial Caco-2 Cells. *Journal of Biological Chemistry*. 2001;276(12):9291-9296. doi:10.1074/jbc.M006991200

41. Bazzoni G, Martínez-Estrada OM, Orsenigo F, Cordenonsi M, Citi S, Dejana E. Interaction of junctional adhesion molecule with the tight junction components ZO-1, cingulin, and occludin. *Journal of Biological Chemistry*. 2000;275(27):20520-20526. doi:10.1074/jbc.M905251199

42. Abbott NJ, Patabendige AAK, Dolman DEM, Yusof SR, Begley DJ. Structure and function of the blood-brain barrier. *Neurobiol Dis*. 2010;37(1):13-25. doi:10.1016/j.nbd.2009.07.030

43. Stephenson RE, Higashi T, Erofeev IS, et al. Rho Flares Repair Local Tight Junction Leaks. *Dev Cell*. 2019;48(4):445-459.e5. doi:10.1016/j.devcel.2019.01.016

44. Armulik A, Genové G, Betsholtz C. Pericytes: Developmental, Physiological, and Pathological Perspectives, Problems, and Promises. *Dev Cell*. 2011;21(2):193-215. doi:10.1016/J.DEVCEL.2011.07.001

45. Hall CN, Reynell C, Gesslein B, et al. Capillary pericytes regulate cerebral blood flow in health and disease. *Nature*. 2014;508(1):55-60. doi:10.1038/nature13165

46. Brown LS, Foster CG, Courtney J maree, et al. Pericytes and Neurovascular Function in the Healthy and Diseased Brain. 2019;13(June):1-9. doi:10.3389/fncel.2019.00282

47. Alarcon-Martinez L, Yilmaz-Ozcan S, Yemisci M, et al. Capillary pericytes express α-smooth muscle actin, which requires prevention of filamentous-actin depolymerization for detection. *Elife*. 2018;7. doi:10.7554/eLife.34861

48. Rucker HK, Wynder HJ, Thomas WE. Cellular mechanisms of CNS pericytes. *Brain Res Bull*. 2000;51(5):363-369. doi:10.1016/S0361-9230(99)00260-9

49. Bergers G, Song S. The role of pericytes in blood-vessel formation and maintenance. *Neuro Oncol*. 2005;7(4):452-464. doi:10.1215/S1152851705000232

50. Ribatti D, Nico B, Crivellato E. The role of pericytes in angiogenesis. *Int J Dev Biol*. 2011;55(3):261-268. doi:10.1387/ijdb.103167dr

51. Nehls V, Zeitler-Zapf P, Drenckhahn D. Different sequences of expression of band 3, spectrin, and ankyrin during normal erythropoiesis and erythroleukemia. *Am J Pathol*. 1993;142(5):1565. Accessed July 5, 2021. /pmc/articles/PMC1886907/?report=abstract

52. Morikawa S, Baluk P, Kaidoh T, Haskell A, Jain RK, McDonald DM. Abnormalities in pericytes on blood vessels and endothelial sprouts in tumors. *American Journal of Pathology*. 2002;160(3):985-1000. doi:10.1016/S0002-9440(10)64920-6

53. Rustenhoven J, Jansson D, Smyth LC, Dragunow M. Brain Pericytes As Mediators of Neuroinflammation. *Trends Pharmacol Sci*. 2017;38(3):291-304. doi:10.1016/j.tips.2016.12.001

54. Underly RG, Levy M, Hartmann DA, Grant RI, Watson AN, Shih AY. Pericytes as inducers of rapid, matrix metalloproteinase-9-dependent capillary damage during ischemia. *Journal of Neuroscience*. 2017;37(1):129-140. doi:10.1523/JNEUROSCI.2891-16.2016

55. Chen F, Ohashi N, Li W, Eckman C, Nguyen JH. Disruptions of occludin and claudin-5 in brain endothelial cells in vitro and in brains of mice with acute liver failure. *Hepatology*. 2009;50(6):1914-1923. doi:10.1002/hep.23203

56. Sagare AP, Bell RD, Zhao Z, et al. Pericyte loss influences Alzheimer-like neurodegeneration in mice. *Nat Commun*. 2013;4. doi:10.1038/NCOMMS3932

57. Nakagawa S, Deli MA, Kawaguchi H, et al. A new blood-brain barrier model using primary rat brain endothelial cells, pericytes and astrocytes. *Neurochem Int*. 2009;54(3-4):253-263. doi:10.1016/j.neuint.2008.12.002

58. Puech C, Hodin S, Forest V, et al. Assessment of HBEC-5i endothelial cell line cultivated in astrocyte conditioned medium as a human blood-brain barrier model for ABC drug transport studies. *Int J Pharm*. 2018;551(1-2):281-289. doi:10.1016/j.ijpharm.2018.09.040

59. Shan Y, Tan S, Lin Y, et al. The glucagon-like peptide-1 receptor agonist reduces inflammation and blood-brain barrier breakdown in an astrocyte-dependent manner in experimental stroke. *J Neuroinflammation*. 2019;16(1). doi:10.1186/s12974-019-1638-6

60. Tiwary S, Morales JE, Kwiatkowski SC, Lang FF, Rao G, McCarty JH. Metastatic brain tumors disrupt the blood-brain barrier and alter lipid metabolism by inhibiting expression of the endothelial cell fatty acid transporter Mfsd2a. *Sci Rep*. 2018;8(1):1-13. doi:10.1038/s41598-018-26636-6

61. Argaw AT, Asp L, Zhang J, et al. Astrocyte-derived VEGF-A drives blood-brain barrier disruption in CNS inflammatory disease. *Journal of Clinical Investigation*. 2012;122(7):2454-2468. doi:10.1172/JCI60842

62. Argaw AT, Gurfein BT, Zhang Y, Zameer A, John GR. VEGF-mediated disruption of endothelial CLN-5 promotes blood-brain barrier breakdown. *Proc Natl Acad Sci U S A*. 2009;106(6):1977-1982. doi:10.1073/pnas.0808698106

63. Zhang ZG, Zhang L, Jiang Q, et al. VEGF enhances angiogenesis and promotes blood-brain barrier leakage in the ischemic brain. *Journal of Clinical Investigation*. 2000;106(7):829-838. doi:10.1172/JCI9369

64. Chapouly C, Argaw AT, Horng S, et al. Astrocytic TYMP and VEGFA drive blood-brain barrier opening in inflammatory central nervous system lesions. *Brain*. 2015;138(6):1548-1567. doi:10.1093/brain/awv077

65. Chen F, Ohashi N, Li W, Eckman C, Nguyen JH. Disruptions of occludin and claudin-5 in brain endothelial cells in vitro and in brains of mice with acute liver failure. *Hepatology*. 2009;50(6):1914-1923. doi:10.1002/hep.23203

66. Y Y, EY E, JF T, W L, GA R. Matrix metalloproteinase-mediated disruption of tight junction proteins in cerebral vessels is reversed by synthetic matrix metalloproteinase inhibitor in focal ischemia in rat. *J Cereb Blood Flow Metab*. 2007;27(4):697-709. doi:10.1038/SJ.JCBFM.9600375

67. Yang Y, Rosenberg GA. MMP-mediated disruption of claudin-5 in the blood-brain barrier of rat brain after cerebral ischemia. *Methods in Molecular Biology*. 2011;762:333-345. doi:10.1007/978-1-61779-185-7_24

68. Girouard H, Iadecola C. HIGHLIGHTED TOPIC Regulation of the Cerebral Circulation Neurovascular coupling in the normal brain and in hypertension, stroke, and Alzheimer disease. *J Appl Physiol*. 2006;100:328-335. doi:10.1152/japplphysiol.00966.2005.-The

69. Herron PO, Chhatbar PY, Levy M, et al. Neural correlates of single-vessel haemodynamic responses in vivo. *Nature*. 2016;534(7607):378-382. doi:10.1038/nature17965

70. G Y, Y Z, ME R, C I. Attenuation of activity-induced increases in cerebellar blood flow in mice lacking neuronal nitric oxide synthase. *Am J Physiol Heart Circ Physiol*. 2003;285(1). doi:10.1152/AJPHEART.00043.2003

71. Ma J, Ayata C, Huang PL, Fishman MC, Moskowitz MA. Regional cerebral blood flow response to vibrissal stimulation in mice lacking type I NOS gene expression. *https://doi.org/101152/ajpheart19962703H1085*. 1996;270(3 39-3). doi:10.1152/AJPHEART.1996.270.3.H1085

72. Lindauer U, Megow D, Matsuda H, Dirnagl U. Nitric oxide: A modulator, but not a mediator, of neurovascular coupling in rat somatosensory cortex. *Am J Physiol Heart Circ Physiol*. 1999;277(2 46-2):799-811. doi:10.1152/ajpheart.1999.277.2.h799

73. Faraci FM, Breese KR. Nitric oxide mediates vasodilatation in response to activation of N- methyl-D-aspartate receptors in brain. *Circ Res*. 1993;72(2):476-480. doi:10.1161/01.RES.72.2.476

74. Hillman EMC. Coupling Mechanism and Significance of the BOLD Signal: A Status Report. doi:10.1146/annurev-neuro-071013-014111

75. Iadecola C. Neurovascular regulation in the normal brain and in Alzheimer's disease. *Nat Rev Neurosci*. 2004;5(5):347-360. doi:10.1038/nrn1387

76. Chen BR, Kozberg MG, Bouchard MB, Shaik MA, Hillman EMC. A critical role for the vascular endothelium in functional neurovascular coupling in the brain. *J Am Heart Assoc*. 2014;3(3):1-14. doi:10.1161/JAHA.114.000787

77. DC R. The roles of intracellular protein-degradation pathways in neurodegeneration. *Nature*. 2006;443(7113):780-786. doi:10.1038/NATURE05291

78. Iliff JJ, Wang M, Liao Y, et al. CEREBROSPINAL FLUID CIRCULATION A Paravascular Pathway Facilitates CSF Flow Through the Brain Parenchyma and the Clearance of Interstitial Solutes , Including Amyloid b. 2012;4(147).

79. Iliff JJ, Wang M, Zeppenfeld DM, et al. Cerebral Arterial Pulsation Drives Paravascular CSF – Interstitial Fluid Exchange in the Murine Brain. 2013;33(46):18190-18199. doi:10.1523/JNEUROSCI.1592-13.2013

80. Nedergaard M, Goldman SA. Glymphatic failure as a final common pathway to dementia. *Science (1979)*. 2020;370(6512):50-56. doi:10.1126/science.abb8739

81. Rasmussen MK, Mestre H, Nedergaard M. Fluid Transport in the Brain. *Physiol Rev*. 2021;(585). doi:10.1152/physrev.00031.2020

82. Xie L, Kang H, Xu Q, et al. Sleep Drives Metabolite Clearance from the Adult Brain. 2013;(October):373-378.

83. Kiviniemi V, Wang X, Korhonen V, et al. Ultra-fast magnetic resonance encephalography of physiological brain activity-Glymphatic pulsation mechanisms? *Journal of Cerebral Blood Flow and Metabolism*. 2016;36(6):1033-1045. doi:10.1177/0271678X15622047

84. Jessen NA, Munk ASF, Lundgaard I, Nedergaard M. The Glymphatic System: A Beginner's Guide. *Neurochem Res*. 2015;40(12):2583-2599. doi:10.1007/s11064-015-1581-6

85. Hablitz LM, Plá V, Giannetto M, et al. Circadian control of brain glymphatic and lymphatic fluid flow. *Nature Communications 2020 11:1*. 2020;11(1):1-11. doi:10.1038/s41467-020-18115-2

86. Mortensen KN, Sanggaard S, Mestre H, et al. Impaired Glymphatic Transport in Spontaneously Hypertensive Rats. *Journal of Neuroscience*. 2019;39(32):6365-6377. doi:10.1523/JNEUROSCI.1974-18.2019

87. Kim YK, Nam K il, Song J. The Glymphatic System in Diabetes-Induced Dementia. *Front Neurol*. 2018;9:867. doi:10.3389/FNEUR.2018.00867

88. Nayak L, Lee EQ, Wen PY. Epidemiology of brain metastases. *Curr Oncol Rep*. 2012;14(1):48-54. doi:10.1007/s11912-011-0203-y

89. Voutouri C, Kirkpatrick ND, Chung E, et al. Experimental and computational analyses reveal dynamics of tumor vessel cooption and optimal treatment strategies. doi:10.1073/pnas.1818322116

90. Zagzag D, Amirnovin R, Greco MA, et al. Vascular apoptosis and involution in gliomas precede neovascularization: A novel concept for glioma growth and angiogenesis. *Laboratory Investigation*. 2000;80(6):837-849. doi:10.1038/labinvest.3780088

91. Bergers G, Hanahan D. Modes of resistance to anti-angiogenic therapy. *Nat Rev Cancer*. Published online 2008. doi:10.1038/nrc2442.Modes

92. Neuwelt EA, Greig NH, Raffel C, et al. Mechanisms of Disease: The Blood-Brain Barrier. *Neurosurgery*. 2004;54(1):131-142. doi:10.1227/01.NEU.0000097715.11966.8E

93. Zhang RD, Price JE, Fujimaki T, Bucana CD, Fidler IJ. Differential permeability of the blood-brain barrier in experimental brain metastases produced by human neoplasms implanted into nude mice. *American Journal of Pathology*. 1992;141(5):1115-1124. Accessed September 14, 2020. /pmc/articles/PMC1886664/?report=abstract

94. JV L, EG A, B M. VEGFR-2 expression in brain injury: its distribution related to brain-blood barrier markers. *J Neural Transm (Vienna)*. 2006;113(4):487-496. doi:10.1007/S00702-005-0407-0

95. Wen L, Tan Y, Dai S, et al. Drug Delivery VEGF-mediated tight junctions pathological fenestration enhances doxorubicin-loaded glycolipid-like nanoparticles traversing BBB for glioblastoma-targeting therapy VEGF-mediated tight junctions pathological fenestration enhances doxorubicin-loaded glycolipid-like nanoparticles traversing BBB for glioblastoma-targeting therapy. Published online 2017. doi:10.1080/10717544.2017.1386731

96. Dvorak HF. Vascular permeability factor/vascular endothelial growth factor: A critical cytokine in tumor angiogenesis and a potential target for diagnosis and therapy. *Journal of Clinical Oncology*. 2002;20(21):4368-4380. doi:10.1200/JCO.2002.10.088

97. Liu T, Ma W, Xu H, et al. PDGF-mediated mesenchymal transformation renders endothelial resistance to anti-VEGF treatment in glioblastoma. *Nat Commun*. 2018;9(1). doi:10.1038/s41467-018-05982-z

98. Wang Q, He Z, Huang M, et al. Vascular niche IL-6 induces alternative macrophage activation in glioblastoma through HIF-2α. *Nat Commun*. 2018;9(1). doi:10.1038/s41467-018-03050-0

99. Fukumura D, Kloepper J, Amoozgar Z, Duda DG, Jain RK. Enhancing cancer immunotherapy using antiangiogenics: Opportunities and challenges. *Nat Rev Clin Oncol*. 2018;15(5):325-340. doi:10.1038/nrclinonc.2018.29

100. Goel S, Duda DG, Xu L, et al. Normalization of the Vasculature for Treatment of Cancer and Other Diseases. *Physiol Rev*. 2011;91:1071-1121. doi:10.1152/physrev.00038.2010.-New

101. Liebner S, Fischmann A, Rascher G, et al. Claudin-1 and claudin-5 expression and tight junction morphology are altered in blood vessels of human glioblastoma multiforme. *Acta Neuropathol*. 2000;100(3):323-331. doi:10.1007/s004010000180

102. Ma J, Wang P, Liu Y, Zhao L, Li Z, Xue Y. Krüppel-Like Factor 4 Regulates Blood-Tumor Barrier Permeability via ZO-1, Occludin and Claudin-5. *J Cell Physiol*. 2014;229(7):916-926. doi:10.1002/jcp.24523

103. Lyle LT, Lockman PR, Adkins CE, et al. Alterations in pericyte subpopulations are associated with elevated blood-tumor barrier permeability in experimental brain metastasis of breast cancer. *Clinical Cancer Research*. 2016;22(21):5287-5299. doi:10.1158/1078-0432.CCR-15-1836

104. Bao X, Wu J, Xie Y, et al. Protein Expression and Functional Relevance of Efflux and Uptake Drug Transporters at the Blood–Brain Barrier of Human Brain and Glioblastoma. *Clin Pharmacol Ther*. 2020;107(5):1116-1127. doi:10.1002/cpt.1710

105. Zhou W, Chen C, Shi Y, et al. Targeting Glioma Stem Cell-Derived Pericytes Disrupts the Blood-Tumor Barrier and Improves Chemotherapeutic Efficacy. *Cell Stem Cell*. 2017;21(5):591-603.e4. doi:10.1016/j.stem.2017.10.002

106. Verhoeven D, Buyssens N. Desmin-positive stellate cells associated with angiogenesis in a tumour and non-tumour system. *Virchows Arch B Cell Pathol Incl Mol Pathol*. 1987;54(1):263-272. doi:10.1007/BF02899222

107. Watkins S, Robel S, Kimbrough IF, Robert SM, Ellis-Davies G, Sontheimer H. Disruption of astrocyte-vascular coupling and the blood-brain barrier by invading glioma cells. *Nat Commun*. 2014;5:4196. doi:10.1038/ncomms5196

108. Farin A, Suzuki SO, Weiker M, Goldman JE, Bruce JN, Canoll P. Transplanted glioma cells migrate and proliferate on host brain vasculature: A dynamic analysis. *Glia*. 2006;53(8):799-808. doi:10.1002/glia.20334

109. Nagano N, Sasaki H, Aoyagi M, Hirakawa K. Invasion of experimental rat brain tumor: early morphological changes following microinjection of C6 glioma cells. *Acta Neuropathol*. 1993;86(2):117-125. doi:10.1007/BF00334878

110. Gril B, Paranjape AN, Woditschka S, et al. Reactive astrocytic S1P3 signaling modulates the blood-tumor barrier in brain metastases. *Nat Commun*. 2018;9(1):1-18. doi:10.1038/s41467-018-05030-w

111. Hall EJ, Giaccia AJ. Radiobiology for the Radiologist, 6th Edition. Published online 2006. doi:10.1016/j.ijrobp.2006.06.027

112. Walker AJ, Ruzevick J, Malayeri AA, et al. Postradiation imaging changes in the CNS: How can we differentiate between treatment effect and disease progression? *Future Oncology*. 2014;10(7):1277-1297. doi:10.2217/fon.13.271

113. Li YQ, Ballinger JR, Nordal RA, Su ZF, Wong CS. Hypoxia in radiation-induced blood-spinal cord barrier breakdown. *Cancer Res*. 2001;61(8):3348-3354.

114. Yuan H, Gaber MW, Boyd K, Wilson CM, Kiani MF, Merchant TE. Effects of fractionated radiation on the brain vasculature in a murine model: Blood-brain barrier permeability, astrocyte proliferation, and ultrastructural changes. *Int J Radiat Oncol Biol Phys*. 2006;66(3):860-866. doi:10.1016/j.ijrobp.2006.06.043

115. Wilson CM, Gaber MW, Sabek OM, Zawaski JA, Merchant TE. Radiation-Induced Astrogliosis and Blood-Brain Barrier Damage Can Be Abrogated Using Anti-TNF Treatment. *Int J Radiat Oncol Biol Phys*. 2009;74(3):934-941. doi:10.1016/j.ijrobp.2009.02.035

116. Lim WH, Choi SH, Yoo RE, et al. Does radiation therapy increase gadolinium accumulation in the brain?: Quantitative analysis of T1 shortening using R1 relaxometry in glioblastoma multiforme patients. *PLoS One*. 2018;13(2):1-14. doi:10.1371/journal.pone.0192838

117. Murrell DH, Zarghami N, Jensen MD, Chambers AF, Wong E, Foster PJ. Evaluating changes to blood-brain barrier integrity in brain metastasis over time and after radiation treatment. *Transl Oncol*. 2016;9(3):219-227. doi:10.1016/j.tranon.2016.04.006

118. Fauquette W, Amourette C, Dehouck MP, Diserbo M. Radiation-induced blood-brain barrier damages: An in vitro study. *Brain Res*. 2012;1433:114-126. doi:10.1016/j.brainres.2011.11.022

119. Diserbo M, Agin A, Lamproglou I, et al. Blood-brain barrier permeability after gamma whole-body irradiation: an in vivo microdialysis study. *Can J Physiol Pharmacol*. 2002;80(7):670-678. doi:10.1139/y02-070

120. NV L, MK L, ED P, LKh E. Endothelial cell population dynamics in rat brain after local irradiation. *Br J Radiol*. 1991;64(766):934-940. doi:10.1259/0007-1285-64-766-934

121. Rubin DB, Drab EA, Ward WF. Physiological and biochemical markers of the endothelial cell response to irradiation. *Int J Radiat Biol*. 1991;60(1-2):29-32. doi:10.1080/09553009114551461

122. Li YQ, Chen P, Haimovitz-Friedman A, Reilly RM, Wong CS. Endothelial apoptosis initiates acute blood-brain barrier disruption after ionizing radiation. *Cancer Res*. 2003;63(18):5950-5956.

123. Peña LA, Fuks Z, Kolesnick RN. Radiation-induced apoptosis of endothelial cells in the murine central nervous system: Protection by fibroblast growth factor and sphingomyelinase deficiency. *Cancer Res*. 2000;60(2):321-327.

124. Kim WK, Kim JH, Yoon K, et al. Salinomycin, a p-glycoprotein inhibitor, sensitizes radiation-treated cancer cells by increasing DNA damage and inducing G2 arrest. *Invest New Drugs*. 2012;30(4):1311-1318. doi:10.1007/s10637-011-9685-6

125. Wang Y, Chen Q, Jin S, et al. Up-regulation of P-glycoprotein is involved in the increased paclitaxel resistance in human esophageal cancer radioresistant cells. *Scand J Gastroenterol*. 2012;47(7):802-808. doi:10.3109/00365521.2012.683042

126. Nagane M, Yasui H, Sakai Y, et al. Activation of eNOS in endothelial cells exposed to ionizing radiation involves components of the DNA damage response pathway. *Biochem Biophys Res Commun*. 2015;456(1):541-546. doi:10.1016/j.bbrc.2014.12.002

127. Kim JE, Ryu HJ, Kang TC. Status Epilepticus Induces Vasogenic Edema via Tumor Necrosis Factor-α/ Endothelin-1-Mediated Two Different Pathways. *PLoS One*. 2013;8(9):1-13. doi:10.1371/journal.pone.0074458

128. Ho ML, Rojas R, Eisenberg RL. Cerebral edema. *American Journal of Roentgenology*. 2012;199(3):258-273. doi:10.2214/AJR.11.8081

129. Kazmierski R, Michalak S, Wencel-Warot A, Nowinski WL. Serum tight-junction proteins predict hemorrhagic transformation in ischemic stroke patients. *Neurology*. 2012;79(16):1677-1685. doi:10.1212/WNL.0b013e31826e9a83

130. Rosenberg GA, Yang Y. Vasogenic edema due to tight junction disruption by matrix metalloproteinases in cerebral ischemia. *Neurosurg Focus*. 2007;22(5):1-9. doi:10.3171/FOC.2007.22.5.5

131. Winkler L, Blasig R, Breitkreuz-Korff O, et al. Tight junctions in the blood–brain barrier promote edema formation and infarct size in stroke – Ambivalent effects of sealing proteins: *https://doi.org/101177/0271678X20904687*. 2020;41(1):132-145. doi:10.1177/0271678X20904687

132. Kevil CG, Keith Payne D, Mire E, Alexander JS. *Vascular Permeability Factor/Vascular Endothelial Cell Growth Factor-Mediated Permeability Occurs through Disorganization of Endothelial Junctional Proteins**.; 1998. Accessed December 19, 2020. http://www.jbc.org/

133. Murakami T, Felinski EA, Antonetti DA. Occludin phosphorylation and ubiquitination regulate tight junction trafficking and vascular endothelial growth factor-induced permeability. *Journal of Biological Chemistry*. 2009;284(31):21036-21046. doi:10.1074/jbc.M109.016766

134. Sitohy B, Nagy JA, Dvorak HF. Anti-VEGF/VEGFR therapy for cancer: Reassessing the target. *Cancer Res*. 2012;72(8):1909-1914. doi:10.1158/0008-5472.CAN-11-3406

135. Inai T, Mancuso M, Hashizume H, et al. Inhibition of vascular endothelial growth factor (VEGF) signaling in cancer causes loss of endothelial fenestrations, regression of tumor vessels, and

appearance of basement membrane ghosts. *American Journal of Pathology*. Published online 2004. doi:10.1016/S0002-9440(10)63273-7

136. Deissler HL, Deissler H, Lang GE. Inhibition of vascular endothelial growth factor (VEGF) is sufficient to completely restore barrier malfunction induced by growth factors in microvascular retinal endothelial cells. *British Journal of Ophthalmology*. 2011;95(8):1151-1156. doi:10.1136/bjo.2010.192229

137. Lee ST, Seo Y, Bae JY, et al. Loss of Pericytes in Radiation Necrosis after Glioblastoma Treatments. *Mol Neurobiol*. 2018;55(6):4918-4926. doi:10.1007/s12035-017-0695-z

138. Bell RD, Winkler EA, Sagare AP, et al. Pericytes Control Key Neurovascular Functions and Neuronal Phenotype in the Adult Brain and during Brain Aging. *Neuron*. 2010;68(3):409-427. doi:10.1016/j.neuron.2010.09.043

139. Sato Y. Persistent vascular normalization as an alternative goal of anti-angiogenic cancer therapy. *Cancer Sci*. 2011;102(7):1253-1256. doi:10.1111/j.1349-7006.2011.01929.x

140. Sándor N, Walter FR, Bocsik A, et al. Low Dose Cranial Irradiation-Induced Cerebrovascular Damage Is Reversible in Mice. *PLoS One*. 2014;9(11). doi:10.1371/JOURNAL.PONE.0112397

141. Y Y, DJ B, M T, et al. Vascular Cell Senescence Contributes to Blood-Brain Barrier Breakdown. *Stroke*. 2016;47(4):1068-1077. doi:10.1161/STROKEAHA.115.010835

142. O A, W S, H S, et al. Integrative proteomics and targeted transcriptomics analyses in cardiac endothelial cells unravel mechanisms of long-term radiation-induced vascular dysfunction. *J Proteome Res*. 2015;14(2):1203-1219. doi:10.1021/PR501141B

143. C P, AM C, J del V, et al. Increased permeability of blood-brain barrier on the hippocampus of a murine model of senescence. *Mech Ageing Dev*. 2007;128(9):522-528. doi:10.1016/J.MAD.2007.07.002

144. J DV, J DV, G M, et al. Time-course of blood-brain barrier disruption in senescence-accelerated mouse prone 8 (SAMP8) mice. *Int J Dev Neurosci*. 2009;27(1):47-52. doi:10.1016/J.IJDEVNEU.2008.10.002

145. Coppé JP, Desprez PY, Krtolica A, Campisi J. The senescence-associated secretory phenotype: The dark side of tumor suppression. *Annual Review of Pathology: Mechanisms of Disease*. 2010;5:99-118. doi:10.1146/annurev-pathol-121808-102144

146. Muñoz-Espín D, Serrano M. Cellular senescence: From physiology to pathology. *Nat Rev Mol Cell Biol*. 2014;15(7):482-496. doi:10.1038/nrm3823

147. C T, JA B, I H, et al. Radiation-induced astrocyte senescence is rescued by Δ133p53. *Neuro Oncol*. 2019;21(4):474-485. doi:10.1093/NEUONC/NOZ001

148. Meldolesi J. Astrocytes: News about brain health and diseases. *Biomedicines*. 2020;8(10):1-14. doi:10.3390/biomedicines8100394

149. Schaue D, Micewicz ED, Ratikan JA, Xie MW, Cheng G, McBride WH. Radiation & Inflammation. *Semin Radiat Oncol*. 2015;25(1):4. doi:10.1016/J.SEMRADONC.2014.07.007

150. Constanzo J, Midavaine É, Fouquet J, et al. Brain irradiation leads to persistent neuroinflammation and long-term neurocognitive dysfunction in a region-specific manner. *Prog Neuropsychopharmacol Biol Psychiatry*. 2020;102:109954. doi:10.1016/J.PNPBP.2020.109954

151. Arvanitis CD, Ferraro GB, Jain RK. The blood-brain barrier and blood-tumour barrier in brain tumours and metastases. doi:10.1038/s41568-019-0205-x

152. Demeule M, Régina A, Jodoin J, et al. Drug transport to the brain: Key roles for the efflux pump P-glycoprotein in the blood-brain barrier. *Vascul Pharmacol*. 2002;38(6):339-348. doi:10.1016/S1537-1891(02)00201-X

153. Strugar J, Rothbart D, Harrington W, Criscuolo GR. Vascular permeability factor in brain metastases: Correlation with vasogenic brain edema and tumor angiogenesis. *J Neurosurg*. 1994;81(4):560-566. doi:10.3171/jns.1994.81.4.0560

154. Thorsen F, Fite B, Mahakian LM, et al. Multimodal imaging enables early detection and characterization of changes in tumor permeability of brain metastases. *Journal of Controlled Release*. 2013;172(3):812-822. doi:10.1016/j.jconrel.2013.10.019

155. Jung BY, Lee EJ, Bae JM, Choi YJ, Lee EK, Kim DB. Differentiation between Glioblastoma and Solitary Metastasis: Morphologic Assessment by Conventional Brain MR Imaging and Diffusion-Weighted Imaging. *Investig Magn Reson Imaging*. 2021;25(1):23. doi:10.13104/imri.2021.25.1.23

156. Meier R, Pahud de Mortanges A, Wiest R, Knecht U. Exploratory Analysis of Qualitative MR Imaging Features for the Differentiation of Glioblastoma and Brain Metastases. *Front Oncol*. 2020;10(December):1-13. doi:10.3389/fonc.2020.581037

157. Hengel K, Sidhu G, Choi J, et al. Attributes of brain metastases from breast and lung cancer. *Int J Clin Oncol*. 2013;18(3):396-401. doi:10.1007/s10147-012-0392-x

158. Storm AJ, van der Kogel AJ, Nooter K. Effect of X-irradiation on the pharmacokinetics of methotrexate in rats: Alteration of the blood-brain barrier. *Eur J Cancer Clin Oncol*. 1985;21(6):759-764. doi:10.1016/0277-5379(85)90275-5

159. Kogel AJ van der. Radiation-induced damage in the central nervous system: an interpretation of target cell responses. *Br J Cancer Suppl*. 1986;7(SUPPL. 7):207. Accessed August 21, 2021. https://www.ncbi.nlm.nih.gov/pmc/articles/PMC2149792/

160. Remler MP, Marcussen WH, Tiller-Borsich J. The late effects of radiation on the blood brain barrier. *Int J Radiat Oncol Biol Phys*. 1986;12(11):1965-1969. doi:10.1016/0360-3016(86)90133-1

161. Yuan H, Gaber MW, Boyd K, Wilson CM, Kiani MF, Merchant TE. Effects of fractionated radiation on the brain vasculature in a murine model: Blood-brain barrier permeability, astrocyte proliferation, and ultrastructural changes. *Int J Radiat Oncol Biol Phys*. 2006;66(3):860-866. doi:10.1016/j.ijrobp.2006.06.043

162. DX Q, R Z, J T, JX L, YH H. Influence of radiation on the blood-brain barrier and optimum time of chemotherapy. *Int J Radiat Oncol Biol Phys*. 1990;19(6):1507-1510. doi:10.1016/0360-3016(90)90364-P

163. Brightman MW, Hori M, Rapoport SI, Reese TS, Westergaard E. Osmotic opening of tight junctions in cerebral endothelium. *Journal of Comparative Neurology*. 1973;152(4):317-325. doi:10.1002/cne.901520402

164. Rapoport SI, Hori M, Klatzo I. Testing of a hypothesis for osmotic opening of the blood-brain barrier. *Am J Physiol*. 1972;223(2):323-331. doi:10.1152/ajplegacy.1972.223.2.323

165. Zylber-Katz E, Gomori JM, Schwartz A, Lossos A, Bokstein F, Siegal T. Pharmacokinetics of methotrexate in cerebrospinal fluid and serum after osmotic blood-brain barrier disruption in patients with brain lymphoma. *Clin Pharmacol Ther*. 2000;67(6):631-641. doi:10.1067/mcp.2000.106932

166. Morikawa N, Mori T, Abe T, Kawashima H, Takeyama M, Hori S. Pharmacokinetics of etoposide and carboplatin in cerebrospinal fluid and plasma during hyperosmotic disruption of the blood brain barrier and intraarterial combination chemotherapy. *Biol Pharm Bull*. 1999;22(4):428-431. doi:10.1248/bpb.22.428

167. Hynynen K, Mcdannold N. Noninvasive MR Imaging–guided Focal Opening of the Blood-Brain Barrier in Rabbits. *Radiology*. 2001;(220):640-646.

168. Aryal M, Arvanitis CD, Alexander PM, McDannold N. Ultrasound-mediated blood-brain barrier disruption for targeted drug delivery in the central nervous system. *Adv Drug Deliv Rev*. 2014;72:94-109. doi:10.1016/j.addr.2014.01.008

169. Meairs S. Facilitation of drug transport across the blood–brain barrier with ultrasound and microbubbles. *Pharmaceutics*. 2015;7(3):275-293. doi:10.3390/pharmaceutics7030275

170. Legon W, Adams S, Bansal P, et al. A retrospective qualitative report of symptoms and safety from transcranial focused ultrasound for neuromodulation in humans. *Sci Rep*. 2020;10(1):1-10. doi:10.1038/s41598-020-62265-8

171. Mcmahon D, Bendayan R, Hynynen K. Acute effects of focused ultrasound-induced increases in blood-brain barrier permeability on rat microvascular transcriptome. *Sci Rep*. 2017;7(March):1-15. doi:10.1038/srep45657

172. Kovacsa ZI, Kima S, Jikariaa N, et al. Disrupting the blood-brain barrier by focused ultrasound induces sterile inflammation. *Proc Natl Acad Sci U S A*. 2017;114(1):E75-E84. doi:10.1073/pnas.1614777114

173. Lajoie JM, Shusta E v. Targeting receptor-mediated transport for delivery of biologics across the blood-brain barrier. *Annu Rev Pharmacol Toxicol*. 2015;55:613-631. doi:10.1146/annurev-pharmtox-010814-124852

174. Daniels TR, Bernabeu E, Rodríguez JA, et al. The transferrin receptor and the targeted delivery of therapeutic agents against cancer. *Biochim Biophys Acta Gen Subj*. 2012;1820(3):291-317. doi:10.1016/j.bbagen.2011.07.016

175. Weaver M, Laske DW. Transferrin receptor ligand-targeted toxin conjugate (Tf-CRM107) therapy of malignant gliomas. *J Neurooncol*. 2003;65(1):3-14. doi:10.1023/A:1026246500788

176. Angeli E, Nguyen TT, Janin A, Bousquet G. How to make anticancer drugs cross the blood-brain barrier to treat brain metastases. *Int J Mol Sci*. 2020;21(1). doi:10.3390/ijms21010022

177. M D, A R, C C, et al. Identification and design of peptides as a new drug delivery system for the brain. *J Pharmacol Exp Ther*. 2008;324(3):1064-1072. doi:10.1124/JPET.107.131318

178. Thomas FC, Taskar K, Rudraraju V, et al. Uptake of ANG1005, a novel paclitaxel derivative, through the blood-brain barrier into brain and experimental brain metastases of breast cancer. *Pharm Res*. 2009;26(11):2486-2494. doi:10.1007/s11095-009-9964-5

179. Kumthekar P, Tang SC, Brenner AJ, et al. ANG1005, a Brain-Penetrating Peptide–Drug Conjugate, Shows Activity in Patients with Breast Cancer with Leptomeningeal Carcinomatosis and Recurrent Brain Metastases. *Clinical Cancer Research*. 2020;26(12):2789-2799. doi:10.1158/1078-0432.CCR-19-3258

180. Montay-Gruel P, Acharya MM, Petersson K, et al. Long-term neurocognitive benefits of FLASH radiotherapy driven by reduced reactive oxygen species. *Proc Natl Acad Sci U S A*. 2019;166(22):10943-10951. doi:10.1073/pnas.1901777116

181. Montay-Gruel P, Markarian M, Allen BD, et al. Ultra-High-Dose-Rate FLASH Irradiation Limits Reactive Gliosis in the Brain. *Radiat Res*. 2020;194(6):636-645. doi:10.1667/RADE-20-00067.1

182. Velalopoulou A, Karagounis I v, Cramer GM, et al. FLASH Proton Radiotherapy Spares Normal Epithelial and Mesenchymal Tissues While Preserving Sarcoma Response. *Cancer Res*. 2021;81(18):canres.1500.2021. doi:10.1158/0008-5472.CAN-21-1500

183. Butler JM, Rapp SR, Shaw EG. Managing the cognitive effects of brain tumor radiation therapy. *Curr Treat Options Oncol*. 2006;7(6):517-523. doi:10.1007/s11864-006-0026-5

184. Butler RW, Fairclough DL, Katz ER, et al. Intellectual functioning and multi-dimensional attentional processes in long-term survivors of a central nervous system related pediatric malignancy. *Life Sci*. 2013;93(17):611-616. doi:10.1016/j.lfs.2013.05.017

185. Seymour ZA, Chan JW, Sneed PK, et al. Dose response and architecture in volume staged radiosurgery for large arteriovenous malformations: A multi-institutional study. *Radiotherapy and Oncology*. 2020;144:180-188. doi:10.1016/j.radonc.2019.09.019

186. Adams HP. Cancer and Cerebrovascular Disease. *Curr Neurol Neurosci Rep*. 2019;19(10):1-10. doi:10.1007/s11910-019-0985-0

187. Zaorsky NG, Zhang Y, Tchelebi LT, Mackley HB, Chinchilli VM, Zacharia BE. Stroke among cancer patients. *Nat Commun*. 2019;10(1). doi:10.1038/s41467-019-13120-6

188. Huang R, Zhou Y, Hu S, Ren G, Cui F, Zhou PK. Radiotherapy Exposure in Cancer Patients and Subsequent Risk of Stroke: A Systematic Review and Meta-Analysis. *Front Neurol*. 2019;10(March):1-12. doi:10.3389/fneur.2019.00233

189. Wells EM, Ullrich NJ, Seidel K, et al. Longitudinal assessment of late-onset neurologic conditions in survivors of childhood central nervous system tumors: A Childhood Cancer Survivor Study report. *Neuro Oncol*. 2018;20(1):132-142. doi:10.1093/neuonc/nox148

190. King AA, Seidel K, Di C, et al. Long-term neurologic health and psychosocial function of adult survivors of childhood medulloblastoma/PNET: A report from the Childhood Cancer Survivor Study. *Neuro Oncol*. 2017;19(5):689-698. doi:10.1093/neuonc/now242

191. Roongpiboonsopit D, Kuijf HJ, Charidimou A, et al. Evolution of cerebral microbleeds after cranial irradiation in medulloblastoma patients. *Neurology*. 2017;88(8):789-796. doi:10.1212/WNL.0000000000003631

192. Hersh DS, Moore K, Nguyen V, et al. Evaluation and treatment of children with radiation-induced cerebral vasculopathy. *J Neurosurg Pediatr*. 2019;24(6):680-688. doi:10.3171/2019.7.PEDS19188

193. Tanyildizi Y, Keweloh S, Neu MA, et al. Radiation-induced vascular changes in the intracranial irradiation field in medulloblastoma survivors: An MRI study. *Radiotherapy and Oncology*. 2019;136:50-55. doi:10.1016/j.radonc.2019.03.017

194. Seymour ZA, Chan JW, Sneed PK, et al. Dose response and architecture in volume staged radiosurgery for large arteriovenous malformations: A multi-institutional study. *Radiotherapy and Oncology*. 2020;144:180-188. doi:10.1016/j.radonc.2019.09.019

195. Gauden AJ, McRobb LS, Lee VS, et al. Occlusion of Animal Model Arteriovenous Malformations Using Vascular Targeting. *Transl Stroke Res*. 2020;11(4):689-699. doi:10.1007/s12975-019-00759-y

196. Hasegawa H, Yamamoto M, Shin M, Barfod BE. Gamma knife radiosurgery for brain vascular malformations: Current evidence and future tasks. *Ther Clin Risk Manag*. 2019;15:1351-1367. doi:10.2147/TCRM.S200813

197. Starke RM, Mccarthy DJ, Chen C jen, et al. Hemorrhage risk of cerebral dural arteriovenous fistulas following Gamma Knife radiosurgery in a multicenter international consortium. *J Neurosurg*. 2020;132(April):1209-1217. doi:1–9. doi:10.3171/2018.12.JNS182208.

198. Tofilon PJ, Fike JR. The radioresponse of the central nervous system: A dynamic process. *Radiat Res*. 2000;153(4):357-370. doi:10.1667/0033-7587(2000)153[0357:TROTCN]2.0.CO;2

199. Milan T. Makale, PhD, Carrie R. McDonald, PhD, Jona Hattangadi-Gluth, MD, and Santosh Kesari, MD P. Brain irradiation and long-term cognitive disability: Current concepts. *Nat Rev Neurol*. 2017;13(1):52.64. doi:10.1038/nrneurol.2016.185.

200. Montay-Gruel P, Meziani L, Yakkala C, Vozenin MC. Expanding the therapeutic index of radiation therapy by normal tissue protection. *British Journal of Radiology*. 2019;92(1093). doi:10.1259/bjr.20180008

201. Vozenin MC, Hendry JH, Limoli CL. Biological Benefits of Ultra-high Dose Rate FLASH Radiotherapy: Sleeping Beauty Awoken. *Clin Oncol*. 2019;31(7):407-415. doi:10.1016/j.clon.2019.04.001

202. Favaudon V, Caplier L, Monceau V, et al. Ultrahigh dose-rate FLASH irradiation increases the differential response between normal and tumor tissue in mice. *Sci Transl Med*. 2014;6(245). doi:10.1126/scitranslmed.3008973

203. Jaccard M, Durán MT, Petersson K, et al. High dose-per-pulse electron beam dosimetry: Commissioning of the Oriatron eRT6 prototype linear accelerator for preclinical use. *Med Phys*. 2018;45(2):863-874. doi:10.1002/mp.12713

204. Jaccard M, Petersson K, Buchillier T, et al. High dose-per-pulse electron beam dosimetry: Usability and dose-rate independence of EBT3 Gafchromic films. *Med Phys*. 2017;44(2):725-735. doi:10.1002/mp.12066

205. Petersson K, Jaccard M, Germond JF, et al. High dose-per-pulse electron beam dosimetry - A model to correct for the ion recombination in the Advanced Markus ionization chamber. *Med Phys*. 2017;44(3):1157-1167. doi:10.1002/mp.12111

206. Jorge PG, Jaccard M, Petersson K, et al. Dosimetric and preparation procedures for irradiating biological models with pulsed electron beam at ultra-high dose-rate. *Radiotherapy and Oncology*. 2019;139:34-39. doi:10.1016/j.radonc.2019.05.004

207. Craver BM, Acharya MM, Allen BD, et al. 3D surface analysis of hippocampal microvasculature in the irradiated brain. *Environ Mol Mutagen*. 2016;57(5). doi:10.1002/em.22015

208. Förstermann U, Sessa WC. Nitric oxide synthases: Regulation and function. *Eur Heart J*. 2012;33(7). doi:10.1093/eurheartj/ehr304

209. Iwase K, Miyanaka K, Shimizu A, et al. Induction of endothelial nitric-oxide synthase in rat brain astrocytes by systemic lipopolysaccharide treatment. *Journal of Biological Chemistry*. 2000;275(16):11929-11933. doi:10.1074/jbc.275.16.11929

210. Lin LH, Taktakishvili O, Talman WT. Identification and localization of cell types that express endothelial and neuronal nitric oxide synthase in the rat nucleus tractus solitarii. *Brain Res*. 2007;1171(1):42-51. doi:10.1016/j.brainres.2007.07.057

211. Michel T, Feron O. Nitric oxide synthases: Which, where, how, and why? *Journal of Clinical Investigation*. 1997;100(9):2146-2152. doi:10.1172/JCI119750

212. Günzel D, Yu ASL. Claudins and the modulation of tight junction permeability. *Physiol Rev*. 2013;93(2):525-569. doi:10.1152/physrev.00019.2012

213. Paul D, Cowan AE, Ge S, Pachter JS. Novel 3D analysis of Claudin-5 reveals significant endothelial heterogeneity among CNS microvessels. *Microvasc Res*. 2013;86(1):1-10. doi:10.1016/j.mvr.2012.12.001

214. Yuan H, Gaber MW, McColgan T, Naimark MD, Kiani MF, Merchant TE. Radiation-induced permeability and leukocyte adhesion in the rat blood–brain barrier: modulation with anti-ICAM-1 antibodies. *Brain Res*. 2003;969(1-2):59-69. doi:10.1016/S0006-8993(03)02278-9

215. King AA, Seidel K, Di C, et al. Long-term neurologic health and psychosocial function of adult survivors of childhood medulloblastoma/PNET: A report from the Childhood Cancer Survivor Study. *Neuro Oncol*. 2017;19(5):689-698. doi:10.1093/neuonc/now242

216. v. Nagesh, C.I. Tsien, T.L. Chenevert, B.D. Ross, T.S. Lawrence, L. Junck and YC. Radiation-Induced Changes in Normal Appearing White Matter in Patients with Cerebral Tumors: A Diffusion Tensor

Imaging Study. *Int J Radiat Oncol Biol Phys*. 2008;70(4):1002-1010. https://www.ncbi.nlm.nih.gov/pmc/articles/PMC3624763/pdf/nihms412728.pdf

217. Seo YS, Ko IO, Park H, et al. Radiation-Induced Changes in Tumor Vessels and Microenvironment Contribute to Therapeutic Resistance in Glioblastoma. *Front Oncol*. 2019;9(November):1-10. doi:10.3389/fonc.2019.01259

218. Reinhold HS, Calvo W, Hopewell JW, van den Berg AP. Development of blood vessel-related radiation damage in the fimbria of the central nervous system. *Int J Radiat Oncol Biol Phys*. Published online 1990. doi:10.1016/0360-3016(90)90264-K

219. Simmons DA, Lartey FM, Schüler E, et al. Reduced cognitive deficits after FLASH irradiation of whole mouse brain are associated with less hippocampal dendritic spine loss and neuroinflammation. *Radiotherapy and Oncology*. 2019;139:4-10. doi:10.1016/j.radonc.2019.06.006

220. Iovino F, Orihuela CJ, Moorlag HE, Molema G, Bijlsma JJE. Interactions between Blood-Borne Streptococcus pneumoniae and the Blood-Brain Barrier Preceding Meningitis. *PLoS One*. 2013;8(7). doi:10.1371/journal.pone.0068408

221. Heiss C, Rodriguez-Mateos A, Kelm M. Central Role of eNOS in the Maintenance of Endothelial Homeostasis. doi:10.1089/ars.2014.6158

222. Wiggermann V, Lapointe E, Litvin L, et al. Longitudinal advanced MRI case report of white matter radiation necrosis. *Ann Clin Transl Neurol*. 2018;6(2):acn3.704. doi:10.1002/acn3.704

223. Kessler AT, Bhatt AA. Brain tumour post-treatment imaging and treatment-related complications. *Insights Imaging*. 2018;9(6):1057-1075. doi:10.1007/s13244-018-0661-y

224. Fouillade C, Curras-Alonso S, Giuranno L, et al. FLASH irradiation spares lung progenitor cells and limits the incidence of radio-induced senescence. *Clinical Cancer Research*. 2020;26(6):1497-1506. doi:10.1158/1078-0432.CCR-19-1440

225. Palmer TD, Willhoite AR, Gage FH. Vascular niche for adult hippocampal neurogenesis. *Journal of Comparative Neurology*. 2000;425(4):479-494. doi:10.1002/1096-9861(20001002)425:4<479::AID-CNE2>3.0.CO;2-3

226. Monje ML, Mizumatsu S, Fike JR, Palmer TD. Irradiation induces neural precursor-cell dysfunction. *Nat Med*. 2002;8(9):955-962. doi:10.1038/nm749

227. Bourhis J, Montay-Gruel P, Gonçalves Jorge P, et al. Clinical translation of FLASH radiotherapy: Why and how? *Radiotherapy and Oncology*. 2019;139:11-17. doi:10.1016/j.radonc.2019.04.008

228. Wilson JD, Hammond EM, Higgins GS, Petersson K. Ultra-High Dose Rate (FLASH) Radiotherapy: Silver Bullet or Fool's Gold? *Front Oncol*. 2020;9(January):1-12. doi:10.3389/fonc.2019.01563

229. Bourhis J, Sozzi WJ, Jorge PG, et al. Treatment of a first patient with FLASH-radiotherapy. *Radiotherapy and Oncology*. 2019;139:18-22. doi:10.1016/j.radonc.2019.06.019

230. Velalopoulou A, Karagounis I v., Cramer GM, et al. Flash proton radiotherapy spares normal epithelial and mesenchymal tissues while preserving sarcoma response. *Cancer Res*. 2021;81(18):4808-4821. doi:10.1158/0008-5472.CAN-21-1500

231. Alaghband Y, Cheeks SN, Allen BD, et al. Neuroprotection of Radiosensitive Juvenile Mice by Ultra-High Dose Rate FLASH Irradiation. *Cancers (Basel)*. 2020;12(6):1-21. doi:10.3390/CANCERS12061671

232. Shen CJ, Terezakis SA. The Evolving Role of Radiotherapy for Pediatric Cancers With Advancements in Molecular Tumor Characterization and Targeted Therapies. *Front Oncol*. 2021;11(September). doi:10.3389/fonc.2021.679701

233. Denunzio NJ, Yock TI. Modern radiotherapy for pediatric brain tumors. *Cancers (Basel)*. 2020;12(6):1-16. doi:10.3390/cancers12061533

234. Kwapis JL, Alaghband Y, Keiser AA, et al. Aging mice show impaired memory updating in the novel OUL updating paradigm. *Neuropsychopharmacology*. 2020;45(2):337-346. doi:10.1038/s41386-019-0438-0

235. Klein EA, Richards D, Cohn A, et al. Clinical validation of a targeted methylation-based multi-cancer early detection test using an independent validation set. *Annals of Oncology*. 2021;32(9):1167-1177. doi:10.1016/j.annonc.2021.05.806

236. Keiser AA, Kramár EA, Dong T, et al. Systemic HDAC3 inhibition ameliorates impairments in synaptic plasticity caused by simulated galactic cosmic radiation exposure in male mice. *Neurobiol Learn Mem*. 2021;178. doi:10.1016/j.nlm.2020.107367

237. Verstraelen P, Garcia-Diaz Barriga G, Verschuuren M, et al. Systematic Quantification of Synapses in Primary Neuronal Culture. *iScience*. 2020;23(9):101542. doi:10.1016/j.isci.2020.101542

238. Acharya MM, Martirosian V, Chmielewski NN, et al. Stem cell transplantation reverses chemotherapy-induced cognitive dysfunction. 2016;75(4):676-686. doi:10.1158/0008-5472.CAN-14-2237.Stem

239. Allen BD, Apodaca LA, Syage AR, et al. Attenuation of neuroinflammation reverses Adriamycin-induced cognitive impairments. *Acta Neuropathol Commun*. 2019;7(1). doi:10.1186/s40478-019-0838-8

240. Acharya MM, Green KN, Allen BD, et al. Elimination of microglia improves cognitive function following cranial irradiation. *Sci Rep*. 2016;6. doi:10.1038/srep31545

241. Hermkens DMA, Stam OCG, de Wit NM, et al. Profiling the unique protective properties of intracranial arterial endothelial cells. *Acta Neuropathol Commun*. 2019;7(1). doi:10.1186/s40478-019-0805-4

242. Christie LA, Acharya MM, Parihar VK, Nguyen A, Martirosian V, Limoli CL. Impaired cognitive function and hippocampal neurogenesis following cancer chemotherapy. *Clinical Cancer Research*. 2012;18(7):1954-1965. doi:10.1158/1078-0432.CCR-11-2000

243. Haruwaka K, Ikegami A, Tachibana Y, et al. Dual microglia effects on blood brain barrier permeability induced by systemic inflammation. *Nature Communications 2019 10:1*. 2019;10(1):1-17. doi:10.1038/s41467-019-13812-z

244. da Fonseca ACC, Matias D, Garcia C, et al. The impact of microglial activation on blood-brain barrier in brain diseases. *Front Cell Neurosci*. 2014;8(November):1-13. doi:10.3389/fncel.2014.00362

245. Schwartzkroin PA, Wester K. Long-lasting facilitation of a synaptic potential following tetanization in thein vitro hippocampal slice. *Brain Res*. 1975;89(1):107-119. doi:10.1016/0006-8993(75)90138-9

246. Acharya MM, Baulch JE, Klein PM, et al. New concerns for neurocognitive function during deep space exposures to chronic, low dose-rate, neutron radiation. *eNeuro*. 2019;6(4):1-15. doi:10.1523/ENEURO.0094-19.2019

247. Costa RP, Mizusaki BEP, Sjöström PJ, van Rossum MCW. Functional consequences of pre- and postsynaptic expression of synaptic plasticity. *Philosophical Transactions of the Royal Society B: Biological Sciences*. 2017;372(1715). doi:10.1098/rstb.2016.0153

248. Sanderson TM, Georgiou J, Collingridge GL. Illuminating Relationships Between the Pre- and Post-synapse. *Front Neural Circuits*. 2020;14(April):1-13. doi:10.3389/fncir.2020.00009

249. Lynch MA. Long-Term Potentiation and Memory. Published online 2004. doi:10.1152/physrev.00014.2003.-One

250. Parihar VK, Allen BD, Tran KK, et al. Targeted overexpression of mitochondrial catalase prevents radiation-induced cognitive dysfunction. *Antioxid Redox Signal*. 2015;22(1). doi:10.1089/ars.2014.5929

251. Apodaca LA, Baddour AAD, Garcia C, et al. Human neural stem cell-derived extracellular vesicles mitigate hallmarks of Alzheimer's disease. *Alzheimers Res Ther*. 2021;13(1):1-18. doi:10.1186/s13195-021-00791-x

252. Martin SJ, Grimwood PD, Morris RGM. Synaptic Plasticity and Memory. *AnnRevNeurosci*. 2000;(23):649-711.

253. Diering GH, Huganir RL. The AMPA Receptor Code of Synaptic Plasticity. *Neuron*. 2018;100(2):314-329. doi:10.1016/j.neuron.2018.10.018

254. Hinkle JJ, Olschowka JA, Love TM, Williams JP, O'Banion MK. Cranial irradiation mediated spine loss is sex-specific and complement receptor-3 dependent in male mice. *Sci Rep*. 2019;9(1):1-12. doi:10.1038/s41598-019-55366-6

255. Parihar VK, Angulo MC, Allen BD, et al. Sex-Specific Cognitive Deficits Following Space Radiation Exposure. *Front Behav Neurosci*. 2020;14. doi:10.3389/fnbeh.2020.535885

256. Dickstein DL, Biron KE, Ujiie M, Pfeifer CG, Jeffries AR, Jefferies WA. Aβ peptide immunization restores blood-brain barrier integrity in Alzheimer disease. *The FASEB Journal*. 2006;20(3):426-433. doi:10.1096/fj.05-3956com

257. Mondo E, Becker SC, Kautzman AG, et al. A developmental analysis of juxtavascular microglia dynamics and interactions with the vasculature. *Journal of Neuroscience*. 2020;40(34):6503-6521. doi:10.1523/JNEUROSCI.3006-19.2020

258. Lou N, Takano T, Pei Y, Xavier AL, Goldman SA, Nedergaard M. Purinergic receptor P2RY12-dependent microglial closure of the injured blood-brain barrier. *Proc Natl Acad Sci U S A*. 2016;113(4):1074-1079. doi:10.1073/pnas.1520398113

259. Varatharaj A, Galea I. The blood-brain barrier in systemic inflammation. *Brain Behav Immun*. 2017;60:1-12. doi:10.1016/j.bbi.2016.03.010

260. Allen BD, Limoli CL. Breaking barriers: Neurodegenerative repercussions of radiotherapy induced damage on the blood-brain and blood-tumor barrier. *Free Radic Biol Med*. 2022;178:189-201. doi:10.1016/j.freeradbiomed.2021.12.002

261. Bernardo-Castro S, Sousa JA, Brás A, et al. Pathophysiology of Blood–Brain Barrier Permeability Throughout the Different Stages of Ischemic Stroke and Its Implication on Hemorrhagic Transformation and Recovery. *Front Neurol*. 2020;11(December):1-24. doi:10.3389/fneur.2020.594672

262. Zhang CE, Wong SM, Uiterwijk R, et al. Blood–brain barrier leakage in relation to white matter hyperintensity volume and cognition in small vessel disease and normal aging. *Brain Imaging Behav*. 2019;13(2):389-395. doi:10.1007/s11682-018-9855-7

263. Szu JI, Binder DK. The role of astrocytic aquaporin-4 in synaptic plasticity and learning and memory. *Front Integr Neurosci*. 2016;10(FEB2016):1-16. doi:10.3389/fnint.2016.00008

264. Maxim PG, Loo BW, Bailat C, Montay-Gruel P, Limoli CL VMC. FLASH Radiation Therapy: A new treatment modality. In: Dyk JV, editor. The Modern Technology of Radiation Oncology: A Compendium for Medical Physicists and Radiation Oncologists. *Med Phys*. Published online 2020:488-500. doi:10.1002/mp.15053

265. Kacem H, Almeida A, Cherbuin N, Vozenin MC. Understanding the FLASH effect to unravel the potential of ultra-high dose rate irradiation. *Int J Radiat Biol*. 2022;98(3):506-516. doi:10.1080/09553002.2021.2004328

266. Limoli, C. L. Vozenin MC. Reinventing Radiobiology in the Light of FLASH Radiotherapy. *Ann Rev Cancer Biol*. 2023;7:In Press.

267. Montay-Gruel P, Acharya MM, Jorge PG, et al. Hypofractionated FLASH-RT as an effective treatment against glioblastoma that reduces neurocognitive side effects in mice. *Clinical Cancer Research*. 2021;27(3):775-784. doi:10.1158/1078-0432.CCR-20-0894

268. Stupp R, Hegi ME, Mason WP, et al. Effects of radiotherapy with concomitant and adjuvant temozolomide versus radiotherapy alone on survival in glioblastoma in a randomised phase III study: 5-year analysis of the EORTC-NCIC trial. *Lancet Oncol*. 2009;10(5):459-466. doi:10.1016/S1470-2045(09)70025-7

269. Brown PD, Gondi V, Pugh S, et al. Hippocampal Avoidance During Whole-Brain Radiotherapy Plus Memantine for Patients With Brain Metastases: Phase III Trial NRG Oncology CC001. *Journal of Clinical Oncology*. 2020;38(10):1019-1029.

270. Gondi V, Pugh SL, Tome WA, et al. Preservation of memory with conformal avoidance of the hippocampal neural stem-cell compartment during whole-brain radiotherapy for brain metastases (RTOG 0933): A phase II multi-institutional trial. *Journal of Clinical Oncology*. 2014;32(34):3810-3816. doi:10.1200/JCO.2014.57.2909

271. Vogel-Ciernia A, Matheos DP, Barrett RM, et al. The neuron-specific chromatin regulatory subunit BAF53b is necessary for synaptic plasticity and memory. *Nat Neurosci*. 2013;16(5):552-561. doi:10.1038/nn.3359

272. Wright DS, Bodinayake KK KJL. Investigating Memory Updating in Mice Using the Objects in Updated Locations Task. *Curr Protoc Neurosci*. 2020;91(1):e87. doi:10.1002/cpns.87

273. W.C. Clapp, J.P. Hamm, I.J. Kirk TJT. Translating LTP from animals to humans: A novel method for non-invasive assessment of cortical plasticity. *Biol psychiatry*. 2012;71(6):496-502. doi:10.1016/j.biopsych.2011.08.021.Translating

274. Mantovani C, Gastino A, Cerrato M, Badellino S, Ricardi U, Levis M. Modern Radiation Therapy for the Management of Brain Metastases From Non-Small Cell Lung Cancer: Current Approaches and Future Directions. *Front Oncol*. 2021;11(November):1-24. doi:10.3389/fonc.2021.772789

275. McKay MJ. Brain metastases: increasingly precision medicine—a narrative review. *Ann Transl Med*. 2021;9(21):1629-1629. doi:10.21037/atm-21-3665

276. Geinisman Y. Structural synaptic modifications associated with hippocampal LTP and behavioral learning. *Cerebral Cortex*. 2000;10(10):952-962. doi:10.1093/cercor/10.10.952

277. Nabavi S, Fox R, Proulx CD, Lin JY, Tsien RY, Malinow R. Engineering a memory with LTP and LTP (LONGER VERSION). 2015;511(7509):348-352. doi:10.1038/nature13294.Engineering

278. Klein PM, Parihar VK, Szabo GG, et al. Detrimental impacts of mixed-ion radiation on nervous system function. *Neurobiol Dis*. 2021;151. doi:10.1016/j.nbd.2021.105252

279. Parihar VK, Maroso M, Syage A, et al. Persistent nature of alterations in cognition and neuronal circuit excitability after exposure to simulated cosmic radiation in mice. *Exp Neurol*. 2018;305. doi:10.1016/j.expneurol.2018.03.009

280. Froidevaux P, Grilj V, Bailat C, Geyer WR, Bochud F, Vozenin MC. FLASH irradiation does not induce lipid peroxidation in lipids micelles and liposomes. *Radiation Physics and Chemistry*. 2023;205(December 2022):110733. doi:10.1016/j.radphyschem.2022.110733

281. Paolicelli RC, Sierra A, Stevens B, et al. Microglia states and nomenclature: A field at its crossroads. *Neuron*. 2022;110(21):3458-3483. doi:10.1016/j.neuron.2022.10.020

282. Salter MW, Beggs S. Sublime microglia: Expanding roles for the guardians of the CNS. *Cell*. 2014;158(1):15-24. doi:10.1016/j.cell.2014.06.008

283. Wake H, Moorhouse AJ, Miyamoto A, Nabekura J. Microglia: Actively surveying and shaping neuronal circuit structure and function. *Trends Neurosci*. 2013;36(4):209-217. doi:10.1016/j.tins.2012.11.007

284. Elmore MRP, Najafi AR, Koike MA, et al. Colony-stimulating factor 1 receptor signaling is necessary for microglia viability, unmasking a microglia progenitor cell in the adult brain. *Neuron*. 2014;82(2):380-397. doi:10.1016/j.neuron.2014.02.040

285. Allen BD, Syage AR, Maroso M, et al. Mitigation of helium irradiation-induced brain injury by microglia depletion. *J Neuroinflammation*. 2020;17(1):1-18. doi:10.1186/s12974-020-01790-9

286. Prinz M, Jung S, Priller J. Microglia Biology: One Century of Evolving Concepts. *Cell*. 2019;179(2):292-311. doi:10.1016/j.cell.2019.08.053

287. Li Q, Barres BA. Microglia and macrophages in brain homeostasis and disease. *Nat Rev Immunol*. 2018;18(4):225-242. doi:10.1038/nri.2017.125

288. Markarian M, Krattli RP, Baddour JD, et al. Glia-selective deletion of complement c1q prevents radiation-induced cognitive deficits and neuroinflammation. *Cancer Res*. 2021;81(7):1732-1744. doi:10.1158/0008-5472.CAN-20-2565

289. Elmore MRP, Hohsfield LA, Kramár EA, et al. Replacement of microglia in the aged brain reverses cognitive, synaptic, and neuronal deficits in mice. *Aging Cell*. 2018;17(6). doi:10.1111/acel.12832

290. Acharya MM, Baulch JE, Lusardi TA, et al. Adenosine kinase inhibition protects against cranial radiation-induced cognitive dysfunction. *Front Mol Neurosci*. 2016;9(JUNE). doi:10.3389/fnmol.2016.00042

291. Yang H, Wang H, Andersson U. Targeting Inflammation Driven by HMGB1. *Front Immunol*. 2020;11(March):1-9. doi:10.3389/fimmu.2020.00484

292. Moore C, Hsu CC, Chen WM, Chen BPC, Han C, Story M et al. Personalized Ultrafractionated Stereotactic Adaptive Radiotherapy (PULSAR) in Preclinical Models Enhances Single- Agent Immune Checkpoint Blockade. *Int J Radiat Oncol Biol Phys*. 2021;110(5):1306-1316. doi:10.1016/j.ijrobp.2021.03.047

293. Svend Strangaard OBP. Cerebral Autoregulation. *Stroke*. 1984;15(3):413-416.

294. Nathaniel H. Greene, MDa and Lorri A. Lee M. Modern and Evolving Understanding of Cerebral Perfusion and Autoregulation. *Adv Anesth*. 2012;30(1):97-129. doi:10.1016/j.aan.2012.08.003.Modern

295. Gorbunov N V., Kiang JG. Brain Damage and Patterns of Neurovascular Disorder after Ionizing Irradiation. Complications in Radiotherapy and Radiation Combined Injury. *Radiat Res*. 2021;196(1):1-16. doi:10.1667/RADE-20-00147.1

296. Hou C, Gong G, Wang L, Su Y, Lu J, Yin Y. The Study of Cerebral Blood Flow Variations during Brain Metastases Radiotherapy. *Oncol Res Treat*. 2022;45(3):130-137. doi:10.1159/000521291

297. Keyeux A, Brucher JM, Ochrymowicz-Bemelmans D, Charlier AA. Late effects of X irradiation on regulation of cerebral blood flow after whole-brain exposure in rats. *Radiat Res*. 1997;147(5):621-630. doi:10.2307/3579629

298. LG Cockerham CF. Effect of antihistamines, disodium cromoglycate (DSCG) or methysergide on post-irradiation cerebral blood flow and mean systemic arterial blood pressure in primates after 25 Gy, whole-body, gamma irradiation. *J Radiation Research*. 1995;36(2):77-90.

299. Wynnie Wai Man Lam, MBBS, FRCR, Stella Sin Yee Ho Mp, Sing Fai Leung, FRCR, FHKAM, Ka Sing Wong, MD M, Constantine Metreweli, FRCR F. Cerebral Blood Flow Measurement by Color Velocity Imaging in Radiation-Induced Carotid Stenosis. *Ultrasound*. 2003;22(1):1055-1060.

300. Katsura M, Sato J, Akahane M, Furuta T, Mori H, Abe O. Recognizing radiation-induced changes in the central nervous system: Where to look and what to look for. *Radiographics*. 2021;41(1):224-248. doi:10.1148/rg.2021200064

301. Choi B, Kang NM, Nelson JS. Laser speckle imaging for monitoring blood flow dynamics in the in vivo rodent dorsal skin fold model. *Microvasc Res*. 2004;68(2):143-146. doi:10.1016/j.mvr.2004.04.003